DEVELOPMENT, FABRICATION, AND GROUND TEST OF AN INFLATABLE STRUCTURE SPACE-FLIGHT EXPERIMENT

THESIS

Thomas Lee Philley Jr., First Lieutenant, USAF

AFIT/GA/ENY/03-3

DEPARTMENT OF THE AIR FORCE
AIR UNIVERSITY

AIR FORCE INSTITUTE OF TECHNOLOGY

Wright-Patterson Air Force Base, Ohio

The views expressed in this thesis are those of the author and do not reflect the official policy or position of the United States Air Force, Department of Defense, or the United States Government.

AFIT/GA/ENY/03-3

DEVELOPMENT, FABRICATION, AND GROUND TEST OF AN INFLATABLE STRUCTURE SPACE-FLIGHT EXPERIMENT

THESIS

Presented to the Faculty
Department of Aeronautics and Astronautics
Graduate School of Engineering and Management
Air Force Institute of Technology
Air University
Air Education and Training Command
in Partial Fulfillment of the Requirements for the
Degree of Master of Science in Astronautical Engineering

Thomas Lee Philley Jr., B.S.
First Lieutenant, USAF

March 2003

AFIT/GA/ENY/03-3

DEVELOPMENT, FABRICATION, AND GROUND TEST OF AN INFLATABLE STRUCTURE SPACE-FLIGHT EXPERIMENT

Thomas Lee Philley Jr., B.S.

First Lieutenant, USAF

Approved:

Richard G. Cobb (Chairman)	Date
Anthony N. Palazotto (Member)	Date
William E. Wiesel (Member)	Date

Acknowledgements

First and foremost, I give honor to my Lord and Savior, Jesus Christ, for it is He who has brought me to where I am today. He gives me the strength and wisdom to make it through each and every day, and without Him, I am nothing.

I would also like to express my sincere appreciation to my thesis advisor, Major Richard Cobb, for his guidance and instruction throughout this thesis effort. His experience and insights were greatly valued throughout the entire process. I would also like to thank all my instructors who committed their time to ensuring I learned the material I needed. I would like to thank the laboratory technicians as well as the technicians in the AFIT model shop. Without them, I would have been lost.

Additionally, I could not have accomplished this task without the love and support of my family, friends, and especially my wife. She sacrificed her time and efforts to give me the support and encouragement I needed. Thank you for all that you are for me.

Thomas Lee Philley Jr.

Table of Contents

List of Figures

List of Tables

List of Symbols

Symbol Page

List of Abbreviations

Abstract

Since the first satellite launches of the 1950's, the requirements placed on space systems have evolved from the earliest beacons of Sputnik to the current state of the art technology. As requirements increase, space systems tend to grow in size and complexity, which in turn significantly increases the weight and cost of the system. In the current age of increasing requirements and limited budgets, the use of inflatable rigidizable structures provides a solution to reduce the costs associated with design, fabrication and launch of a space system while simultaneously increasing the deployment reliability and mission success of the system. However, due to insufficient data correlating ground tests to space flight results, the use of inflatable rigidizable structures in both the Air Force and industry has been very limited. Therefore, the goal of this research effort is to validate the ground testing methodology by correlating ground tests to space flight results of inflatable tubes.

The Rigidizable Inflatable Get-Away-Special Experiment is a self-contained Space Shuttle experiment that will test the deployment and structural characteristics of three inflatable rigidizable tubes. Once inflated and rigidized, each tube will be excited using piezoelectric transducers in order to collect vibration data for structural characterization. This thesis will present the follow on to the preliminary design of the experiment along with the initial fabrication processes and ground testing results.

DEVELOPMENT, FABRICATION, AND GROUND TEST OF AN INFLATABLE STRUCTURE SPACE-FLIGHT EXPERIMENT

I. Introduction

1.1 Background

Space assets are vital in today's world. These assets are used daily by members of both the commercial sector and the Department of Defense (DoD) community. Space has become an every day part of life during peace time and war time. As technology advances, more demands are placed on space systems. An increase in demands results in an increase in system complexity, which for most cases leads to a drastic increase in the size and weight of the system. This increase in size and weight poses two key problems. The first is associated with the fact that an increase in the size and weight amplifies the cost to launch and deploy the system. The second problem is found in the current constraints imposed by the launch vehicle. Regardless of how well developed a space system is or how revolutionary the technology may be, if the size and weight exceed the limitations of the launch vehicle, the capabilities of that system will never be utilized in the space environment. It is for these reasons that an alternate method must be found. One solution is to incorporate the use of inflatable, rigidizable structures into future space systems.

An inflatable, rigidizable structure is one that just prior to inflation is highly flexible in order to enable efficient packaging. In most cases, the volume required to package these structures is drastically reduced from that of a comparable rigid system. Upon inflation, the structure is deployed to a predefined shape. Due to the predefined nature of the structure, this process becomes very reliable because of the absence of complex joints and mechanical components. Once fully deployed, the

structure is rigidized thus obtaining a high degree of structural strength and stiffness comparable to that of traditional mechanical structures.

The use of inflatable structures in space is not a new concept. The National Aeronautics and Space Administration (NASA) began research in the area of inflatable structures in the early years of space exploration due to the fact that "the launch capabilities of the US (United States) vehicles were very limited (40)" During this time, inflatable structures were the only option to achieve the mission requirements. However, do to the unfamiliarity with how these structures would react in a space environment, along with the development of larger launch vehicles, the early space community turned to methods that could be more easily accomplished (12).

Since the early research and development efforts of NASA, strides have been made by the DoD and the commercial sector to incorporate inflatable technology into the next generation of space systems. The Air Force Research Laboratory's Directed Energy Directorate (AFRL/DE) has recognized the importance of inflatable technology in their efforts to launch and deploy large aperture optical telescopes that "provide continuous, synoptic, detailed coverage of the battlefield with the potential to provide real-time information on weather patterns and environmental disasters (28)." Commercial contributors have also made numerous advances in their efforts to incorporate inflatable technology into space systems requiring large on orbit hardware component configurations, to include solar arrays, sunshields, aerobrakes, and radar antennas (25). Significant advances have been made in the development, manufacturing, and on-orbit testing of inflatable structures, which allows space systems to take advantage of the decreased packing size and weight that inflatables offer. However, there is much less research in the area of developing inflatable, rigidizable structures for use in the space environment.

The majority of the current work performed in the research and development of inflatable, rigidizable structures has been primarily focused on analytical modelling and ground testing. Very little work has been conducted in an effort to correlate

the results of ground testing to actual space-flight results. Space presents a very unique environment. While the temperature, pressure, and gravity of space can all be duplicated through various means on earth, the affects of all three cannot be tested simultaneously. Therefore the exact performance of a space based inflatable, rigidizable structure cannot be accurately predicted until a method is determined to correlate the ground testing of these structures to the actual space-flight results.

1.2 Scope of Project

The primary goal of the Rigidized Inflatable Get-Away-Special (GAS) Experiment (RIGEX) is to correlate ground test data to space flight results in an effort to increase the use of inflatable, rigidizable technology for space applications. A GAS experiment is one that is mounted inside a canister that is attached to the side wall inside the Space Shuttle cargo bay, and is often referred to as a 'GAS can'. By utilizing the GAS can technology, RIGEX will be kept in a self-contained area while being exposed to the vacuum, temperature, and zero gravity affects of the space environment simultaneously. The RIGEX project will collect on-orbit data regarding inflation, deployment, rigidization, and structural characterization. Upon the completion of the on-orbit data collection, the experiment will be returned to Earth for further analysis and testing in an effort to verify the accuracy and improve upon the methods used in ground testing.

The goal of this thesis was to improve upon the current RIGEX design, fabricate one inflatable, rigidizable tube deployment assembly, and test the fabricated portion of the experiment in an effort to collect data for the deployment of the inflatable, rigidizable tube in the Earth's gravitational environment. This research effort is a continuation of the work performed at the Air Force Institute of Technology (AFIT) by John D. DiSebastian III from August 2000 through March 2001 (17), and Thomas G. Single from August 2001 through March 2002 (36).

1.3 Previous RIGEX Research

The first work done on the RIGEX project was conducted in an effort to produce a preliminary design for the experiment. This effort worked towards the goal of providing a system that would be capable of providing data on space rigidized structures. Numerous options were evaluated regarding all aspects off the project. Figure 1.1 shows the conceptual drawing of RIGEX that was a result of the preliminary design. Once an initial design of the experiment was complete, some preliminary work was accomplished in an effort to develop an event calendar that would outline the sequencing of events necessary to accomplish the mission (17).

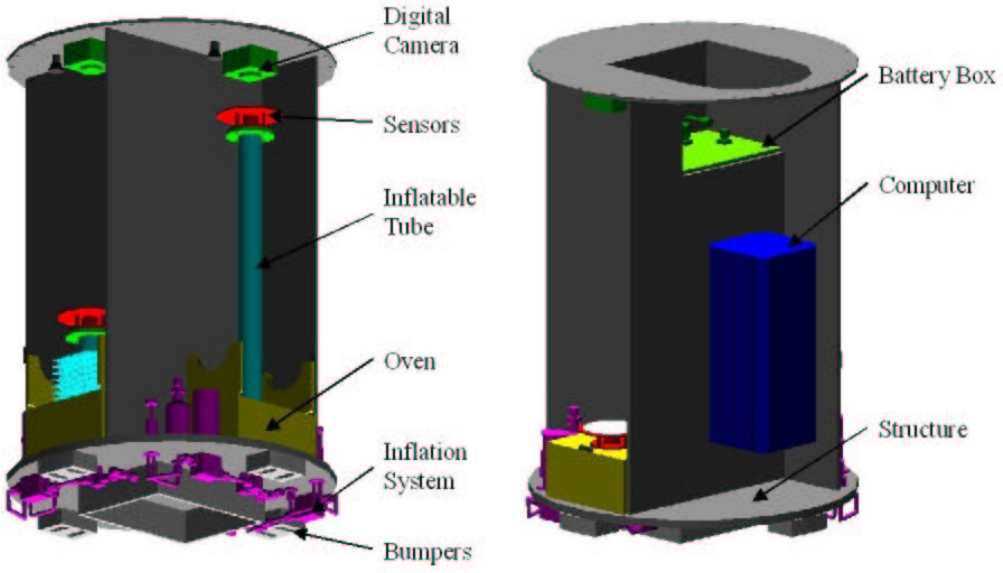

Figure 1.1 RIGEX Preliminary Design Conceptual Drawing

Upon completion of the preliminary design, follow on research was conducted specifically in regards to the actual inflatable, rigidizable tubes that would be used as part of the RIGEX mission. The study of the tubes focused on determining the natural frequencies and damping ratios of the tubes, as well as determining the feasibility of applying standard beam theory as an analysis method for the tubes. Several factors were analyzed throughout this research including the effects pressure and temperature had on the vibrational properties of the tubes. The results of this

research found what were thought to be the modes of the tube, however, the analysis used to determine these values proved very difficult due to the complexity of the data collected within the experiment. In addition, it was determined that simple beam theory was not adequate for the analysis of the tubes due to torsional modes not adequately captured in the model (36).

A final area of research was conducted in an effort to optimize the RIGEX heater box. This work was done by Michael Maddux at AFIT during the Summer of 2002. Initially the heater box was designed to be 6.5 inches wide by 4.5 inches deep by 3.125 inches tall as shown in Figure 1.2 (17). However, after extensive testing and analysis, it was determined that the current design would not be capable of heating the tube to a temperature adequate for deployment. In addition, the current design for the heater box did not provide adequate space for the folded tube to be mounted within the box.

Figure 1.2 Original Heater Box Design

To resolve the issues with the heater box, the original design was first modified to give the new heater box dimensions of 6 inches wide by 4.5 inches deep by 5 inches tall. This modification allowed the tube to be easily mounted within the

heater box and also provided better heat transfer to the tube due to the fact that the heaters were now in closer proximity to the tube itself. Additionally, the interior of the heater box was lined with an aluminum coating and all heaters within the box were coated with a flat black paint (26). These additional modifications as with the change in size increased the ability of the heater box to properly heat the inflatable, rigidizable tube in preparation for deployment.

1.4 Objectives

Through the previous work that has been accomplished, AFIT developed the following mission statement for the RIGEX project (17):

> *To verify and validate ground testing of inflation and rigidization methods for inflatable space structures against a zero-gravity space environment.*

With this defined, the following are the primary and secondary objectives specifically for the research effort that will be conducted in the current phase of the overall RIGEX project.

Primary Objective:

– *Design and fabricate test hardware necessary to collect ground based data on the RIGEX inflatable, rigidizable tube deployment.*

Secondary Objectives:

– *Perform vibrational analysis on the inflatable, rigidizable tube in an effort to characterize its structural properties.*

– *Determine the affects varying the boundary conditions has on the structural properties of the inflatable, rigidizable tube .*

This research focused on the ground testing aspect of the RIGEX project. One inflatable, rigidizable tube assembly was fabricated and the deployment of the tube was tested. Various data collection methods as well as ground deployment testing methodologies were developed and implemented on the tube assembly. Once the deployment of the tube was demonstrated, and a sufficient amount of data collected, a

preliminary vibrational analysis was performed on the tube. This analysis collected data in an effort to determine the natural frequency, damping ratio, and bending mode of the tube. Upon completion of testing, the data collected throughout the course of this research was used to predict the performance of the inflatable, rigidizable tube in space.

1.5 Assumptions/Constraints

The primary constraints that are placed on the RIGEX project stem from the NASA Goddard Space Flight Center (GSFC) Shuttle Small Payloads Project Office (SSPPO) concerning the criteria that an experiment must meet for integration into a GAS can. The primary constraint associated with all GAS can experiments is the user envelope. Table 1.1 outlines the primary constraints set forth by NASA (17).

Table 1.1 NASA GAS Constraints

Constraint	Limit
Weight	200 lbs
Size	19.75 inches (diameter)
	28.25 inches (height)
Flight Time	14 days

The ground testing associated with this experiment will be limited to the inflatable, rigidizable tubes manufactured by L'Garde, Inc. Each tube is composed of a proprietary three ply carbon fiber material that has been designated by L'Garde as L5 (36). The L5 material is designed to remain rigid while below a specified glass transient temperature (T_g) and once heated above the T_g value the material softens. For the purposes of this experiment, the T_g value has been set by L'Garde at $125°C$. Each tube was z-folded by L'Garde prior to inflation, as shown in Figure 1.3. In addition, each tube is assumed to be identical throughout all tests conducted.

Vibrational tests throughout this experiment will focus only on the bending modes of the tubes, and will specifically focus on the first and second bending modes.

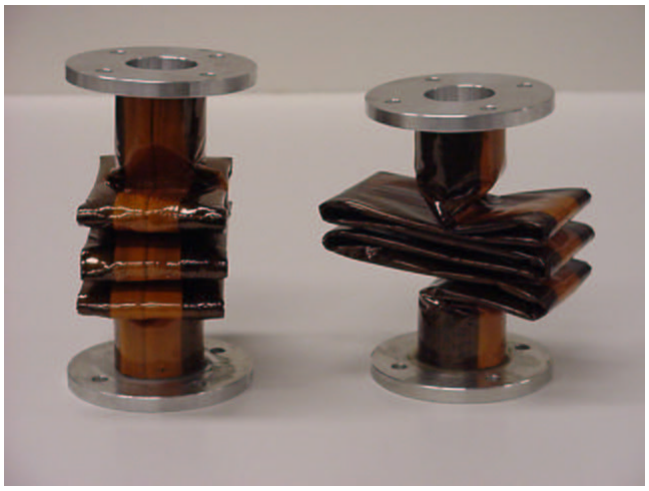

Figure 1.3 Inflatable, Rigidizable Tube: Z-Fold Configuration

This limitation will allow the results found to be correlated to the results of previous experimentation conducted on the RIGEX inflatable, rigidizable tubes.

The final constraint placed upon the ground testing of RIGEX is the available test equipment, primarily the vacuum tank which will be used for testing. The vacuum tank places a constraint on any test article which will be tested in it by the fact that the entrance to the tank has a diameter of only eighteen inches. Therefore, any structure built to test the deployment of the inflatable, rigidizable tubes in vacuum, must fit through the eighteen inch diameter entrance to the vacuum tank.

1.6 Methodology

In order to correlate RIGEX ground test data to the actual space flight results, the ground tests must simulate, as accurately as possible, the space flight configuration. This was done by first developing a test structure identical to that which would be flown. The current RIGEX structure has a diameter of 19.75 inches which, given the constraints outlined in Section 1.5, will not fit through the entrance of the vacuum tank. The overall RIGEX hardware includes three redundant tube assemblies that will be tested. Therefore, in order to adhere to the physical constraints of the vacuum tank, only one tube assembly was built and tested with the philos-

ophy that each addition assembly would operate identical to the assembly tested. This allowed the RIGEX components to be tested as they will be flown given the equipment limitations.

The vibrational testing of the inflatable, rigidizable tubes was conducted in two phases. First, the tube was tested independent of the RIGEX structure. This allowed for the modal frequencies and damping of the tube itself to be determined. The tube was first mounted firmly to a vibrational testing table, and then mounted to a test stand that was in turn be mounted to the table. This allowed flexibility to be added to the mounted base, thus providing the change in boundary conditions. The tube was then mounted to the RIGEX test structure and various tests were performed to determine what effects the structure has on the structural properties of the tube.

Once vibrational tests were complete, the z-folded tube was mounted to the test structure, and the deployment of the tube was tested. This was done by mounting the structure inside the vacuum tank and following the deployment procedures that will be used for on-orbit testing. This allowed the tube to be deployed under conditions similar to those that would be seen in space. By simulating the space environment, ground test results could later be compared to the actual space flight results in order to determine the affects gravity plays on the accurate deployment of the tube. Each test was monitored by various temperature and pressure sensors as well as visually by a digital camera mounted to the test structure.

In order to conduct the tests outlined above, a variety of equipment was used. Piezoelectric transducers (PZT) were used to excite the tube during vibrational testing. A signal produced by a single axis accelerometer mounted to the tube was used in conjunction with a reference signal to produce a frequency response function. A laser vibrometer was also used to validate results. The RIGEX vibrational tests were all conducted in ambient conditions, while the deployment tests were conducted in a vacuum. All tests however were conducted within the AFIT Vibrations Laboratory.

1.7 Summary of Thesis

In the following chapters, the design and fabrication of the RIGEX test structure along with the initial ground testing of the experiment is presented. Chapter 2 presents the topic of inflatable structures and give details on the progress this technology has made over time. It outlines the theory behind the methods that will be used for the preliminary vibrational analysis of RIGEX, and then gives an overview of the previous work that has been completed to date on RIGEX. Chapter 3 discusses the setup and procedures used in to conduct the various tests.

Chapter 4 presents the results achieved through the preliminary RIGEX ground tests, along with a discussion of the results. Finally, Chapter 5 incorporates a summary of the presented material along with recommendations for future work to be accomplished on the RIGEX project.

II. Literature Review

2.1 Inflatable Structures

2.1.1 Overview. Inflatable structures are flexible, lightweight structures that prior to inflation can be packaged into a very small volume. These structures can be divided into two main categories, purely inflatable and inflatable, rigidizable structures. Both categories of inflatables are identical in the fact that once pressurized, they inflate to a predefined form that can vary to encompass a wide variety of shapes and sizes. However, purely inflatable structures require additional inflation gas in order to maintain pressurization by compensating for leaks. The pressure maintained provides the necessary structural support. Inflatable, rigidizable structures take a slightly different approach. Once the structure is initially pressurized, the structural material itself is rigidized thus allowing the structural support to be maintained once the inflation gas is vented. Numerous research efforts have focused on the use of purely inflatable structures in space application, however very little has been done in the area of inflatable, rigidizable structures.

The use of inflatable structures for space applications is not a new concept. Since the late 1950s, there has been a constant, although limited at times, interest in the use of such structures to optimize the various technological advances in space. The use of inflatables in space became a necessity in the early days of space exploration given the limited capabilities of the first generation launch vehicles. However, as advances were made in launch capabilities, a turn was made to the more traditional and familiar mechanical systems. In the space industry today, this limitation in launch vehicle capabilities has once again been reached. As shown in Table 2.1 (17, 6, 5), even with today's technologically advanced launch systems, there still remains limitations to the size and weight of a system if it is to be placed in orbit. As the requirements placed on space systems increase, the complexity and necessary size and weight of these structures grow drastically. This once again limits the abil-

Table 2.1 Current Launch Systems Specifications

Launch System	Maximum LEO (kg)	Payload GEO (kg)	Payload Diameter (m)	Fairing Length (m)
Atlas II	8640	1050	4.2	12.0
Atlas V	20520	8670	5	23.4
Delta II	5089	3890	2.9	8.5
Delta IV	23040	13130	5	22.4
STS	24400	n/a	4.5	18.0
Ariane 5 (ESA)	18000	12000	4.5	12.0
H-2 (Japan)	10500	6600	4.6	5.0
Long March (China)	13600	2250	3.8	6.0
Proton (Russia)	20900	2500	4.1	15.6/7.5

ity to apply state-of-the-art technology to space assets unless an alternative to the traditional and familiar mechanical systems is implemented.

As the size and weight of space systems grow, problems arise not only in conjunction with finding a compatible launch system, but also in the program costs. Typically the costs associated with a particular space system are directly proportional to the weight of the system being launched. On average, the cost associated with placing a satellite in orbit range from approximately $\$11K/kg$ for a low earth orbit (LEO) to approximately $\$83.1K/kg$ for a geosynchronous earth orbit (GEO) (45). Therefore, as the weight increases, the cost does so as well. There are many benefits associated with using inflatable structures to combat the problems associated with the technological needs of current and future space systems. Perhaps the primary advantage exploited by satellite designers is the low weight and packaging efficiency that inflatable structures offer.

Weight and volume restrictions are issues that constantly plague space systems. As requirements grow, the necessary weight and volume needed to meet the requirements also grows. Eventually, a compromise must be made between increasing the size of the space system and meeting more of the requirements or reducing the size and eliminating requirements. In some cases, this compromise will reduce the capabilities of the system. Inflatable structures offer the possibility of reducing the overall weight structural weight, typically, by fifty percent from that required by

traditional mechanical structures. In addition, inflatables can typically be packaged in a volume less than twenty-five percent of that necessary for standard mechanical structures, and can be packaged in essentially any shape depending on particular mission requirements (12).

Weight and volume though are not the only issues that must be dealt with in the design of a space structure. The strength of the structure is also an issue. "Inflatable structures are inherently strong (12)." This is due to the fact that inflatable structures are able to absorb loads over a large surface area. Mechanical systems are restricted given that typically loads are concentrated in certain points which must then be reinforced (12). The Atlas missile program relied on the strength of inflatable structures in that the missile itself was inflated by the fuel which in turn gave the missile the strength needed to sustain the loads exhibited during launch (40).

In addition to the strength of the structure, the deployed structure must also be highly reliable. Inflatable structures have a very high deployment reliability, given that an inflatable system is essentially self correcting. This is due partly to the predefined form of the structure and also due to the fact that if an error occurs and the system resists deployment, the deployment force increases due to a build up of pressure, there is less risk of an inaccurate or incomplete deployment. If properly designed, an inflatable structure only has a single point of failure corresponding to the initiation of the inflation gas. Based also on the same reasons, the deployment results of inflatables are highly repeatable. When compared to mechanically deployed system containing numerous joints and hinges, the reliability and ability to repeat the deployment multiple times is drastically reduced (12).

Inflatable structures currently provide many advantages to the space community. They offer a means to reduce the weight and packaging volume of a system while maintaining the structural strength and increasing the deployment reliability. As the demands placed on space systems increase, and the size and complexity of these systems grow, designers are forced to find alternate means to the traditional

mechanical systems. Inflatables provide a solution that will allow designers to incorporate revolutionary technology into future space assets.

2.1.2 History. Beginning in the early years of space exploration, the potential uses for inflatable structures in space were tested. Despite their immature designs and lack of testing, inflatables were looked upon as a means for accomplishing space missions in the 1950's. Although primitive in design, many of these early technology demonstrations were very advanced for their time. Over the past fifty years, numerous steps have been made towards the increased usage of inflatables in space. Several of the experiments which contributed to validating this technology are described in the following sections.

2.1.2.1 Goodyear Inflatable Structures. Goodyear was a pioneer in the use of inflatable structures in space. Throughout the 1950's and 1960's, they developed concepts that would incorporate inflatable structures into their search radar antenna, radar calibration sphere, and lenticular inflatable parabolic reflector. The search radar antenna used a truss structure covered with a metallic mesh for the aperture surface and had a length of 10 meters and width of 3 meters. The radar calibration sphere was based on the a concept of using hexagonal shaped panels bonded together at their edges to form a sphere that once inflated would measure approximately 6 meters in diameter. The lenticular inflatable parabolic reflector was composed of a lenticular reflector supported on its periphery by a toroidal structure. The reflector was fabricated by bonding together "pie shaped (20)" metalized membrane gores into a parabolic surface. The overall structure measured 12 meters in diameter while the reflector itself maintained a diameter of 10 meters (20).

2.1.2.2 NASA Inflatable Satellites. NASA was also a key contributor to inflatable technology through their efforts to incorporate inflatable structures into

Figure 2.1 NASA Echo I Satellite

space missions. NASA's efforts began in May of 1958 with their efforts to develop, fabricate and launch large, high precision space structures. This research began at the NASA Langley Research Center (LaRC) and later was assigned to the GSFC. The first in a series of satellites associated with this research was the Echo I balloon.

The Echo I project was the pathfinder program for NASA inflatable satellites. Composed of mylar gores coated with 2000 angstroms of vapor deposited aluminum that were bonded together to form a sphere, Echo I was a passive communications satellite. The Echo I satellite, as shown in Figure 2.1 maintained a diameter of 100 feet, weighed 136 pounds, and was stored in a 26 inch diameter container, and was launched on August 12, 1960 (20). Echo I was successfully deployed once on orbit and remained operational for several months, thus accomplishing its mission. However, an incomplete inflation of the balloon had occurred, and due to a lack of onboard instrumentation, the exact cause remains unknown (40).

NASA went on to produce a number of additional inflatable satellite experiments following the success of Echo I. Table 2.2 outlines the follow on experiments

Table 2.2 NASA Inflatable Satellite Missions

System	Weight (lb)	Diameter (ft)	Launch Date	Life (yrs)	Purpose
Explorer IX	34	12	Feb 1961	3	Hi-Alt. Density
Explorer XIX	34	12	Dec 1963	2	Hi-Alt. Density
Echo II	580	135	Jan 1964	-	Comm.
PAGEOS I	149	100	Jun 1966	5	Earth Survey

developed by NASA (12). Despite the anomaly with the Echo I inflation, the Echo II, PAGEOS, and Explorer satellites were complete successes (40)

2.1.2.3 Contraves Inflatable Structures. The European Space Agency (ESA) displayed interest in the area of inflatable deployable space structures with their sponsorship of the Contraves Space Division in Switzerland for the development of concepts for reflector antenna and sun shade structures. Primarily this research was focused towards axisymmetric reflector antennas for Very Large Baseline Interferometry (VLBI) and sun shade support structures for large telescopes and sensors. These potential for inflatable technology was demonstrated by Contraves in the 1980's with fabrication of a six meter, one third scale model of a VLBI antenna. Additionally, a ten meter by twelve meter land mobile communications reflector antenna was built and evaluated. Based on the results of these two endeavors, Contraves was able to develop a functional scale model of a sun shade support structure for a submillimeter space telescope (20).

2.1.2.4 Inflatable Antenna Experiment. In an effort to identify unique and innovative technologies for use in the space environment, NASA initiated the In-Space Technology Experiments Program (IN-STEP). In an effort to provide a solution to the need for large deployable space antennas, L'Garde, Inc. developed the Inflatable Antenna Experiment (IAE).

The IAE was designed to verify the ability to provide a low cost, low weight solution to manufacturing a fourteen meter diameter flight qualified reflector antenna structure. In addition, the objectives of the IAE were to demonstrate the

deployment reliability of the inflatable structure in a realistic environment as well as measuring the surface precision of the reflector (19). Given these objectives, L'Garde chose to utilize the capabilities of the Space Shuttle launched Spartan experiment platform due to its ability to provide a platform for the IAE, power and the electrical initiation of the experiment. In addition, the Spartan would provide data recording and attitude control capability as well as a means to separate the antenna from the Spartan upon the completion of the experiment (42).

The basic design for the IAE was composed of three main components. The first is the fourteen meter diameter reflector structure and transparent canopy which was a mirror image of the reflector, and used to maintain the gas pressure while on orbit. The second component included a torus structure that provided the support circumferentially to the reflector assembly. The final component consisted of three 28 meter long struts that connected the torus structure to the experiment canister that was in turn mounted to the Spartan platform (19). The complete IAE experiment is shown in Figure 2.2. In order to demonstrate the packing efficiency of the IAE, the experiment was packaged into a canister of only 80 inches long, 43 inches wide and 21 inches high (42).

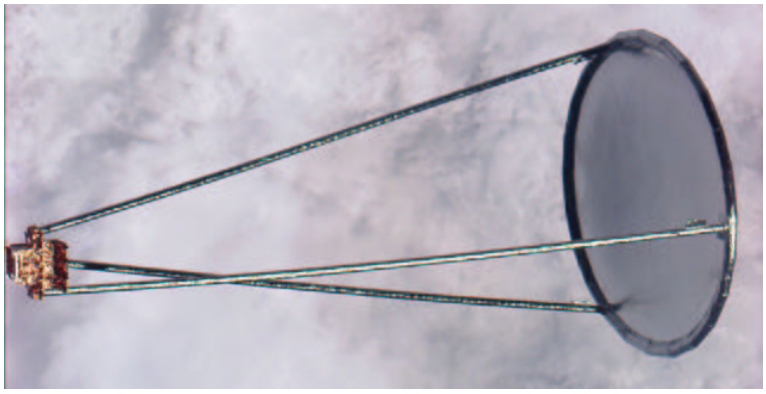

Figure 2.2 Inflatable Antenna Experiment

On May 19, 1996, the IAE was launched on board the STS-77 mission. Upon launch, the IAE weighed only 60 kilograms (18), thus providing a drastic decrease

in weight over traditional mechanical systems. The Spartan containing the IAE was nominally deployed on the second day of the mission and after one and one half orbits, the IAE antenna structure was inflated. Unexpected dynamics during the initial inflation caused the entire structure to rotate, however, the correct final shape was attained. Once the desired orbit for operations was reached, the antenna was jettisoned from the Spartan, thus completing the IAE mission. The overall mission was success in that it provided a vast array of information concerning the deployment of large dynamic structures in space (39), and all at a cost on the order of only one million dollars.

2.1.2.5 ARISE. The technique of VLBI has been used to enhance the resolution of the observations of astronomical objects since 1967. This technique is done by using two or more separated radio telescopes simultaneously observing the same source. By correlating the observations, a large radio telescope whose diameter is equal to the size of the telescope array can be synthesized. However, this concept in the terrestrial sense is limited by the in angular resolution by the Earth's diameter. With this, the Advanced Radio Interferometry between Space and Earth (ARISE) mission was developed as part of NASA's efforts to find concepts capable of improving the angular resolution on observations of celestial objects (41). The ARISE mission concept was developed in order to utilize orbiting antennas on the order of 30 meters in diameter in conjunction with ground based antennas to eliminate the limitation of the Earth's diameter.

In order to accomplish this mission through the use of conventional mechanically deployed technologies, the cost would range from 500 million up to 1 billion dollars to fabricate a 30 meter diameter antenna (41). Therefore, for this mission to be feasible, the antenna cost could not drive the cost of the mission. In addition, the stowed antenna would be required to fit in a volume of less than one cubic meter in order to ensure a launch on either an Atlas of Delta class launch vehicle (33). Given

the mission requirements, an innovative solution was needed, thus incorporating the use of inflatable technology.

The initial conceptual design of the ARISE mission yielded a system that could house an antenna on the order of 30 meters in diameter, weigh on the order of only 100 kilograms, and could be packaged into a volume less than the required one cubic meter. Figure 2.3 illustrates a conceptual drawing of the deployed ARISE structure, which would enable astronomers to achieve very high angular resolution of distant radio sources at a cost of only a few tens of millions of dollars through the use of inflatable technology (33).

Figure 2.3 ARISE Inflatable Spacecraft

2.1.3 Recent Projects. With a foundation set by experiments throughout the past fifty years, many new innovative concepts for the use of inflatable and inflatable, rigidizable concepts in space are being developed. These efforts take on a wide range of missions that could one day revolutionize the satellite industry. The following sections outline some of the state of the art concepts that are currently being developed.

2.1.3.1 Gossamer Space Telescope. AFRL/DE, inspired by the 1996 flight of the IAE is developing a concept that will place an inflatable thirty meter optical telescope in space. They hope that by placing multiple telescopes of this sort

Figure 2.4 NGST Conceptual Drawing and Sunshield Scale Model

into geosynchronous orbits, the total number of satellites required for continuous earth observation will be drastically reduced (28).

The current design calls for the parabolic mirror of the telescope to be produced through a newly developed method using a CP-1 polymer to produce high quality planar films of only twenty microns thick. Once deployed, the thirty meter diameter mirror will be rigidized in order to maintain the shape necessary for the collection of precise images. Current engineers expect the packaged diameter of the mirror to be on the order of one tenth of the deployed diameter, thus bringing the near impossible launch of such a large structure into reality (28).

2.1.3.2 Inflatable Sunshield in Space. NASA is currently developing the technology necessary to accomplish the Next Generation Space Telescope (NGST) mission scheduled to fly in 2007. The current design of the NGST is to produce a near infrared, eight meter aperture telescope that will orbit at the L2 position for approximately five to ten years. In order to optimally operate the telescope, it must be kept at a temperature below $60K$. In order to maintain this temperature, a 32 meter by 14 meter sunshield is required (25). Figure 2.4 shows a conceptual drawing of the NGST and inflatable sunshield design along with a half scale engineering model of the NGST sunshield developed by L'Garde, Inc.

Currently both mechanically deployed and inflatable sunshield options are being analyzed to accomplish this mission. However, several advantages that have

been expressed in conjunction with the use of an inflatable is the fact that it would provide a lighter weight and much smaller launch volume. In addition though, one primary concern NASA has with the use of an inflatable structure for the NGST mission is the potential for the uncontrolled deployment of the sunshield to cause unintentional damage to the telescope (25). The half scale engineering model of the NGST sunshield shown in Figure 2.4 is currently being used by L'Garde in an effort to demonstrate controlled deployment.

2.1.3.3 Inflatable Rigidizable Truss Structure. In an effort to expand the use of inflatables to areas other than antenna structures, L'Garde, Inc. developed a concept that would use inflatable, rigidizable tubes to form a truss structure as shown in Figure 2.5. This task was designed to develop the capability to build an inflatable, rigidizable truss structure and to demonstrate the packaging, strength, and vacuum deployment of the structure (22).

Figure 2.5 L'Garde Inflatable Space Truss

The truss itself consisted of 21 legs and 9 joints, and once deployed, the truss measures 60.1 inches in length. The legs of the truss structure are tubes composed of a composite material that are impregnated with a water soluble resin. Once deployed, the resin is rigidized as the water impregnated in the material evaporates. This gives the tubes the stiffness necessary to provide strength to the structure. The

joints are cast aluminum manifolds that allow the legs to be connected and allow the inflation gas to flow freely between joints.

As with all inflatable structures, the distinct advantage is the reduction in weight and packaging volume, although, with the addition of aluminum joints to the truss, the weight as well as the packed volume are increased slightly. However, this increase was seen to be only minimal in the fact that the truss, which measured 60.1 inches in length had a weight of only 1917 grams, and a packaging volume of only 1953 cubic inches (22) as shown in Figure 2.6.

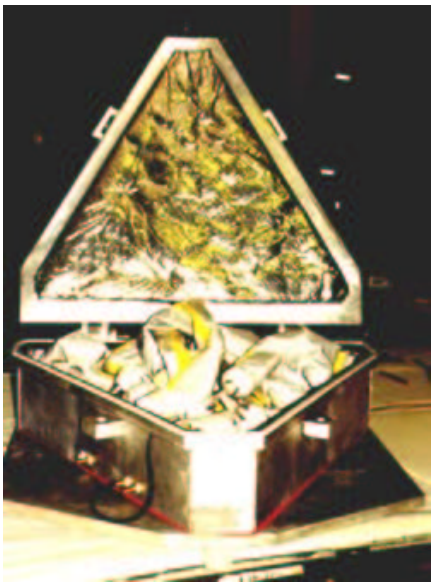

Figure 2.6 L'Garde Packaged Inflatable Space Truss

After testing the structure from packaging through to vacuum deployment, the project was considered a success. It was demonstrated that the tube could withstand the dynamics of deployment, and through vibrational tests, it was shown that the truss possessed a very high stiffness and excellent damping properties (22), thus enabling inflatable, rigidizable structures the potential to be used as load bearing support structures for numerous space applications.

2.1.3.4 PowerSphere Concept. With the development of current microsatellites and nanosatellites, the volume available for subsystems within the satellite is becoming more and more limited. The deployment of traditional mechanical solar arrays requires a large amount of volume and weight as well as additional hardware necessary for pointing accuracy. In order to resolve the conflict of supplying sufficient power in an environment of decreasing volume, a team composed of Aerospace, ILC Dover, Lockheed Martin, and NASA has developed a concept known as the PowerSphere.

The PowerSphere is an ultra lightweight deployable solar array structure that will deploy from a small satellite, and form a sphere around the satellite payload (35). The concept consists of an upper and lower center deployment column along with multiple solar panels that once deployed, piece together to form the sphere. The center deployment columns will use an inflatable, rigidizable tube to provide the central support for the sphere along with any necessary electrical connections. Once inflated and rigidized, the panels will be deployed. While there are still multiple deployment options for the panels that are being analyzed, one such option includes the used of an inflatable, rigidizable tubular hinge. The position of the panels will be preset to form the sphere when each tubular hinge is inflated. Prior to inflation, the panels will be folded at the hinge and packaged into the desired volume. Upon inflation, the hinges and panels return to their preset configuration, thus deploying the PowerSphere (35).

While this concept is still in the early developmental stages, it provides a complete power system which weighs under one kilogram. This concept expands upon the traditional uses of inflatable, rigidizable structures in an innovative manner that allows manufactures to meet the requirements levied by the small satellite community. The PowerSphere illustrates the vast potential inflatables have to revolutionize the space industry.

2.1.4 Testing Methodologies. Adequate inflation test methods is one key area where a significant shortfall exists in the area of inflatable, rigidizable technology. The very nature of inflatable structures, given that they are highly flexible and in most cases exhibit uncontrolled deployment, causes testing to become very difficult. In addition, the light weight that causes inflatable structures to be so attractive to various satellite designers also causes gravity to significantly affect the behavior of the structure. It is for these reasons that additional research is needed in order to modify current testing methods and overcome the challenges presented by inflatable structures.

2.1.4.1 Challenges to Testing. The light weight, efficient packaging, and deployment that drives designers to incorporate inflatable structures into various systems are the same factors that cause numerous challenges in validating the system through testing. The primary challenge to inflatable structures is seen in the deployment. The majority of deployment failures are caused by strain energy within the structure that is unaccounted for. The internal energy during ground testing is significantly larger due to the effects of gravity and tend to mask the key deployment energies that are seen in space (43). Reactions to such forces cause unexpected physical behavior of the system thus initiating additional demands on the guidance and control subsystem.

Additional challenges are seen in the fact that due once again to the light weight nature of inflatables, the static position and dynamics of the structure can not be sufficiently predicted by ground tests (43). The reason for this stems from the fact that even though some inflatable structures are rigidized, often times, gravity causes a distortion in the shape of the structure that cannot be corrected without the removal of gravity. This in turn causes various shifts in the uniformity of the material properties and other physical properties that are necessary to understand for an accurate design.

Other challenges to the testing of inflatables are seen in the fact that there is merely a lack of knowledge concerning the structures. There is currently little experience with ground testing methods therefore, most testing has been conducted in space or simulated zero gravity environments. However, even in these cases, there are limitations to the data that can be collected without modifying the structure which in turn imposes similar problems to those instigated by gravity. Therefore, until a greater base of knowledge is formed there will still remain uncertainty within inflatable structures that limits the ability to accurately test and validate the structures prior to launch.

2.1.4.2 Current Solutions. There are various methods that are currently being implemented to attempt to combat the challenges associated with testing inflatable structures. As with traditional structures, there is various modelling and simulation software being developed along with both ground and flight tests that are attempting to gain the knowledge needed to better understand and thus more accurately test inflatables.

Several efforts have been devoted to determine if current software was capable of modelling inflatable structures. However, it has been seen that most standard software packages designed for structures do not work well for inflatables. Some can be used cautiously, but more applicable software is needed (40). Some studies have been done in order to develop such software that would model the deployment of a single inflatable tube. One such study conducted at the LaRC was able to predict the behavior of a z-folded tube. The study was able to incorporate the effects due to a varying inflation rate, the presence of residual air in the tube, and some effects due to gravitational forces (44). The shortfall in this research however, lies in the fact that once again, a zero gravity test of the identical structure is needed to validate the results.

Actual flight tests are also being conducted to validate various inflatable structures. Flight tests are available through several sources. One method for conducting such experiments is to actually fly the experiment in space. This, although effective in supplying the actual environment, it is not very cost efficient in addition to the fact that often times, years of preparation are required prior to the actual space flight. A second option is through aircraft flights on a parabolic trajectory. While this provides zero gravity for a limited time, it cannot be done in conjunction with a vacuum test, thus once again limiting the validity of the test (43). A combined team from United Space Alliance and the University of Kentucky incorporated this method of testing as they analyzed an inflatable tube with a single fold in the center. They analyzed the tube through extensive ground tests, and compared the ground tests to results found in tests conducted onboard an aircraft flying a parabolic trajectory. The tests showed that gravity had a significant effect on the delayed inflation of the tube past the fold point and that zero gravity deployments occur in less time than those conducted in a one-g environment (37). While these are notable results, the test were limited by the fact that they could not be conducted in a vacuum.

Testing is vital to space systems especially when a new technology is to be incorporated in to operational systems. Current methods of testing provide a stepping stone in the direction of validating the technology, however, if inflatable, rigidizable structures are to be incorporated on an operational level, ground testing methods must be identified that can accurately be correlated to the actual space flight results.

2.2 Vibrational Analysis

Dynamics, the study of the relation between the motion of physical systems and the forces causing motion within the system, is a topic that has intrigued researches for numerous years (29). Every physical system has some type of motion, visible or not, that is a direct result of either internal or external forces acting upon the system. One type of dynamic behavior of particular interest to individuals within

the space industry is the study of vibrations, which can be defined as the oscillation of a particular system about a specified equilibrium position (29).

Understanding vibrations and the vibrational response a particular system has given an excitation force is vital to the success of satellite programs. Vibrations are experienced by a satellite throughout all stages of its life to include launch, initial deployment, and even throughout normal day to day operations as the satellite experience various disturbances, which range from planned attitude correction maneuvers to unexpected micrometeorite impacts. If the vibrational response a satellite will have to each of this various forces is not accounted for, the effects could be disastrous for the mission.

When inflatable structures are incorporated into a satellite program, the need to understand the vibrational response becomes even more prevalent. Due to the highly flexible nature of inflatable structures, there are numerous additional complexities within the vibrational response of the system. As with traditional systems, if the vibrational response of an inflatable system is not fully understood, the success of the mission will be compromised.

Vibrations is a very complex field of study. Vibrational responses can stem from either single or multi degree-of-freedom systems which can be excited by either deterministic or stochastic inputs. Each input can then in turn produce either a discrete or continuous response that could be either linear or non-linear in nature (11). Fortunately though, often times the process can be simplified by linearizing the system for a particular interval of interest and modelling a multi degree-of-freedom system as merely a combination of multiple single degree-of-freedom systems. This in turn allows an analysis to be performed that will determine the natural frequencies and damping for the system, which provides a basis for vibrational analysis. To accomplish this task, the following equations and models are commonly used.

In order to initially analyze any system, a model must first be developed. In the case of dynamical analysis, the most simple of such models, a single degree of

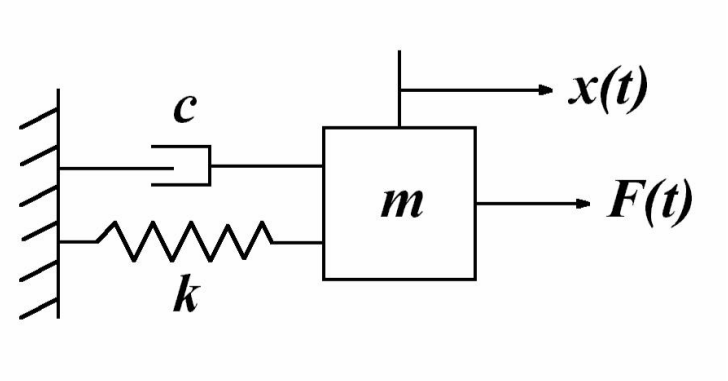

Figure 2.7 Single Degree-of-Freedom System

freedom mass, spring, dashpot system, is shown in Figure 2.7. If motion of this system is constrained to the x(t) direction, where x represents the displacement of the mass (m), the motion of the mass can be defined by the equation 2.1:

$$m\ddot{x} + c\dot{x} + kx = f(t) \tag{2.1}$$

where c is the coefficient of viscous damping, k is the spring constant, $\ddot{x}$ is the acceleration, $\dot{x}$ is the velocity, and $f(t)$ is an input forcing function (29).

An alternate way to express equation 2.1, it to divide the equation through by m and replace the damping and stiffness terms, c and k, with the natural frequency (ω_n) and the viscous damping factor (ζ) through the following relationship. The relationship between k and ω_n is given by equation 2.2:

$$\omega_n = \sqrt{\frac{k}{m}} \tag{2.2}$$

where ω_n is found in radians per second. Additionally, the relationship between c and ζ is given by equation 2.3:

$$\zeta = \frac{c}{2m\omega_n} \tag{2.3}$$

where ζ is a nondimensional quantity used to describe damping (29).

Using equations 2.2 and 2.3, equation 2.1 can be rewritten in the form of equation 2.4:

$$\ddot{x} + 2\zeta\omega_n\dot{x} + \omega_n^2 x = \frac{f(t)}{m} \tag{2.4}$$

In order to find a solution to equation 2.4, it will be assumed that $f(t)$ is equal to zero, and the motion of the system is provided by some initial displacement in either x or $\dot{x}$. This assumption will remain throughout the course of this derivation. If the system is also assumed to be underdamped ($0 < \zeta < 1$), the response $x(t)$ can now be found through equation 2.5 (14):

$$x(t) = X_{max}e^{-\zeta\omega_n t}\sin(\omega_d t + \phi) \tag{2.5}$$

where X_{max} defines the maximum amplitude of the response, ϕ is the phase shift of the response, and ω_d is the damped natural frequency as defined by equation 2.6:

$$\omega_d = \omega_n\sqrt{1-\zeta^2} \tag{2.6}$$

Assuming all the parameters of the system were known, the above equations would directly identify the response of the system. However, often times, the amount of damping for any given system is not known (29). Therefore, in order to determine the response of the system, the damping value must be found experimentally. This can be done through a variety of methods, two of which include the Logarithmic Decrement Method and the Half Power Method.

2.2.1 Logarithmic Decrement Method. The Logarithmic Decrement Method is a convenient method for finding the damping of a single degree of freedom system. However, due to the technique used, it difficult to use in a multi-degree of freedom system. The basic concept applied in this method is to measure the damping of the system by the amount the peak amplitude of the response decreases after a time frame equal to an integer multiple of the period of vibration (T), where a period is

given by equation 2.7:

$$T = \frac{2\pi}{\omega_d} \tag{2.7}$$

This allows for the exponential envelope produced by the time response data to be found and in turn used to calculate ζ (14). To derive the equations necessary to calculate the ζ value, equation 2.5 will be used.

By first finding the response at time t and then dividing by the response at time $t+nT$, where n is any integer value, the decrement (r_n) is found by equation 2.8:

$$r_n = \frac{x(t)}{x(t+nT)} = \frac{Ae^{-\zeta\omega_n t}\sin(\omega_d t + \phi)}{Ae^{-\zeta\omega_n (t+nT)}\sin(\omega_d (t+nT) + \phi)} \tag{2.8}$$

With n being an integer, it can be shown that $\sin(\omega_d t + \phi) = \sin(\omega_d (t + nT) + \phi)$. Therefore, by simplifying equation 2.8, r_n is given by equation 2.9 (14):

$$r_n = e^{\zeta\omega_n nT} \tag{2.9}$$

Taking the natural logarithm of equation 2.9 and substituting equation 2.7 for T and equation 2.6 for ω_d and simplifying the fraction, the following expression is found for the per radian decrement (α):

$$\alpha = \frac{\zeta}{\sqrt{1-\zeta^2}} = \frac{1}{2\pi n}\ln r_n \tag{2.10}$$

Finally, solving equation 2.10 for ζ, the viscous damping factor of the system is found to be (14):

$$\zeta = \sqrt{\frac{\alpha^2}{1+\alpha^2}} \tag{2.11}$$

Therefore, by taking the time response data of a single degree-of-freedom system, and calculating the decrement, the viscous damping factor can be found. This method can be expanded to incorporate a multi-degree of freedom system, however,

the frequency response approach of the Half Power Method provides a much easier means of accomplishing this task.

2.2.2 Half Power Method. The Half Power Method provides a frequency domain approach to calculating the damping of either a single degree of freedom or multi degree-of-freedom system. This is accomplished by taking the frequency response function (FRF) of a particular system and find the frequencies at which the value is 3 dB less than the peak value. Given that in a multi degree-of-freedom system, each mode of the system is illustrated by a distinct peak on the plot of the FRF, the damping for each degree of freedom can be easily calculated.

In order to illustrate the process for this method, it is first necessary to convert the time domain description of the system to a system FRF, which can be found through a variety of methods. Given the system differential equation shown in equation 2.4, the FRF can be found by simply taking the Laplace transform of equation 2.4, and solving for transfer function, $\frac{X(s)}{F(s)}$. By substituting $s = j\omega$ into the transfer function, the FRF of the system is found.

A second approach for finding the system FRF is to incorporate the use of the Fourier transform. The Fourier transform is defined by equation pair shown in equations 2.12 and 2.13:

$$x(t) = \int_{-\infty}^{\infty} X(\omega) e^{i\omega t} d\omega \tag{2.12}$$

$$X(\omega) = \frac{1}{2\pi} \int_{-\infty}^{\infty} x(t) e^{i\omega t} dt \tag{2.13}$$

$X(\omega)$ is defined as the Fourier transform of the time response, $x(t)$, which is the response of the system transformed into the frequency domain. By applying the same transform to the input signal through equation 2.14:

$$F(\omega) = \frac{1}{2\pi} \int_{-\infty}^{\infty} f(t) e^{i\omega t} dt \tag{2.14}$$

Where $F(\omega)$ is the Fourier transform of the input signal, $f(t)$. The Fourier transform of the time domain response can then be related to the Fourier transform of the input signal by the relationship shown in equation 2.15:

$$X(\omega) = G(\omega)F(\omega) \tag{2.15}$$

By applying the relationship shown in equation 2.15, the system FRF, $G(\omega)$ can be found (29, 14).

While both the Laplace transform and the Fourier transform provide a method for finding the FRF of the system, both methods are limited by the information needed for the transform. In the Laplace transform, the differential equation is needed and for the Fourier transform, the time domain response function is needed. Often times, in experimental analysis, the differential equation is very difficult to accurately model, and even if an accurate model is developed, the solution to the differential equation can be equally difficult to find. In addition, both methods require either a continuous model or a continuous data stream. Due to the fact that in experimental analysis, data is collected at discrete time steps, the above methods for finding the system FRF are not valid.

2.2.2.1 Frequency Response Function Development. To account for the discrete data collected during experimental analysis, the Fourier transform shown in equations 2.12 and 2.13 can be modified. This in turn creates what is known as the discrete Fourier transform, which is simply an approximation of the continuous Fourier transform. To implement this method, the continuous time Fourier series is defined by equations 2.16, 2.17 and 2.18:

$$x(t) = a_\circ + 2\sum_{k=1}^{\infty} a_k \cos\frac{2\pi k}{T}t + b_k \sin\frac{2\pi k}{T}t \tag{2.16}$$

$$a_k = \frac{1}{T}\int_0^T x(t)\cos\frac{2\pi k}{T}tdt \tag{2.17}$$

$$b_k = \frac{1}{T}\int_0^T x(t)\sin\frac{2\pi k}{T}tdt \tag{2.18}$$

Where T is the period of the time domain response function $x(t)$. The continuous time Fourier series can then be rewritten in complex form as shown in equation 2.19:

$$X_k = a_k + ib_k = \frac{1}{T}\int_0^T x(t)e^{-i\frac{2\pi k}{T}t}dt \tag{2.19}$$

By making approximations of the coefficients defined in equation 2.19, the definition of X_k can be rewritten as shown in equation 2.20:

$$X_k = \frac{1}{T}\sum_{r=0}^{N-1} x_r e^{-i\frac{2\pi k}{T}r\Delta}\Delta \tag{2.20}$$

$$x_r = x(t = r\Delta) \tag{2.21}$$

Where Δ is defined as the sample period, N is the number of samples, and x_r is the sampled time response. Using these relationships, the period, T, can be redefined as $T = N\Delta$. By rearranging terms, equation 2.20 can be written in its final form for the discrete Fourier transform as shown in equation 2.22:

$$X_k = \frac{1}{N}\sum_{r=0}^{N-1} x_r e^{-i\frac{2\pi k}{N}r} \tag{2.22}$$

The same process can then be repeated for the input signal to give the relationship shown in equation 2.22:

$$F_k = \frac{1}{N}\sum_{r=0}^{N-1} f_r e^{-i\frac{2\pi k}{N}r} \tag{2.23}$$

Where F_k is the discrete Fourier transform of f_r given that f_r is the sampled time response of the input signal (14). Using the discrete Fourier transform of the input and the output, the power spectral densities (PSD) of the system can be defined by

the relationships shown in equations 2.24, 2.25, 2.26 and 2.27:

$$S_{ff_k} = F_k^T F_k \tag{2.24}$$

$$S_{xx_k} = X_k^T X_k \tag{2.25}$$

$$S_{fx_k} = F_k^T X_k \tag{2.26}$$

$$S_{xf_k} = X_k^T F_k \tag{2.27}$$

Where F_k^T and X_k^T are the Hermitian transposes of the F_k and X_k matrices.

With the discrete Fourier transform of the input and output defined in equations 2.22 and 2.23 and their relationships to the various system PSD functions shown in equations 2.24, 2.25, 2.26 and 2.27, the next step towards finding the system FRF is to relate the PSD functions of the system to the system FRF. The first step in this process is to define the cross-correlation between the input and the output. Equation 2.28 defines the cross-correlation for the system (14):

$$R_{xf}(\tau) = E[f(t)x(t+\tau)] \tag{2.28}$$

Where τ is some distinct step in time. In addition, based on the convolution integral, which incorporates the impulse response function $h(t)$ of the system, the relationship shown in equation 2.29 between the output and input is given:

$$x(t) = \int_{-\infty}^{\infty} h(\eta) f(t-\eta) d\eta \tag{2.29}$$

By incrementing the output one time step, τ, equation 2.29 becomes:

$$x(t+\tau) = \int_{-\infty}^{\infty} h(\eta) f(t+\tau-\eta) d\eta \tag{2.30}$$

Which can in turn be used to update equation 2.28. Thus, the cross-correlation (R_{xf}) is defined in terms of the impulse response function as shown in equation 2.31:

$$R_{xf}(\tau) = E[f(t) \int_{-\infty}^{\infty} h(\eta) f(t + \tau - \eta) d\eta] \tag{2.31}$$

Since $x(t)$ is not a function of η, equation 2.31 can be rewritten as:

$$R_{xf}(\tau) = \int_{-\infty}^{\infty} h(\eta) E[f(t) f(t + \tau - \eta)] d\eta \tag{2.32}$$

Given the definition of the cross-correlation shown in equation 2.28, the auto-correlation (R_{ff}) of the input can be similarly defined as:

$$R_{ff}(\tau) = E[f(t) f(t + \tau)] \tag{2.33}$$

Using the relationship shown in equation 2.33, the cross-correlation can be redefined in terms of the auto-correlation as shown in equation 2.34 (14):

$$R_{xf}(\tau) = \int_{-\infty}^{\infty} h(\eta) R_{ff}(\tau - \eta) d\eta \tag{2.34}$$

By definition, the FRF of a system can be defined by taking the Fourier transform of the impulse response function as shown in equation 2.35:

$$G(\omega) = \int_{-\infty}^{\infty} h(t) e^{-i\omega t} dt \tag{2.35}$$

By taking the Fourier transform of both sides of equation 2.34, and manipulating the terms, the relationship shown in equation 2.36 is found:

$$S_{fx}(\omega) = S_{ff}(\omega) \int_{-\infty}^{\infty} h(\eta) e^{-i\omega\eta} d\eta \tag{2.36}$$

By substituting in the relationship shown in equation 2.35, the definition of the system FRF is found to be:

$$G(\omega) = \frac{S_{fx}(\omega)}{S_{ff}(\omega)} = \frac{S_{xx}(\omega)}{S_{xf}(\omega)} \tag{2.37}$$

Equation 2.37 can in turn can be used in conjunction with equations 2.23, 2.24, 2.25 and 2.26 to give the final definition of the system FRF in terms of the discrete Fourier transform of both the input signal and output time response as shown in equation 2.38:

$$G(\omega) = \frac{F^T(\omega)X(\omega)}{F^T(\omega)F(\omega)} = \frac{X^T(\omega)X(\omega)}{X^T(\omega)F(\omega)} \tag{2.38}$$

These relationships hold true assuming there is no noise present within the system. If noise is present, additional terms will be seen within the relationship accounting for the PSD of the noise (14).

2.2.2.2 Damping Ratio Identification. In order to determine the damping ratio of the system using the half power method, it will be assumed that a system posses the FRF seen in equation 2.39:

$$G(s) = \frac{\omega_n^2}{s^2 + 2\zeta\omega_n s + \omega_n^2} \tag{2.39}$$

In addition, it will be assumed that the system is only lightly damped ($\zeta < \frac{1}{2\sqrt{2}}$). With the assumptions made, equation 2.39 can be evaluated over all frequencies, to give $G(j\omega)$ as:

$$G(j\omega) = \frac{\omega_n^2}{\omega_n^2 - \omega^2 + 2\zeta\omega\omega_n j} \tag{2.40}$$

By further evaluation of equation 2.40 at the point were $\omega = \omega_n$, the value of the FRF is shown to be:

$$G(j\omega_n) = \frac{1}{2\zeta j} \tag{2.41}$$

and in turn has a magnitude of:

$$|G(j\omega_n)| = \frac{1}{2\zeta} \tag{2.42}$$

Given that the system is only lightly damped, it can also be assumed that $\omega_n \cong \omega_d \cong \omega_r$ (14), where ω_d is defined by equation 2.6, and ω_r, the resonant frequency, is given by equation 2.43 to be:

$$\omega_r = \omega_n\sqrt{1-2\zeta^2} \tag{2.43}$$

thus showing that $\frac{1}{2\zeta}$ is approximately equal to the peak magnitude of the FRF at the point of resonance (14).

The frequency of the points at which the magnitude of the FRF is 3 dB less than the peak magnitude must now be found. This 3 dB drop in magnitude corresponds to a magnitude amplification of $\frac{1}{\sqrt{2}}$ times the peak value. To locate these frequencies, the terms in equation 2.40 are rearranged, and then set equal to the peak value multiplied by the magnitude amplification factor as shown in equation 2.44:

$$\frac{1}{2\sqrt{2}\zeta} = |\frac{1}{1-(\frac{\omega}{\omega_n})^2+2\zeta(\frac{\omega}{\omega_n})j}| \tag{2.44}$$

By squaring both sides of equation 2.44, manipulating the result, the following expression can be achieved:

$$(\frac{\omega}{\omega_n})^4 - 2(1-2\zeta^2)(\frac{\omega}{\omega_n})^2 + (1-8\zeta^2) = 0 \tag{2.45}$$

which in turn can be used to find the two ω values where the magnitude falls to 3 dB below the peak value (14).

To find the ω values, the roots of equation 2.45 must be found. The first step in accomplishing this task is to realize that the assumption that $\zeta < \frac{1}{2\sqrt{2}}$ is necessary

in order to ensure that the $1-8\zeta^2$ term is greater than zero, thus resulting in positive roots for the equation. It is then necessary to assume a solution of:

$$(\frac{\omega^2}{\omega_n^2} - \frac{\omega_1^2}{\omega_n^2})(\frac{\omega^2}{\omega_n^2} - \frac{\omega_2^2}{\omega_n^2}) = 0 \tag{2.46}$$

where it is also assumed for the remainder of this derivation, that $\omega_1 < \omega_n < \omega_2$. Equation 2.46 is then multiplied through to give equation 2.47:

$$(\frac{\omega}{\omega_n})^4 - (\frac{\omega_1^2 + \omega_2^2}{\omega_n^2})(\frac{\omega}{\omega_n})^2 + (\frac{\omega_1^2\omega_2^2}{\omega_n^4}) = 0 \tag{2.47}$$

and by equating the coefficients of equations 2.45 and 2.47, the following relationships are found:

$$\frac{\omega_1^2 + \omega_2^2}{\omega_n^2} = 2(1 - 2\zeta^2) \tag{2.48}$$

$$\frac{\omega_1^2\omega_2^2}{\omega_n^4} = 1 - 8\zeta^2 \tag{2.49}$$

In order to find the damping of the system using the two frequencies, ω_1 and ω_2, one additional relationship is required. By forming the equation $(\frac{\omega_2-\omega_1}{\omega_n})^2$, it can be shown that this relates to equations 2.48 and 2.49 by the relationship shown in equation 2.50:

$$(\frac{\omega_2 - \omega_1}{\omega_n})^2 = 2(1 - 2\zeta^2) - 2\sqrt{1 - 8\zeta^2} \tag{2.50}$$

Applying a binomial expansion to the relationship shown in equation 2.50 and given the fact that $2\omega_n = \omega_1 + \omega_2$, the following solution for ζ is found (14):

$$\zeta = (\frac{\omega_2 - \omega_1}{\omega_2 + \omega_1}) \tag{2.51}$$

Therefore, by first locating the peak magnitude for a given system FRF, and by then finding the corresponding ω_1 and ω_2 values for that peak, the viscous damping factor can be found. Unlike the Logarithmic Decrement Method, the Half Power

Method can then be easily applied to not only a single degree of freedom system, but also a multi-degree of freedom system by simply applying the same technique to each magnitude peak shown on the system FRF.

2.3 Summary

The concept of inflatable structures in space is one that has been in practice since the beginning phases of space exploration. This chapter outlined the evolution of inflatable space structures since the 1950's, and discussed current programs that are utilizing the advantages presented by the use of inflatable, rigidizable technology. In addition, the testing methodologies used in conjunction with inflatable structures was presented. However, despite the previous use of inflatables in space, their operational uses are limited due to the lack of validated ground testing procedures.

Also discussed in this chapter were the necessities for vibrational analysis in regards to space structures. Within this discussion of vibrational testing, the fundamentals of the logarithmic decrement and half power methods for identifying the damping ratio of a system were defined. It was then shown how the half power method could be directly applied to an experimental platform that collects discrete time response signals in order to allow the half power method to be used throughout RIGEX vibrational testing.

The next chapter will outline the details of the RIGEX ground testing process. A description of each system within RIGEX will be discussed in order to show the modifications that were made to the preliminary design of the experiment. The procedures used for testing all aspects of the experiment will then be described.

III. Experimental Methodology

3.1 Overview

The dynamics of structures in space due to the lack of gravity provide unique challenges to experiment designers. Due to the high cost of conducting space missions, an improper design could risk millions of dollars if the experiment fails to operate nominally. Therefore, accurate testing of the experiment prior to launch is essential. In order to accurately test space experiments, ground tests must be correlated to space flight results so that the behavior of various structures can be accounted for. RIGEX testing will accomplish this task through ground tests in both ambient and vacuum conditions, and will then be completed with the space flight test of the experiment. Upon completion, data from all tests will be compiled and analyzed.

The goal of RIGEX testing is two fold. First, a test structure was built that simulates one inflatable, rigidizable tube assembly in order to test the deployment and rigidization of the tube. This was done by following the draft specifications outlined in the preliminary design of RIGEX. By maintaining these specifications, all tests simulated the actual flight configuration. This will allow the correlation of the results upon completion of the RIGEX space flight.

The second task was to determine the natural frequencies and viscous damping ratios of the tube. In order to obtain frequency response functions for the tube, an input excitation force was applied to the tube by piezoelectric transducers, and an output signal was generated by a single axis accelerometer. By varying the boundary conditions of the tube, data was collected showing how the frequencies and damping varied throughout each test. By compiling this data, an approximation can be made as to how the values will change once RIGEX is on orbit.

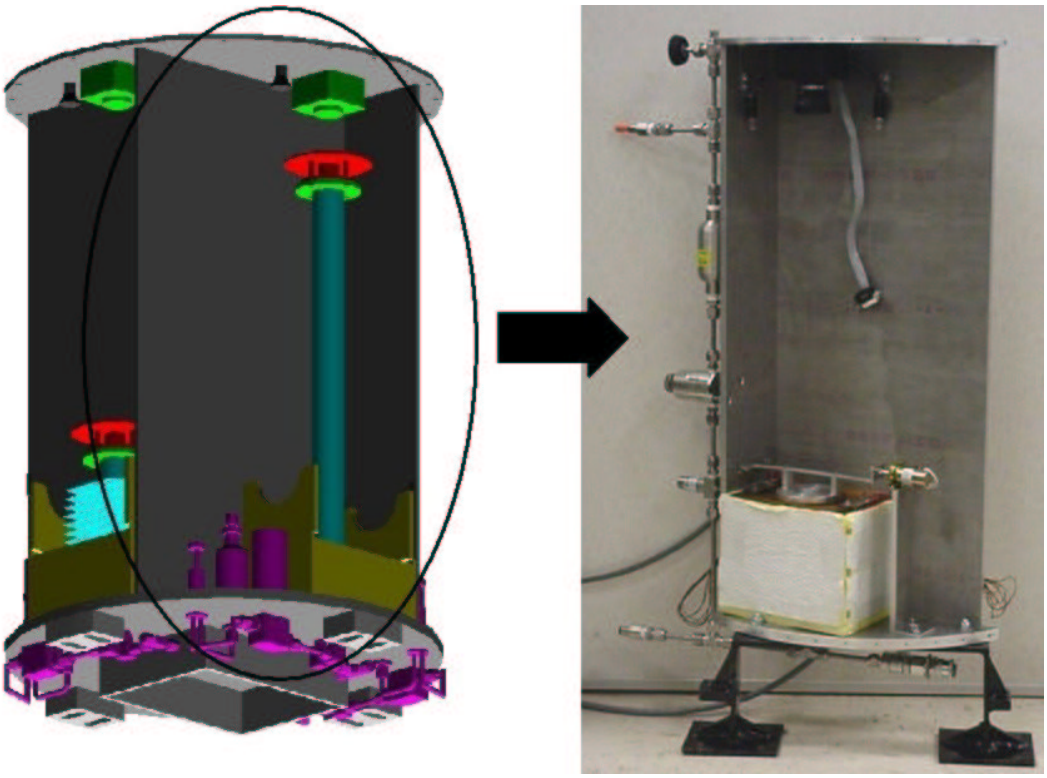

Figure 3.1 Test Structure Assembly

3.2 Experiment Assembly

In order to accomplish the necessary testing in an environment that would simulate the RIGEX flight configuration, a testing unit was built to the specifications outlined in the preliminary design. In the course of fabricating the test unit, several modifications to the original design were needed in order to accomplish the mission. The following sections define the assembly and components used in fabricating the test unit.

3.2.1 Test Structure. As stated in Section 1.5, a limiting factor to ground testing was the size the vacuum tank opening. Given that the opening has a diameter of only eighteen inches, a one quarter bay model of the preliminary design structure was designed for use as the RIGEX test structure. The test structure included one inflatable, rigidizable tube assembly, and is shown in Figure 3.1.

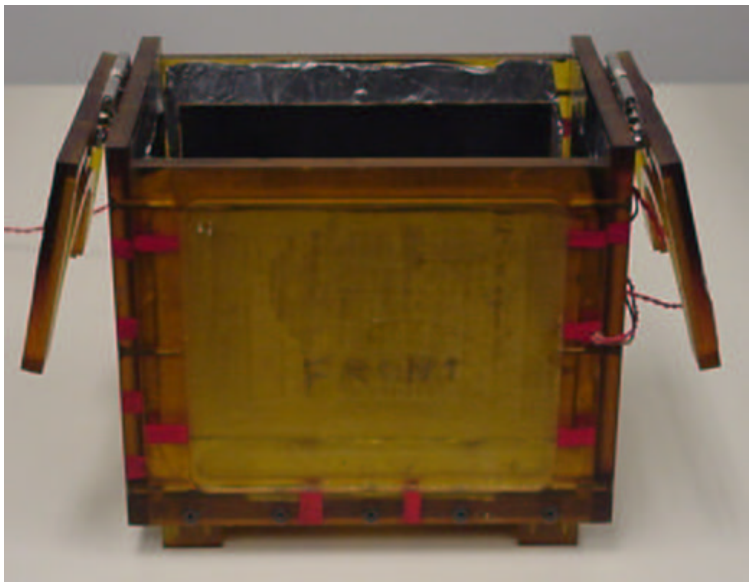

Figure 3.2 Modified Heater Box

The structure stood 26.25 inches tall, and the top and bottom plate each have a radius of curvature equal to that of a circle with a diameter of 19.75 inches. This yields a maximum width of 12.0625 inches and a maximum depth of 5.625 inches, thus enabling the structure to be placed inside the vacuum tank. The two plates used for the walls along with the top plate are made from 0.25 inch thick aluminum while the bottom plate is made from 0.5 inch thick aluminum.

Additionally, for the purposes of this experiment the structure was assembled by screwing the plates together, which differs slightly from the preliminary design which calls for the structure to be welded. The reason for this modification was to enable disassembly of the structure in order to mount various components as necessary to conduct the experiment.

3.2.2 Heater Box. As determined by previous testing, modifications were made to the preliminary design of the RIGEX heater box. As shown in Figure 3.2, the dimensions of the box were changed to 6 inches wide by 4.25 inches deep by 5 inches tall, in order to allow better heat transfer to the tube. The heater box

is made from a 0.25 inch thick Ultem 1000, PEI, Polyetherimide material (8), and the interior of the box was coated with aluminum in order to increase the surface reflectivity within the box. The heaters used to provide heat to the box are a foil backed heater produced by Minco Products, Inc. (1), and in order to increase the surface emissivity of the heaters, a coat of flat black paint was applied to each (26).

In addition, previous testing determined that in order to achieve the desired T_g temperature of $125°C$, the box needed to be insulated (26). In order to meet this requirement, additional supports were added to the bottom of the box. These supports were constructed from the same material as the box, and measured 0.5 inches tall. This allowed for 0.5 inches of insulation between the bottom plate of the structure and the box, and by positioning the box away from the side walls of the structure, 0.375 inches of insulation was placed on the sides of the box while 0.25 inches was attached to the front and back. The thickness of the applied insulation was based solely on the available space and necessary position of the box within the test structure. No insulation was attached to the top of the box due to the fact that this would inhibit the ability of the latch and doors to operate properly. In addition, by applying the insulation, the total heat loss of the heater box was reduced from $194.2917W$ to $59.9712W$ as shown by the calculations in Appendix C.

The final modification to the heater box was the latch assembly. The original design called for a latch to be placed on each side of the box's two doors. This however, proved to be unfeasible due to the changes in the box dimensions. Therefore, the latch assembly shown in Figure 3.3 was designed.

The latch is composed of aluminum and is connected to the structure wall by a spring loaded hinge. The latch is held closed by a magnetic solenoid valve, manufactured by Guardian Electric Manufacturing Co., that when activated retracts a pin and releases the latch and thus allowing the doors of the heater box to open. For the flight model, the P5-403-9RS pin-puller, manufactured by TiNi Aerospace,

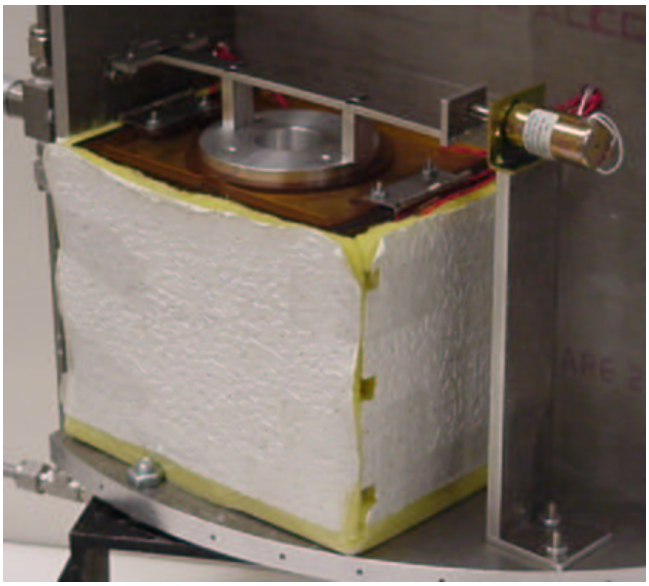

Figure 3.3 Heater Box Latch Assembly

Inc. was chosen (9). However, due to time constraints and the availability of the device, the flight model pin-puller was not used for testing.

3.2.3 Inflation System. The inflation system complies with the preliminary design with the only exception being the mounting position. As shown in Figure 3.4, the inflation system is currently mounted to the side panel of the test structure rather than the bottom plate as specified in the preliminary design. This modification is a result of limited mounting space under the bottom plate due to the fact that only a one quarter section of the complete structure was used for testing. In addition, the mounting of the latch stand used to support the latch solenoid valve limited the ability to mount the inflation system according to the preliminary design.

The inflation system begins with a hand operated valve (A) that is in turn connected to the gas cylinder (B) that is capable of holding the required 347 psia of pressure outlined in the preliminary design (17). The gas cylinder is then connected to the pressure regulator (C). The regulator used is a CPR-1 Series compact stainless steel pressure reducing regulator that is manufactured by GO Regulator, Inc., and

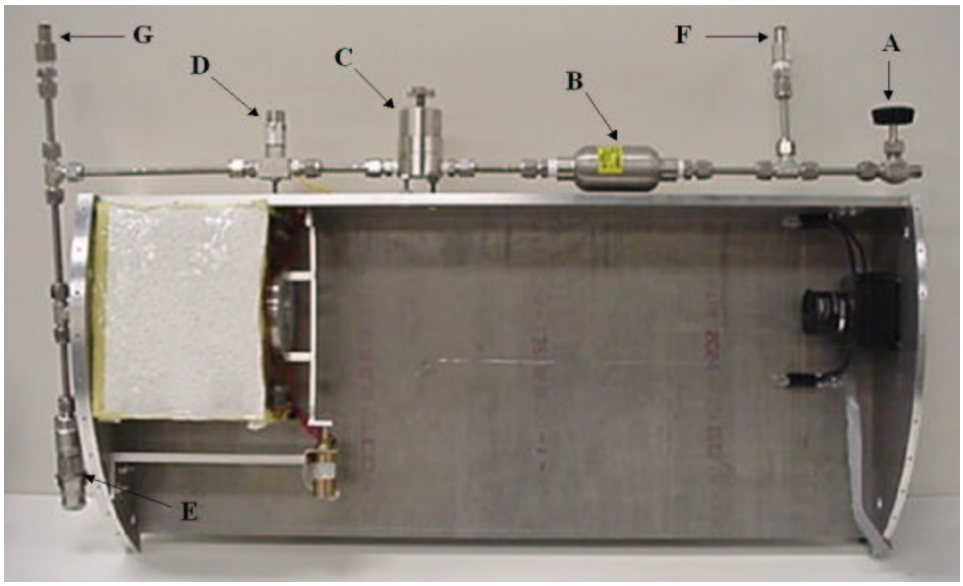

Figure 3.4 Inflation System

is capable of maintaining an outlet pressure of 0 to 10 psig (7). This meets the preliminary design requirement of being capable of regulating the pressure to 4 psia once in vacuum.

Once the gas flows through the pressure reducing regulator, it is then connected to a solenoid valve (D) that is closed until power is provided. The solenoid valve is a Series 9 high performance valve that is manufactured by the Parker Hannifin Corporation (4). From the solenoid valve, the flow of gas has two paths. The first of which connect to the base of the heater box to provide the inflation gas to the tube. This is done by screwing the connection into the base of the box and an o-ring then provides a seal between the base of the box and the bottom end flange of the tube, thus preventing gas leakage. The second path taken connects to an RL4 series pressure relief valve (E) produced by the Parker Hannifin Corporation that prevents the over pressurization of the tube (4).

The inflation system also includes two pressure sensors. These are located just prior to the gas cylinder and just after the solenoid valve. The first pressure sensor (F) is a 500 psig sensor. This enables the gas cylinder to be properly charged with

the required gas needed for the tube inflation. The second pressure sensor (G) is a 15 psig sensor that measures the pressure in the tube itself. This allows the pressure regulator and the pressure relief valve to be set prior to testing in order to ensure the tube is properly inflated. The complete layout of the inflation system is shown in Figure 3.5.

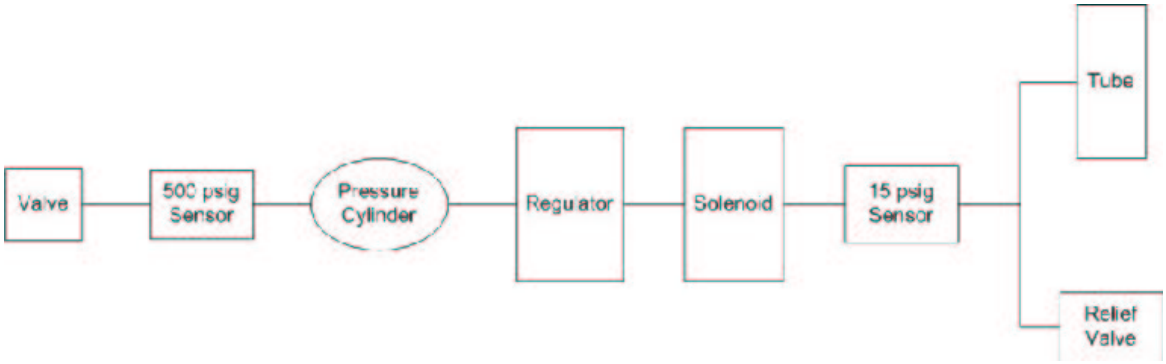

Figure 3.5 Inflation System Schematic

3.2.4 Digital Imaging System. The digital imaging system is composed of two components. The first is a digital camera manufactured by the ELECTRIM Corporation (3). The camera allows the testing within the vacuum chamber to be monitored as well as is used as a tool to determine the accuracy of the deployment during the space flight. The camera was mounted to the top plate of the test structure and was positioned so that the top end flange of the tube prior to deployment was the center of the image.

The second component present in the digital imaging system is a basic background lighting system. The lighting system is composed of a two simple mini-bayonet base fixtures mounted to the side and back walls of the test structure slightly lower than the camera lens as to not impart any shadows on the image. Each fixture is powered by a 24 volt source, and uses standard incandescent light bulbs. In both the ground tests, when tests are conducted within the vacuum tank, and during the actual space flight, when the GAS can is sealed, no ambient light will be present

Figure 3.6 Digital Imaging System

to enable the camera to capture images. Therefore, by providing light to the experiment, the capability is given to take digital images throughout both the ground testing and space flight. Figure 3.6 shows the digital imaging system mounted to the RIGEX test structure.

3.3 Test Setup and Procedures

To accomplish the RIGEX ground tests, testing was divided into two components, deployment testing and vibrational testing. Each of these components provided vital knowledge necessary to the successful correlation of the RIGEX ground test data to actual space flight results. A variety of aspects were analyzed throughout each component of the ground tests in an effort to determine first and foremost, is the inflation and rigidization of a tube possible, and if so, how does the tube respond within earth's gravitational environment.

The two components of testing incorporated first a tube deployment test to determine the feasibility of the RIGEX mission, and second a series of vibrational tests that allowed the response of the tube to be analyzed given various boundary conditions. Each testing component was designed to accomplish a specific task, that could in turn be compiled to form the basis for the ground test data necessary to

accomplish the RIGEX mission. In order to accomplish this task, ground testing procedures were developed that would most accurately model actual flight test procedures. Table 3.1 outlines the procedures used in the deployment of the inflatable, rigidizable tube.

Table 3.1 Deployment Testing Procedures

Step	Description	Condition
1	Turn on digital camera	
2	Activate camera lights	
3	Adjust camera settings	Exposure = 15 ms, Gain = 235, Bias = 120
4	Initiate $LabVIEW^{TM}$ Program	Use default settings specified
5	Activate heater box heaters	
6	Begin digital image capture	
7	Release latch	Tube Temperature $\geq 125°C$
8	Initiate inflation	Activate the inflation system solenoid
9	Deactivate heater box heaters	
10	Vent inflation gas	Tube Temperature $\leq 100°C$
11	Cease digital image capture	
12	Test complete	$LabVIEW^{TM}$ program completed data collection

3.3.1 Deployment Testing. A variety of tasks are involved with the deployment of the inflatable, rigidizable tube. Each component of the experiment must first be tested individually prior to the actual deployment test. The various components within the experiment include the inflation system, heater box, latch system, and digital imaging system. Due to the experimental nature of RIGEX, a failure of any one system could cause failure for the mission, hence the necessity for a thorough testing process.

3.3.1.1 Experiment Configuration. The primary task in configuring the experiment was to supply power to the various systems. Once power was applied to the system, the various sensors needed to collect the data necessary to accomplish the ground testing portion of the RIGEX mission were configured. These sensors

were used to collect the vast amount of data needed to validate the system, and once configured, each system within RIGEX could be accurately tested.

Power was necessary to operate various components within each of the RIGEX systems. The preliminary design of the RIGEX power system provided a single 30 volt source. Due to the availability of various components, given the requirement that all must operate on the same voltage, the 30 volt source was modified, and only a 24 volt source was used. This allowed tests to model actual single voltage flight conditions. The various components requiring power include the heaters within the heater box, the solenoid valve used to release the latch on the heater box, the solenoid valve within the inflation system, and the lights within the digital imaging system. All power was connected to each component through connection plates located on the wall of the vacuum tank as shown in Figure 3.7. Additionally, for the actual flight design, the experiment computer, digital camera, and various sensors and actuators will also require power. However, for the purposes of the current ground tests, power is supplied to these components independent of the RIGEX power system.

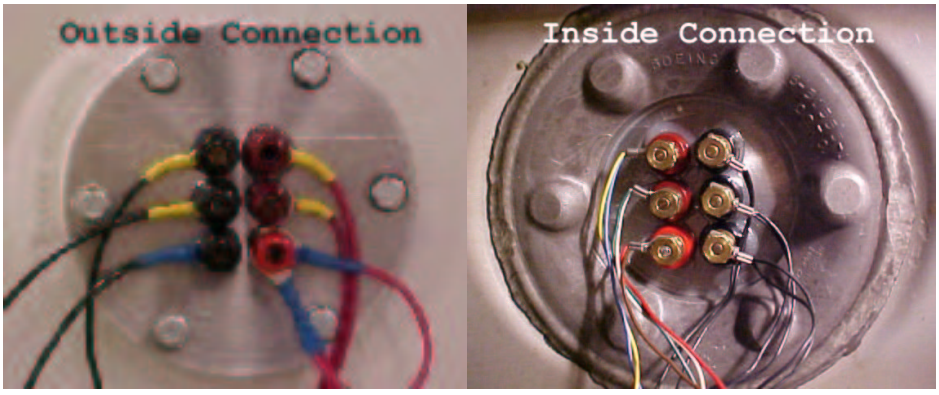

Figure 3.7 Vacuum Tank Power Connections

In addition, each component requiring power was connected to a dedicated 24 volt power supply with the heaters within the heater box being viewed as one component. The reason each component was connected to a separate power source is due to the fact that during testing, power is supplied to each component at various times

Table 3.2 Heater Descriptions

Heater Location	Number	Resistance (Ω)
Top Left	1	9.5
Top Right	2	9.5
Bottom Left	3	9.5
Bottom Right	4	9.5
Left Side	5	27.3
Right Side	6	27.3
Front	7	11.3
Back	8	11.3

as necessary to accomplish the test. By connecting each component to a dedicated power source, the capability to supply power to each component individually is provided. Each dedicated power source maintained the required 24 volts thus meeting the testing objective of supplying only a single voltage. The ability to supply power to each component individually during the space flight will be accomplished through the proper design of the experiment circuitry and flight software.

The heaters within the heater box were configured into three separate circuits as shown in Figure 3.8. By powering the heaters in three separate circuits the output power was maximized for the heaters that contributed the most to heating the tube (26). Table 3.2 defines the numbering used for the eight heaters along with the corresponding resistance values for each. The first of the three circuits incorporated the heaters one and two connected in series and in turn connected in parallel to heaters three and four which were also connected in series. The second circuit included heaters five and six connected in parallel with one another. The final circuit incorporated heaters seven and eight connected in series with one another. Each of the three circuits were connected to one 24 volt power supply in order to provide identical power to each circuit.

The final step in configuring the power to the experiment was to verify that the accurate power was being carried through each connection. The was done by simply

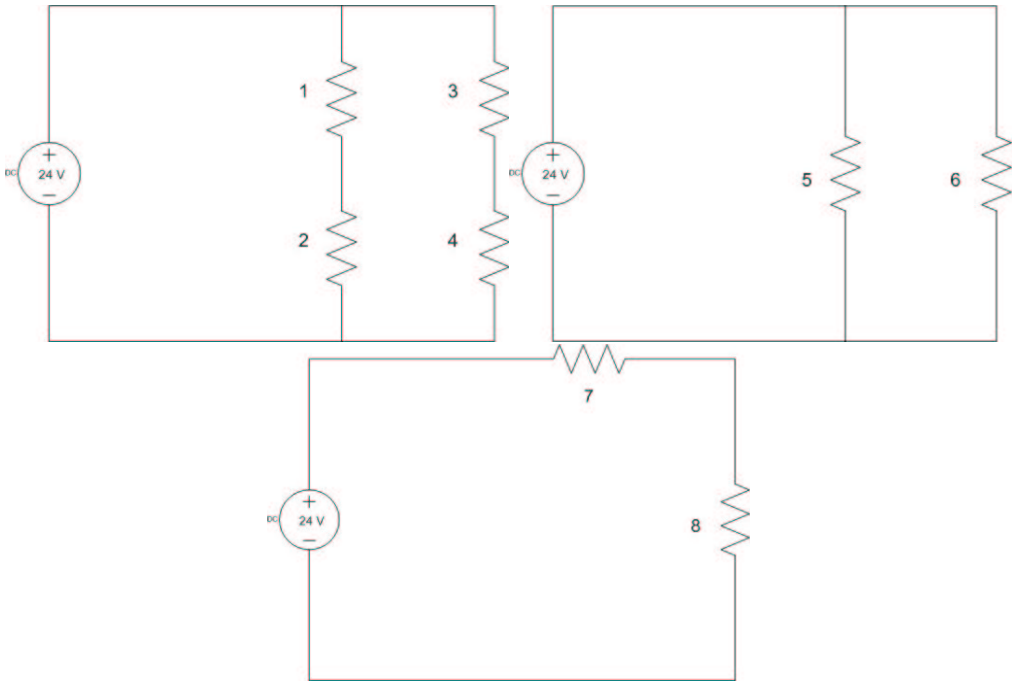

Figure 3.8 Heater Circuits

applying the power to the systems and using a standard voltmeter, all connections were checked to ensure that each maintained a power of 24 volts. Connections that were checked included the actual power supply to ensure that the initial settings were accurate, and then both the connections inside and outside of the vacuum tank were verified to be working properly.

Once the experiment power was configured, the inflation system was configured and tested. Due to the fact that Nitrogen gas (N_2) is to be used on the flight experiment for inflation, N_2 was used for all tests and calibrations in order to maintain continuity between the ground tests and flight experiment. The first step in the configuration process was to set the pressure relief valve to allow a maximum of 10 psig inflation pressure. This was done by connecting the inflation system to a N_2 source that was set to maintain a constant 320 psig. This pressure was an increase over the preliminary design calculation requiring 250 psig. The change was made in order to account for any unnoticed leaks that may be present within the

tube or inflation system and thus ensuring that adequate pressure is maintained until rigidization occurs. The level of increase over the preliminary design was based solely on the maximum pressure capable from the given N_2 source without exceeding the maximum capability of the inflation system components. This would allow the maximum amount of gas to be present within the inflation system once testing began, which would in turn allow the maximum compensation for any leaks that may arise during testing.

With the 320 psig source connected, a previously inflated tube was mounted and connected to the inflation system in order to simulate the accurate volume that would be inflated. With these steps accomplished, the inflation system regulator was opened until a pressure of 10.5 psig was reached. The pressure relief valve was then slowly opened until pressure started to bleed off and settle at 10 psig. The inflation gas was then vented and applied once again to test the functionality of the relief valve.

With the relief valve set, the regulator was then set to maintain a 4 psig pressure within the tube. This task was accomplished by first closing off the inflation system regulator. The inflation gas was then applied, and the regulator was slowly opened until the pressure within the inflatable tube stabilized at 4 psig. The inflation gas was then vented and reapplied in order to test the functionality of the regulator.

The final system to test was the digital imaging system. In order to verify that the digital imaging system functioned properly, the first task was to ensure that the lights were operational. By connecting the lights to the designated power supply and applying power, the functionality of the lights were easily determined. The focus and iris of the digital camera then needed to be set by physically setting the adjustments located on the lens of the camera in order to ensure that images could be collected throughout the tests. This was done by first mounting an inflated tube to the structure and adjusting the focus of the camera. Once the focus was adjusted, the structure was placed in the dark, and with the lights of the digital

imaging system powered on, the iris was adjusted. With these two features set, the inflated tube was removed and a folded tube was mounted to the structure. This allowed verification that images could be collected both prior to inflation and after inflation had occurred. No modifications were made though based on the clarity of the images collected with the folded tube. This is due to the fact that the more important image is that of the inflated tube given that this will tell the accuracy of the deployment.

The next step in the experiment configuration was to ensure data collection methods were in place for the tests. The data necessary for the RIGEX ground tests included pressure readings which were used to determine the functionality of the inflation system and the presence of leaks within the tube itself along with temperature data in order to determine the functionality and effectiveness of the heater box along with giving a method for monitoring the tube to determine when the T_g temperature was reached thus enabling deployment of the tube. To monitor pressure values, a 500 psig pressure transducer was connected to the inflation system just prior to the gas pressure cylinder in order to monitor in the cylinder pressure throughout the experiment, while a 15 psig pressure transducer was connected to the inflation system just prior to the inflatable tube connection in order to monitor the pressure within the tube. To monitor the temperature of the heaters and the tube, six K-type thermocouples were connected directly to the heaters while two K-type thermocouples were connected directly to the tube. Figure 3.9 shows the connection of the thermocouples through the vacuum tank.

In order to capture the data and enable various charts of the data to be reproduced, a $LabVIEW^{TM}$ program was created that monitored all pressure and temperature sensor data. Each thermocouple was connected to a specific channel that in turn relayed the data to the computer. The channels assigned to each thermocouple are outlined in Table 3.3. Each pressure transducer produced a voltage that was sent directly to a multimeter. The multimeter then relayed the voltage

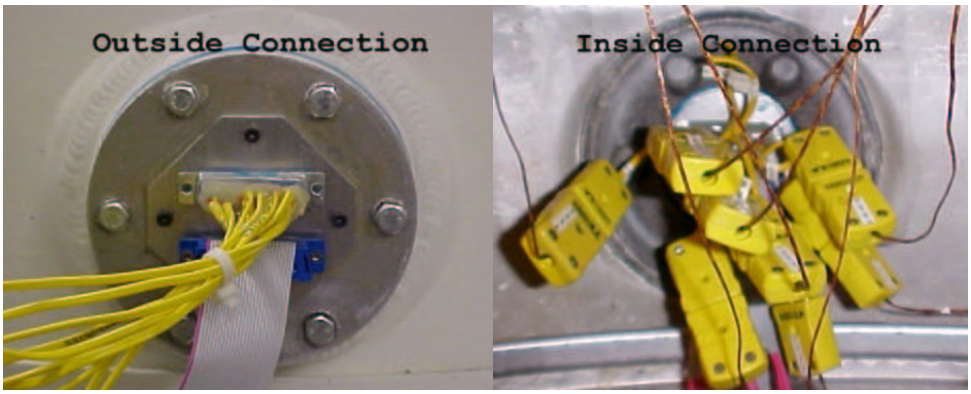

Figure 3.9 Vacuum Tank Thermocouple Connections

to the computer where the $LabVIEW^{TM}$ program converted the voltage signal to a pressure reading. With all connections made, the $LabVIEW^{TM}$ program, once initiated, collected data for a set run time and wrote data to a data file every five seconds (26). This program allowed all data to be monitored in real time thus allowing modifications to be made if need be throughout the test, along with preserving all data from the test for future analysis.

Table 3.3 Temperature Measurement Channels

Thermocouple Channel	Temperature Monitored
0	Heater 7
1	Heater 8
2	Heater 5
3	Heater 6
4	Heater 1
5	Heater 3
6	Inflatable Tube
7	Inflatable Tube

The final task to complete prior to testing was to configure the experiment inside the vacuum tank. This was done by first mounting the test structure inside the tank, and connecting the power to the experiment through the connections shown previously in Figure 3.7. With power connected to the experiment, the thermocouples were then connected as previously shown in Figure 3.9. The final step was then

to charge the inflation system with the N_2 gas, and seal the vacuum tank. Upon the completion of these tasks, the experiment was ready for testing.

3.3.1.2 Deployment Procedures. The deployment process for the initial ground test of RIGEX occurred in two phases. Phase one was conducted using a purely inflatable tube while phase two incorporated the testing of the inflatable, rigidizable tube. The purpose behind dividing the testing into two separate phases allowed for phase one to give initial estimates on how the tube would deploy in order to optimize the testing procedures during phase two so that a successful deployment would be achieved. The difference between the two phases included the fact that phase one testing used air as the inflation gas while phase two modelled the flight design and used N_2 to inflate the tube. An additional difference was that all phase one testing was conducted in ambient conditions rather than incorporating the use of the vacuum tank, while all phase two testing was conducted in vacuum conditions.

The primary goal of phase one testing was to first determine what orientation the structure should be mounted in so that a full deployment could be achieved, and through various deployment tests, the deployment time would also be found. All testing throughout this phase was conducted using a purely inflatable tube, which unlike the tubes used for the actual RIGEX mission, the purely inflatable tube is highly flexible at all times. This allows multiple tests of only the deployment to be conducted without the necessity for heating and refolding the tube.

The goal of phase one testing was accomplished through the use of two test configurations, one with the test structure mounted in the upright position and the second with the test structure mounted in the inverted position. The upright position is defined as the orientation of the structure with the bottom plate being that which the heater box is mounted and the top plate being that which the camera is mounted. The inverted position is defined as the opposite of the upright position. Tests were conducted in the upright configuration first, and then in the inverted configuration.

The steps taken to inflate the tube during both configurations of phase one testing were to:

1. Apply inflation gas to inflation system through an air compressor.
2. Release the latch by activating the latch solenoid.
3. Initiate inflation by activating the inflation system solenoid.
4. Deactivate the latch solenoid to prevent damage to the component.
5. Once the tube is deployed deactivate the inflation system solenoid.

Based on the results of phase one testing, the test structure would be mounted inside the vacuum tank in the desired orientation. Once the experiment was fully connected inside the tank, and the vacuum tank was sealed, phase two testing could commence. Phase two testing was designed to simulate the space flight, and therefore would follow the procedures outlined in Table 3.1.

Upon completion of the deployment test, the test structure was removed from the vacuum tank and the accuracy of the tube deployment was analyzed. In addition, the data collected by the $LabVIEW^{TM}$ program was used to form various charts that could later be used to modify the deployment procedures if need be to conserve power within the experiment.

3.3.2 Vibrational Testing. The purpose behind the vibrational testing of RIGEX was two fold. The first priority of testing was to determine the natural frequencies and the damping ratios of the inflatable rigidizable tube. Once this task was accomplished for the tube, the mounting structure for the tube was varied in order to change the boundary conditions of the test. Given that the primary goal of RIGEX is to correlate ground tests to actual space flight results, the variation in boundary conditions enables a pattern to be developed that will allow correlations to be made between the various tests thus being able to predict how the tube will respond once on orbit.

3.3.2.1 Testing Equipment. A variety of equipment was used in conducting the vibrational tests for RIGEX. Vibrational testing was conducted using two basic equipment configurations, which allowed the results of each test to be validated through the comparisons made between the two data collection methods. Both methods were very similar in concept, however the first incorporated only a single point of data collection while the second allowed for multiple data points thus enabling the actual mode shapes of the tube to be found along with the natural frequencies and damping ratios. However, while on orbit, RIGEX will only be capable of collecting data from a single point. Therefore, to provide ground test results that can be compared to space flight results, all final conclusions will be based only on data collected using the single data collection point.

The first test equipment configuration used a personal computer (PC) running Windows 98 operating system along with the Data Physics Corporation's *SignalCalc 620* software package to control the testing. A transfer function test was selected to run within *SignalCalc 620*, and in turn was used to drive the Hewlett Packard (HP) VXI Plug and Play system. The HP system incorporates eight separate channels that can be used to monitor various signals. For the purposes of this test, only channels one and two were used. Channel one was identified as the reference or driving signal while channel two measured the tube's response signal.

In order to monitor the response of the tube, a single axis accelerometer was attached to the top end flange of the tube and then connected to a power amplifier which was in turn connected to the HP system. In order to provide the excitation force needed to create the vibrations within the tube, two PZT's, manufactured by LaRC, were attached to the tube near the base. Figure 3.10 shows the LaRC PZT as well as the PZT attached to the inflatable, rigidizable tube. The PZT's were then connected to a dedicated power supply and in turn connected to channel one of the HP system.

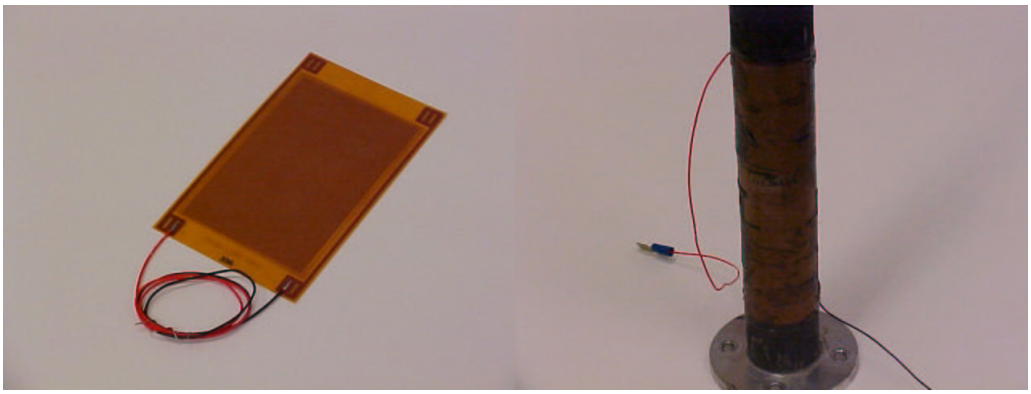

Figure 3.10 Piezoelectric Transducers

Figure 3.11 shows a block diagram of the HP system used throughout vibrational testing. However, this configuration was used only for testing, and differs slightly from the flight configuration, where a complete HP system will not be flown. Therefore, for the actual flight configuration, the HP VXI System block and the PC block will be replaced by the flight computer. All data processing procedures accomplished within the HP system will be programmed into the flight software. If programming capability does not allow for all functions to be accomplished, some post flight data processing will be necessary.

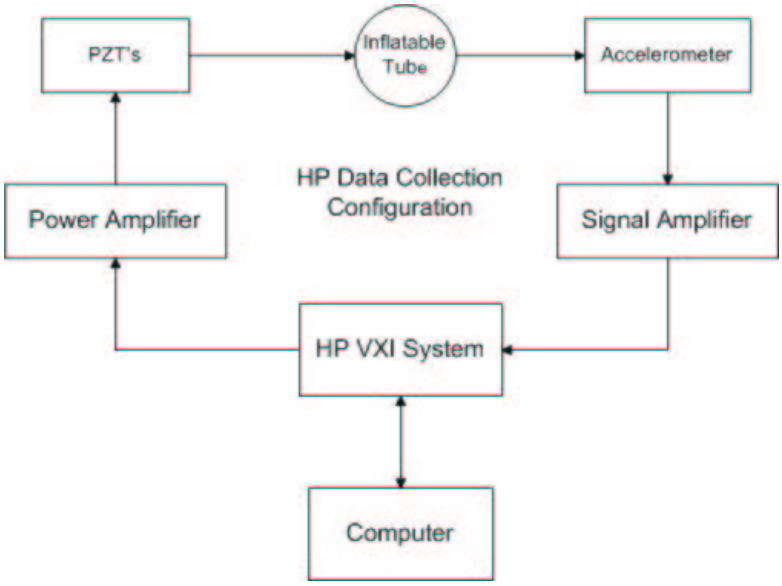

Figure 3.11 HP Data Collection Configuration Block Diagram

The second test equipment configuration used was very similar to the first. The data collection was achieved throughout this method through the use of the Polytec Scanning Vibrometer 300 (PSV). Using the laser vibrometer rather than the single axis accelerometer allowed for multiple data points to be collected thus enabling the actual mode shapes of the tube to be determined. The PSV signal was connected to the driving PC in the same manner as the accelerometer. One difference between the HP system and the PSV is that the PSV system measures the velocity of each scan point as opposed to acceleration measurements in the HP configuration. However, this difference in measurements will not affect the results given that natural frequencies of the system will remain the same. Therefore, the PSV was connected to the velocity input channel while channel one of the PSV system was identified as the reference or driving signal. The configuration of the tube was identical in this method of testing with the exception that no accelerometer was attached to the tube. The PZT's remained on the tube and connected to the power supply which was in turn connected to channel one on the PSV system. A block diagram of the PSV data collection configuration is shown in Figure 3.12.

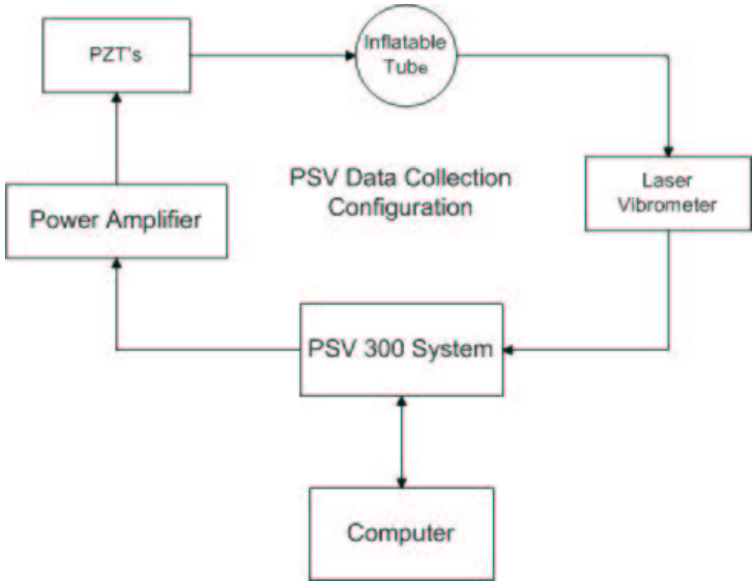

Figure 3.12 PSV Data Collection Configuration Block Diagram

3.3.2.2 Testing Configurations. The RIGEX vibrational testing was conducted with four separate testing configurations in order to allow first a baseline to be set for the ω_n and ζ values and then to provide variations to that baseline in order to determine a pattern associated with modifying the boundary conditions for the tube. In addition, three of the four testing configurations were testing using both equipment configurations in order to provide a means for validating the results. Table 3.4 outlines the various testing configurations used.

Table 3.4 Vibrations Testing Configurations

Test Configuration	**Description**
1a	Table mounted using HP system
1b	Table mounted using PSV system
2a	Stand mounted using HP system
2b	Stand mounted using PSV system
3a	Structure mounted on stand using HP system
3b	Structure mounted on stand using PSV system
4	Structure mounted in vacuum tank using HP system

For each test configuration, the table mounted scenario refers to the tube mounted firmly to a vibration isolation table for the test. This provides a rigid cantilever support in order to compare how the response of the tube compares to that of a standard cantilever beam. The configuration where the tube is described as being stand mounted refers to the tube being mounted onto a metal test stand which is in turn mounted firmly to the table. The test stand provides separation between the tube and the table thus creating a less rigid base. Figure 3.13 shows the inflatable, rigidizable tube mounted firmly to the table and to the test stand as in configurations 1a and 2a.

As stated in Table 3.4, test configuration 2b is identical to 2a except for the use of the laser vibrometer as opposed to the accelerometer. Figure 3.14 shows the setup used for configuration 2b, along with the PC that supports the PSV system and the laser vibrometer used in testing.

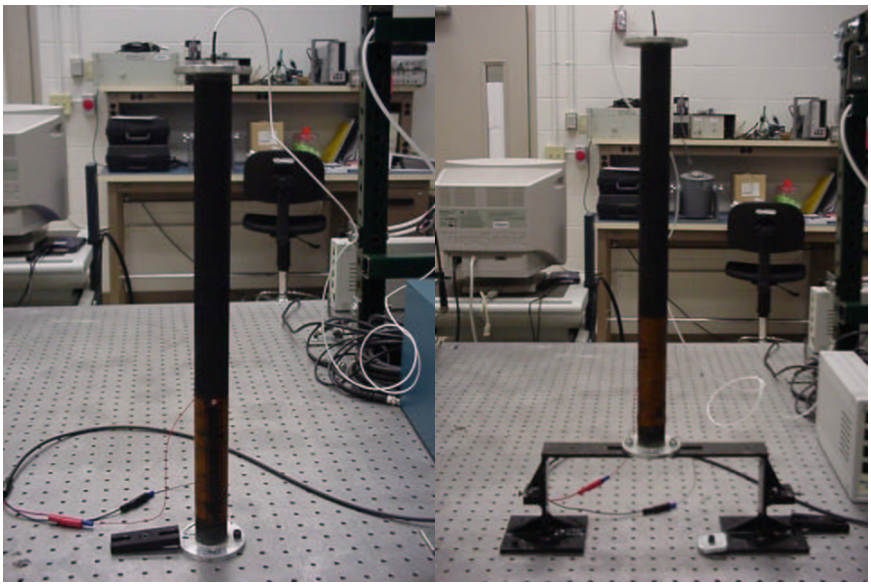

Figure 3.13 Vibrations Test Configurations 1a and 2a

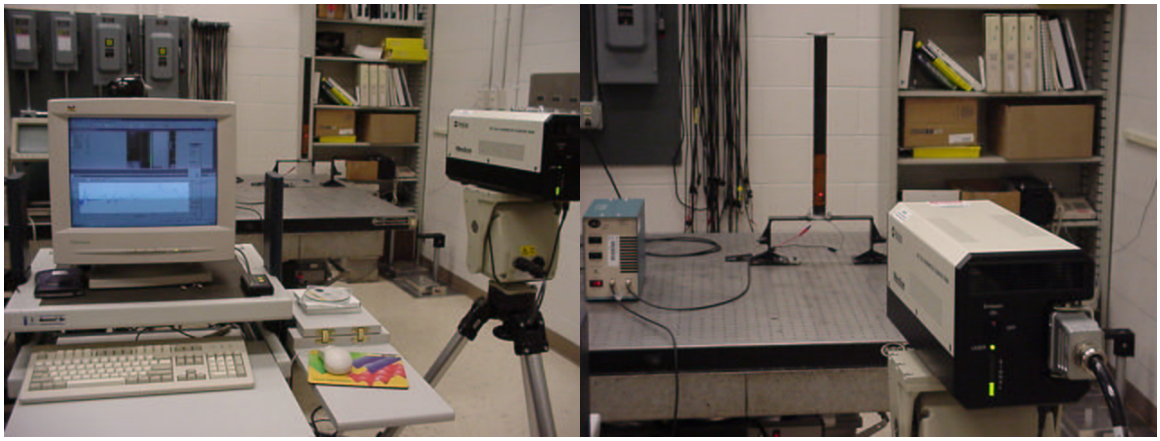

Figure 3.14 Vibrations Test Configuration 2b

The structure mounted configuration refers to the tube being mounted firmly to the RIGEX test structure which is turn mounted to the test stand, which is then mounted firmly to the table. The reason the test stand is used for this test rather than simply mounting the test structure to the table is due to the fact that part of the RIGEX inflation system lies on the bottom side of the test structure base plate, thus prohibiting the structure to be mounted directly to the table. The test stand allows clearance for the inflation system thus enabling the tube to be tested as part of the RIGEX test structure in order to provide a baseline for how mounting the tube within the test structure affects the vibrational properties. Figure 3.15 shows the inflatable, rigidizable tube mounted on the RIGEX test structure in configurations 3a and 3b.

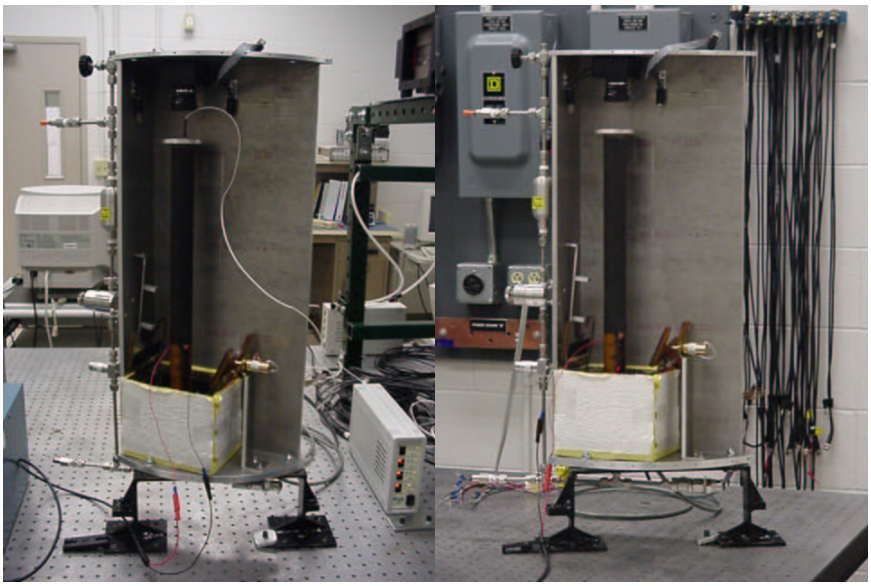

Figure 3.15 Vibrations Test Configurations 3a and 3b

The final test configuration most accurately models the flight configuration in that when mounted inside the GAS canister, RIGEX will be firmly supported in the upright configuration by connecting the top plate of the structure to the top of the GAS canister. Therefore, by mounting the RIGEX test structure in the upright configuration to a support structure within the vacuum tank, vibrational tests

can be conducted in the most accurate manner, simulating the flight configuration. Figure 3.16 shows configuration 4 of the RIGEX vibrations testing.

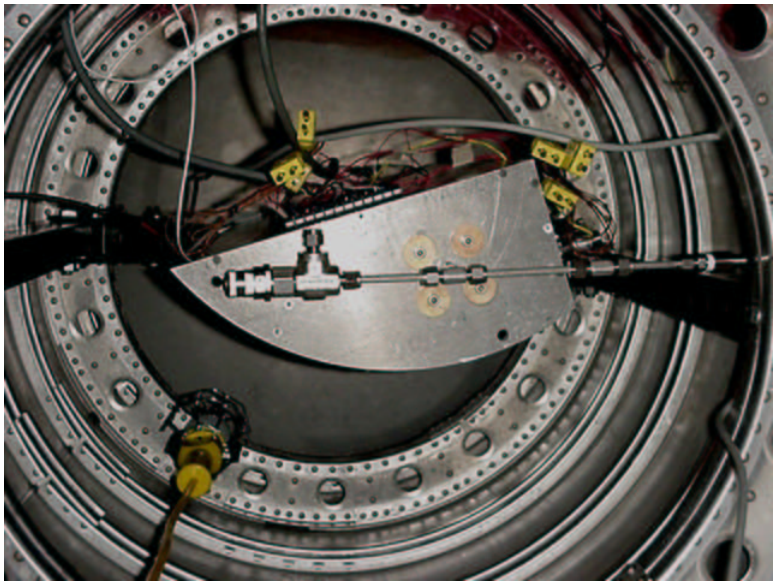

Figure 3.16 Vibrations Test Configuration 4

The final parameter within the testing configurations that must be defined is the choice scan pattern to be used by the PSV system. Test configurations 1b, 2b, and 3b as specified in Table 3.4 use the grid scan pattern. The purpose for the scan patterns is to provide multiple scan points on the tube in order to verify the true bending modes. When a grid pattern is used, both bending and torsional modes can be detected. This provides an accurate representation of how the tube is responding, however for the purposes of this research, only the bending modes are analyzed.

With the various testing configurations defined, the computer systems could be configured for each test. The system parameters for both computer systems were held constant throughout all tests in that, when possible, identical parameters were used for both the HP and the PSV system, and throughout all test configurations, the parameters for each system remained unchanged. This ensured continuity between tests was maintained, thus allowing comparisons to be made between the results obtained from various test configurations, and through both the accelerometer and

the PSV collection methods. Table 3.5 defines the system parameters that were used for each computer system.

Table 3.5 Computer System Test Parameters

HP System	
Parameter	**Setting**
Input Signal	Random
Input Signal Magnitude	5
Frequency Span	1000 Hz
Block Size	8192
Number of Averages	20
Percent Overlap	50
PSV System	
Parameter	**Setting**
Input Signal	Periodic Chirp
Input Signal Magnitude	2
Frequency Span	1000 Hz
Number of Spectral Lines	3200
X Density	40
Y Density	18

As Table 3.5 shows, a few slight differences are seen in the system parameter settings for each computer system. One difference is seen in that the HP system is given a block size specification while the PSV system is given a set number of spectral lines. These two values can be linked together through Equation 3.1:

$$BlockSize = 2.56 \times (Number of Spectral Lines) \tag{3.1}$$

Thus, given that the block size used for the PSV system is equal to the block size of 8192 used in the HP system. One additional difference is shown in that for the HP system a random input signal with magnitude of 5 is used as opposed to the periodic chirp signal with magnitude of 2 that was used in the PSV system. The reason for this variation is due to the cleanliness of the FRF that was produced by each system.

The HP system, given the additional parameters, produced a very clean FRF using a random input, however, the PSV system would not. Therefore, the input signal was modified in the PSV system in order to achieve optimal results. This was due to the fact that the HP system is measuring acceleration data while the PSV system is measuring velocity data. By changing the measurement, the magnitude of the peaks changes. This change in magnitude results in the need for a change to the input signal.

One additional step that must be performed when using the HP system is to set the data range for both the reference signal and the response signal. This task is accomplished by using the auto range feature within *SignalCalc*. By running the auto range feature, the ranges are automatically set to monitor the signal strength throughout the test without being clipped. In addition, prior to operating the PSV system, the laser must first be focused in order to achieve the maximum allowable signal. This is done by simply adjusting the laser focus until the highest value is reached on the built in signal meter. Once these tasks are complete, the test can be run.

The final step in the vibrations testing process is to save the data. When using the HP system, this is done by selecting the desired values and saving them as a $MATLAB^{®}$ data file. This allows the data to later be manipulated and analyzed through the use of various functions within $MATLAB^{®}$. For the purposes of this research, only the FRF and coherence values will be saved for future use. When using the PSV system, the FRF is immediately displayed on the screen and by selecting the various peak values, the ω_n value along with the modal shape is shown. These values are then correlated to those found using the HP system in an effort to validate the results. The modal shape pictures are then used to distinguish between the bending and torsional modes within the system. By using each resource available, an accurate measure can be determined to tell how the ω_n and ζ values vary as the boundary conditions within the experiment change.

For the actual flight configuration, slight modifications will be made in the data processing due to the lack of the HP system in space. Rather than saving actual FRF and coherence values, the time history of the response will be collected. This data will then be processed within the flight computer and saved to a data file. Once the experiment is returned to Earth, the data will be extracted, and $MATLAB^{®}$ code will be used to further process the results in order to determine the actual ω_n and ζ values.

IV. Results and Analysis

4.1 Overview

Ground testing for a space experiment can be considered successful in both success and failure of a test. A successful test can lead to adequate data that can be further analyzed to verify prior predictions while a test failure can show possibly flaws in key operational procedures. Either scenario yields data that accomplishes the goal of the overall testing program which is to ensure the experiment is prepared for flight.

Throughout the course of RIGEX testing, both success and failure was experienced. Successful tests showed that the predicted behavior of the inflatable, rigidizable tube and the various experiment systems accurately represented in some cases the true response. However, in other cases, what initially appeared to be a failed test gave insight and knowledge that can be later used to modify various components of RIGEX in order to ensure a successful mission.

4.2 Deployment Results

The deployment of an inflatable, rigidizable tube, as part of the RIGEX ground testing, was conducted in various stages in order to adequately test each component of the experiment. Once each component was verified and operating within acceptable limits, a complete end to end test was conducted where a tube was heated, inflated, and rigidized. The following sections outline the results found through each stage of deployment testing.

4.2.1 Inflation System. The inflation system was the first to be validated. Prior to mounting the inflation system to the test structure, a simple test was conducted to determine if any leaks were present. By pressurizing the inflation system using an air compressor, it was shown that the inflation system held pressure, and

after checking each connection, no leaks were found. Initially however, some ambiguity was seen in the pressure regulator in that it was very difficult to set to a specific pressure thus causing risk of fluctuation in tube pressure once the inflation process began.

Given the successful operation of the inflation system, the system was mounted to the RIGEX test structure and connected to the heater box. As this point, the purely inflatable tube was mounted inside the heater box for further testing of the inflation system. Once again, after pressurizing the system, it maintained pressure and showed no signs of leaking. However, once the solenoid was activated, and the inflatable tube was pressurized, there appeared to be a leak within the system due to the fact that the pressure reading within the tube slowly decreased. After examining the tube, it was found that leaks were present within the tube itself thus causing the drop in pressure. No additional leaks could be found within the inflation system, however, one point of uncertainty was present in the fact that due to the layout of the experiment, neither the seal between the tube and the heater box through the o-ring, nor the connection where the inflation system screwed into the base of the heater box, could be tested. Every precaution was taken to ensure no leaks were present at these connections by applying high pressure vacuum grease to the o-ring and teflon tape to the heater box connections, however, the quality of these seals remained unknown.

The air compressor was then removed, and N_2 gas was then applied to the inflation system in order to set the pressure relief valve and the regulator. To accomplish this test, a modification was made to the test plan given the results of the previous inflation system test. Given that the purely inflatable tube leaked, it was replaced with a pre-inflated rigidized tube which modelled the dimensions of the tubes that would be inflated and rigidized in the final end to end test. In order to first check for leaks within the tube, the system was pressurized using the N_2 gas

and tested. No leaks were found thus enabling the calibration of the components to continue.

The first step in calibrating the inflation system was to set the pressure relief valve. By first setting the regulator to allow a 10.5 psig pressure within the tube, the pressure relief valve was slowly opened until the pressure began to drop and stabilize at 10 psig. Once this level was reached, the locking nut was set and the inflation gas was vented. In order to check the operation of the valve, the system was once again pressurized with the regulator set for 10.5 psig. The valve operated as expected and the pressure stabilized at 10 psig.

It was then necessary to set the pressure regulator to regulate the 320 psig source down to 4 psig. Using the same configuration as used for setting the pressure relief valve, the regulator was closed off, and the inflation system was pressurized. The regulator was then slowly opened until the pressure stabilized at 4 psig. Once again, this value was set, and the inflation gas was vented. In order to ensure the value was properly set, pressure was applied once more and the pressure within the tube stabilized at 4 psig. However, at this point, the pressure within the tube began to slowly decrease. Each component was tested for leaks, and the source of the leak was found to be within the pressure relief valve. The valve leaked through the exhaust port thus causing the pressure within the system to be drained. To correct the problem, the relief valve was reset and tested once again, and the same problem arose. Therefore, to correct the problem, the valve was fully closed thus setting the relief valve to a pressure of 25 psig. While this was not the optimal solution, it provided a means to seal the inflation system and prevent pressure loss. The regulator was then reset, and the system tested. All components then functioned properly and no leaks were present. For the flight configuration, it is recommended that a more precise pressure relief valve be used that is capable of setting a 10 psig relief pressure. This will ensure that overpressurization does not occur within the tube.

The final step to prepare for the end to end test was to mount the z-folded inflatable, rigidizable tube within the heater box and test the inflation system one final time prior to deployment. Based on the fact that in previous analysis of the tubes, pressure could be applied to a folded tube, this test was determined to be an acceptable means for testing the final seal of the inflation system. However, once pressure was applied to the tube, it began to inflate and crack. Pressure was immediately vented and the tube was removed. While no apparent damaged seemed to have been done to the tube, a new tube was mounted inside the heater box, and no further tests were performed on the inflation system in order to prevent damage to the tubes. This provided one additional source of ambiguity within the inflation system given that the seal made between the tube and the heater box could not be tested prior to inflation.

4.2.2 Digital Imaging System. The first step in testing the digital imaging system was to test the functionality of the lighting portion of the system this was done by first setting the power supply connected to the lights and using a voltmeter, it was verified that all connections maintained the proper 24 volt reading. Once this was validated, power was applied to the lights, and instantaneously, they turned on thus verifying that the lighting portion of the system functioned properly.

With the lights operational, the remaining tasks were to set the focus and the iris of the digital camera. By mounting a pre-inflated tube within the heater box, test images could be taken that would simulate those to be taken in the final end to end test. The focus of the camera was first adjusted and it was found that the once adjusting the camera to the maximum limit in nearness focus, a suitable image was achieved. With a focused image achieved it was then necessary for the iris to be set so that accurate images could be taken in the vacuum tank.

By placing the RIGEX test structure in the dark and then turning on the lights, the actual testing environment was simulated. The iris was then manually

adjusted until an optimal image was collected. The camera was then disconnected, and the structure was mounted inside the vacuum tank. This allowed test images to be conducted in the actual environment where the test would take place. The lights of the system were turned on, and several images were collected. Slight modifications were needed to the iris setting once in the vacuum tank. Once these corrections were made, the settings of the iris and focus adjustments were physically marked on the camera thus allowing the settings to be checked prior to further testing. For the actual flight configuration, it is recommended that a camera be used that is capable of setting all parameters directly through software. This will eliminate the risk of physical settings being shifted during launch.

4.2.3 Purely Inflatable Tube. The use of a purely inflatable tube for portions of the testing served several purposed. First, this allowed multiple inflations of the tube in order to test the inflation rate and the ability of the digital camera to capture images of the inflation process. In addition, throughout the multiple deployments of the purely inflatable tube, it was determined if either the upright or inverted configuration of the test structure was preferred for the end to end test when the inflatable, rigidizable tube would be used. Given the limited number of inflatable, rigidizable tubes, the use of the purely inflatable tube throughout testing proved very useful.

Prior to the inflation system components being configured, the purely inflatable tube was mounted within the heater box in order to test the actual deployment of a tube. With the regulator set to regulate the pressure down to 4 psig, the deployment was first tested with the structure in the upright configuration. Upon the first deployment test, the testing procedure was determined to be invalid. Initial testing procedures called for the activation of the inflation system solenoid prior to the release of the heater box latch. The original thought was that this would allow deployment to begin immediately upon the release of the latch due to the pressure within the tube. This would allow the tube to deploy and essentially rise above the

heater box doors prior to them opening, and thus eliminating an added force to the tube deployment from the opening of the heater box doors. It was thought that this would allow the deployment to be purely accomplished by the inflation rather than having the force of the doors opening initiating the deployment. However, the first test showed that with the tube pressurized inside the unopened heater box, an additional force was placed on the latch which was in turn transferred to the solenoid that would retract the pin thus releasing the heater box latch. This added force proved to be too large of a force for the solenoid to overcome. Therefore, if the tube was pressurized prior to the release of the latch, the latch would not release. This in turn resulted in changing the initial testing procedures to those shown in Section 3.3.1.2, where heater box latch was first released, followed by the activation of the inflation system solenoid.

Once the testing procedures had been changed, tests continued with initial tests being conducted with the Test structure in the upright configuration. In this configuration, and with the regulator set at 4 psig, the tube consistently failed to fully deploy. The 4 psig pressure was achieved, however, once the heater box latch was released and the tube began to inflate, it would press against one side of the heater box and prohibit a full inflation. The tube would then be left only partially inflated with only part of the tube extending outside of the heater box.

A change was then made to determine if a higher initial pressure would create a faster deployment and thus prevent the tube from being wedged between the walls of the heater box. The pressure was first increased by adjusting the regulator to maintain a constant pressure of 6 psig and the identical test was run. The results were the same as before in that the tube only partially deployed do to the tube being wedged against the wall of the heater box. The pressure was then increased to 8 psig and an identical result was shown. It was not until the pressure was increased to 10 psig that the results changed. At this point, the initial inflation pressure was enough to fully deploy the tube, however, the total inflation occurred in under one second,

and immediately once the tube was deployed, the regulator had to be adjusted due to the fact that the pressure would exceed the maximum operating limit for the tube. Due to the fact that inside the vacuum tank, and on the actual flight experiment, this method to resolve the problem proved ineffective.

The test structure was then mounted in the inverted configuration and testing continued. By changing to this configuration gravity became the driving force responsible for the deployment of the tube do to the fact that once the heater box doors opened, gravity would cause the weight of the end flange to fall, thus fully deploying the tube even if no inflation gas was present. Therefore, given this configuration, it was certain that a full deployment would be achieved. However, this configuration would inhibit the ability to determine how accurately the tube deploys given that regardless of the conditions of the test, gravitational forces ensured that the tube deployed fully and in a perfectly straight manner each time when using the purely inflatable tube.

The final test needed in conjunction with the purely inflatable tube was to test the ability of the digital camera to capture the images of the tube deployment. The exposure time of the camera was initially set to 100 milliseconds and the tube was inflated. This proved ineffective in that images were only being collected approximately every 1.5 seconds. Given this, the exposure time was decreased to 50 milliseconds and in turn down to 10 milliseconds. At 10 milliseconds a sporadic representation of the deployment could be seen, however, the resolution of the image was very poor. At 50 milliseconds, the image improved, however, the speed was not adequate. Therefore, the exposure time was set at 25 milliseconds in balance out the quality of the image with the speed at which an image is collected.

With the exposure time set, it was necessary to determine how the images would be saved during the deployment. Using the multiple frame acquisition (MFA) selection within the digital camera software, it was thought this could be accomplished. However, by testing to see the time required for various numbers of images,

this method proved inadequate. In order to collect images throughout the deployment process, at least sixty seconds worth of images were needed. Given that even with an exposure time of 25 milliseconds, images were only collected approximately every second, it was necessary to collect a minimum of sixty images. When this task was attempted using the MFA tool, the elapsed time to collect sixty images totalled approximately ten minutes. Therefore, an alternate method for capturing images during the deployment was needed.

To resolve this issue, a video camera was used to video tape the monitor that would display the time lapsed images taken by the digital camera. This video could then be edited and individual images could be collected from the video. This allowed the digital camera to be operated in its regular capture mode, and thus enabled a smaller exposure time of 15 milliseconds. Prior to further testing, various options should be considered that could increase the computer speed thus allowing images to be collected at a much more rapid rate. In addition, the option of a real time digital video camera that could replace the ELECTRIM digital imaging camera should be explored. This would resolve the image collection issues for both testing and the actual space flight.

4.2.4 Inflatable, Rigidizable Tube. Prior to initiating tests on the inflatable rigidizable tube, one final check was made on the inflation system to ensure all components were functioning properly. This was done as before by mounting a previously inflated, rigidized within the heater box. The pressure cylinder was then pressurized with 320 psig of N_2 gas and was sealed off in order to separate the inflation system from the source used to pressurize the cylinder. This would allow the pressure cylinder and the inflation system alone to be responsible for pressurizing the tube. The inflation system solenoid was activated and a pressure of 4 psig was achieved within the tube. However, with this final test, once the 4 psig pressure was reached, it began to drop off, thus indicating that a leak was once again present within the inflation system.

In order to determine where the leak originated from, the N_2 source was reconnected to the inflation system in order to maintain a constant pressure of 320 psig being applied to the inflation system. This would allow the 4 psig pressure to be maintained given the fact that the 320 psig source would compensate for any leak within the system. The inflation system solenoid was activated once again, and a pressure of 4 psig was reached, but shortly after stabilizing, began to decrease as before. Given that a constant 320 psig source was being applied to the inflation system, this indicated a malfunction within one of the components within the inflation system. By analyzing the pressure readings, the pressure prior to the regulator was being maintained at 320 psig, however the pressure after the regulator was quickly diminishing. This indicated that the problem was present within the pressure regulator.

To determine if the regulator was malfunctioning, adjustments were made to increase the pressure allowed into the tube by the regulator given the assumption that there was perhaps an initial overshoot in the pressure value that stabilized over time to a pressure lower than the value initially set. After adjusting the regulator setting, once again a 4 psig pressure reading was achieved. To determine the validity these results, the inflation gas was then vented, and the test was repeated. The 4 psig pressure was achieved and remained for approximately two hours. The exact cause for the variation in the response of the regulator between each test is unknown, however, at this point the problem appeared to have been resolved, and with the issue resolved, the set up of the complete end to end test of RIGEX could begin.

Based on previous tests, all tests conducted using the inflatable, rigidizable tube were mounted in the vacuum tank in the inverted configuration. This allowed assurance that a full deployment would occur and the tube would not become lodged within the heater box. Based on this, in order to begin testing, the z-folded tube was first mounted within the heater box, and the test structure was then mounted

inside the vacuum tank in order to simulate the space environment in which the actual experiment would operate.

Once mounted inside the vacuum tank, the system was configured as specified in Section 3.3.1.1, and all connections were tested to ensure the RIGEX test structure was properly connected. Before the vacuum tank could be sealed and a vacuum drawn down on the RIGEX test structure, two additional tests were needed. The first of which was to test the functionality of the heater box latch and ensure it was properly set. The latch was set and released several times to verify its functionality and each test of the latch was completely successful. The second test needed was to verify that the digital camera functioned properly. Figure 4.1 shows the image taken from the digital camera with the structure mounted inside the vacuum tank.

Figure 4.1 Digital Image Inside Vacuum Tank: Deployment Test 1

4.2.4.1 Deployment Test 1. Final preparations for the first deployment test of the inflatable, rigidizable tube began once the functionality of all components had been verified. The pressure cylinder within the inflation system was first charged with 320 psig of N_2 gas. In order to ensure the pressure cylinder would maintain pressure within the vacuum, the system was sealed and left to sit for ap-

proximately twenty hours. At the end of this time period, the pressure within the pressure cylinder had dropped to 300 psig. This loss was assumed to be negligible due to the fact that all testing would last a maximum of three hours, and based on the preliminary design, only a pressure of 250 psig was needed to fully inflate the tube. Given this, the pressure cylinder was recharged to 320 psig and the vacuum tank was sealed and a vacuum was drawn down on the RIGEX test structure creating an environment pressure within the vacuum tank of 0.21 psia.

When the vacuum was drawn down on the RIGEX test assembly, the pressure within the inflation system pressure cylinder displayed a rather unique behavior. Based on the fact that all pressures were being measured using psig standards, an increase in approximately 14.7 psig was expected once the pressure was reduced within the vacuum tank. As the pressure within the vacuum tank decreased, the pressure within the pressure cylinder increased as expected. At the point when the experiment was in vacuum, the pressure within the pressure cylinder had increased from its starting pressure of 320 psig to a final reading of 337 psig, resulting in a 17 psig increase. The exact cause of the variation from the expected 14.7 psig increase is unknown.

With the experiment sealed within the vacuum tank, the deployment test was initiated in accordance with the procedures outlined in Table 3.1. Once the heaters were initialized, their profile followed an expected pattern in that they had an initially sharp increase in temperature that seemed to approach a final steady state value as shown in Figure 4.2, until the power to the heaters was terminated once the tube had deployed. As seen in Figure 4.2, all heaters did not maintain equal values in reference to one another. This is due to the different resistance values for each heaters, and is the desired outcome based on previous research. Given that the heaters located on the top and bottom of the heater box contribute the most to heating the tube, they are designed to supply the most heat (26). In addition, a slight dip in the plot is seen just prior to the point where the heaters were turned off, and the decrease

in temperature is seen. This initial dip was due to the opening of the heater box doors at the point of the tube deployment. Once the doors were opened, some heat escaped from the box thus slightly cooling the heaters. Once the tube deployed, the heaters where turned off, thus causing the temperature decrease. Therefore, the temperature profile shown in Figure 4.2 follows the expected profile.

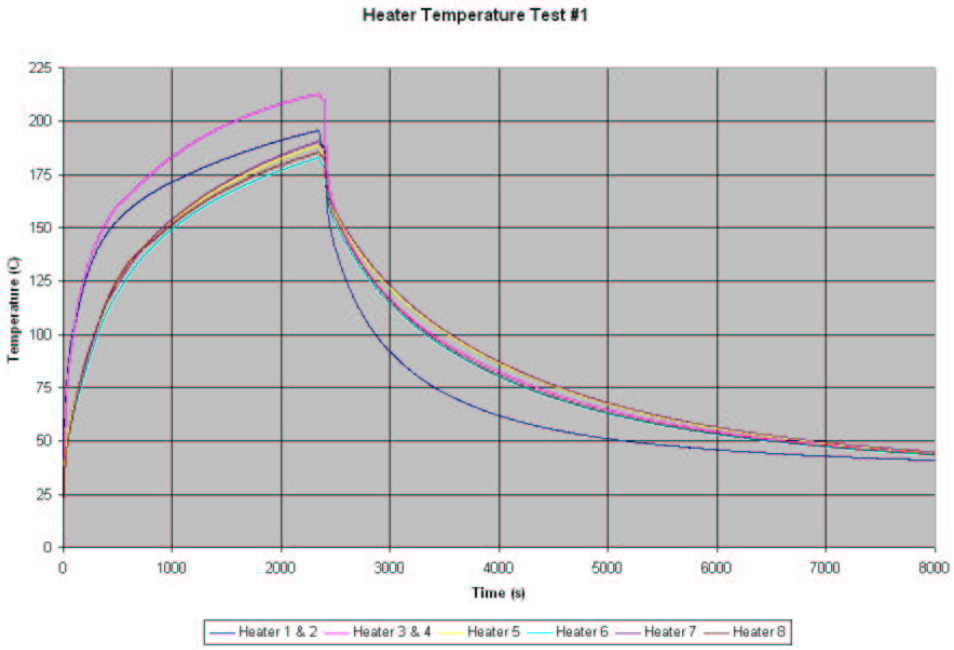

Figure 4.2 Heater Temperature: Deployment Test 1

In order to monitor the temperature of the inflatable, rigidizable tube, two thermocouples were placed within the bottom three inches of the tube. The first was connected just above the bottom end flange while the second was attached inside the first fold of the tube as shown in Figure 4.3. This allowed the temperature of the tube to be monitored in two locations in order to ensure the tube had reached the T_g temperature of $125°C$ before the actual deployment was initiated.

The temperature profile of the tube, as with that of the heaters, followed the expected profile. A plot of the temperatures recorded for each thermocouple is shown in Figure 4.4. As seen in the plot, the two points on the tube heated in similar pat-

Figure 4.3 Tube Thermocouple Locations

terns, but the actual temperatures differed over time. This was due to the fact that the thermocouple mounted just above the bottom end flange was not a valid measurement of the tube temperature due to the fact that at that point, the aluminum of the end flange was affecting the temperature based on the fact that there was a larger mass of material to heat. Therefore, this measurement point was measuring the temperature of the end flange rather than the actual material of the tube. The thermocouple mounted within the fold of the tube measurement increased at a much faster rate due to the fact that there was less material to heat. At the point of deployment, a sharp increase is seen in the temperature of the thermocouple mounted within the fold of the tube. As the tube deployed, the thermocouple which was originally embedded within the fold was exposed to the surroundings. This increased exposure of the thermocouple to the heat source supplied by the heaters resulted in the initial increase in the temperature. The point at which the temperature begin to decrease corresponds to the time at which the heaters were deactivated.

Based on the data shown in Figure 4.4, a clear point at which the entire tube had reached the T_g temperature was not present. Therefore, in order to ensure that the tube was properly heated, the criteria outlined in Table 3.1 for when the tube should be deployed was modified slightly. Despite the one data point that showed the tube had reached $125°C$, the deployment was delayed until both readings

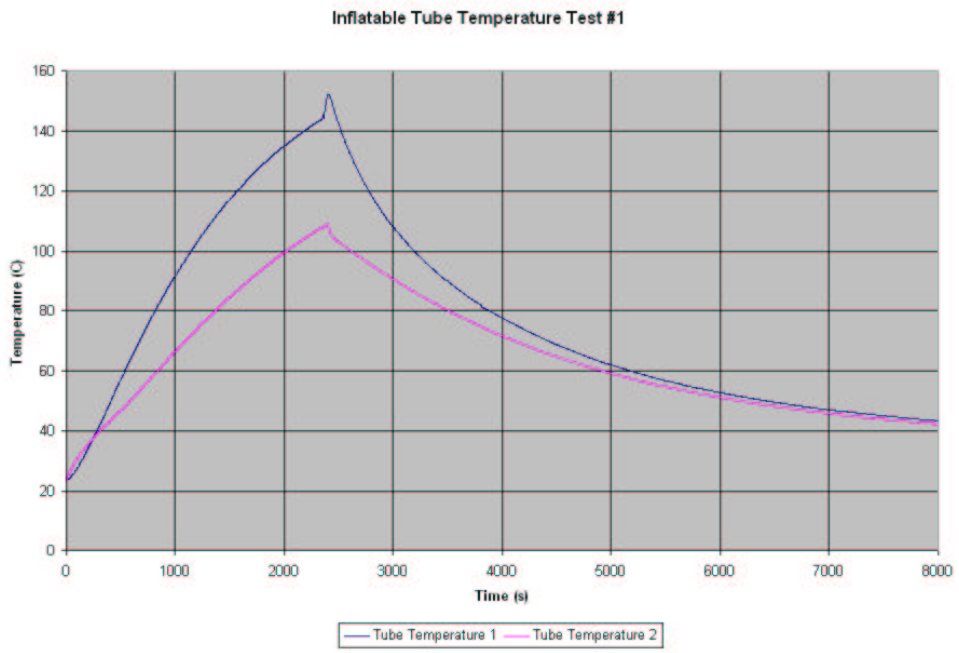

Figure 4.4 Tube Temperature: Deployment Test 1

showed a minimum of $100°C$. The purpose behind the $100°C$ criteria rather than $125°C$ is based on the assumption that since the lower temperature corresponded to the thermocouple mounted just above the bottom end flange, the measurement did not accurately represent the temperature of the tube. Therefore, by waiting until this reading had reached a minimum of $100°C$, the other tube temperature reading had reached approximately $152°C$. Given that this value was well above the T_g temperature, it was assumed that the tube was properly heated and ready for deployment. Further testing, to include an increase in the number of thermocouples monitoring temperatures at various points on the tube, is needed to more accurately determine the point at which the tube is properly heated for deployment.

In addition to temperature measurements, the power and current used by the heaters within the heater box were monitored. The power applied to the heaters was set and maintained at 24 volts throughout the test. Once the heaters were powered on, they began to draw a total current of 3.33 amps. Throughout the course of

the test, this value slowly decreased to a value of 2.66 amps at the point where the deployment sequence was initiated. The standard maximum operating range for a D-cell battery is approximately 1.1 volts (2). This immediately shows a flaw in the preliminary design of the power system in that a battery cell of 20 D-cell batteries will only yield a maximum voltage of 22 volts. Within the design however, there is the capability if increasing the number of batteries within each cell to a total of 21 batteries. This will yield a maximum power of 23.1 volts by connecting all batteries in series with one another. While this still falls short of the testing value of 24 volts, this value can be increased by using higher efficiency batteries that can operate at 1.2 volts.

Given that the deployment occurred in approximately 40 minutes, one battery cell could provide the voltage needed for the time required, however, the current draw limits this capability. Based on D-Cell battery specifications, the maximum current draw capability for each battery is 2 amps, however, this drastically limits the lifetime of the battery to approximately 40 minutes (2). Therefore, with the maximum current of 3.33 amps for the deployment test, it is necessary to connect four battery cells in parallel to one another in order to supply the current necessary to conduct the test. By connecting four cells in parallel, the power source can provide a 4 amp capability for approximately two hours, thus enabling the heating of the tube. This in turn shows that for the RIGEX mission, a maximum of 12 battery cells are needed for the heating of the three inflatable, rigidizable tubes, thus leaving 8 battery cells to power the remaining RIGEX components. While it is estimated that the remaining 8 cells will provide sufficient power for the remaining components, a detailed power analysis is needed.

Once the tube was properly heated, the deployment sequence was initiated. Initially, each component appeared to function as expected, however, several unexpected results were seen. The first unexpected result occurred in the speed at which the deployment occurred. The time lapsed images taken during the deployment are

shown in Appendix A. Due to the fact that the experiment was mounted in the inverted configuration, it was known that the deployment would occur very rapidly, however, it was still expected that a minimum of three to four frames could still be captured once the latch was released and prior to the point where full inflation had occurred. However, the deployment occurred much more rapidly than expected, and only two intermediate frames were captured.

The pressure within the tube demonstrated the second unexpected result. The tube initially reached a pressure of 6 psig which was higher than expected, while the pressure within the pressure cylinder dropped slightly and stabilized as expected due to the loss of N_2 gas used to inflate the tube. As time passed, the pressure within the inflation system pressure cylinder remained fairly constant as expected. However, during this time, the pressure within the tube steadily increased. If a leak were present within the system, the pressure within the pressure cylinder would have slowly decreased to compensate for the leak while the tube pressure remained constant. However, the increase in the tube pressure until the point at which the tube temperature fell below the T_g temperature thus rigidizing the tube. This increase in tube pressure was unexpected and leads to the conclusion that the pressure regulator may have malfunctioned. The plots showing the pressure of both the pressure cylinder and the tube over the course of the test are shown in Appendix A.

The final unexpected result in the fact that the final digital image taken by the digital camera was expected to be an image of the top end flange. However, the image shown in Figure 4.5 was seen. In viewing this image, it appeared that a piece of the tube was laid across the lens of the camera. Given that the design of the test structure allowed for a clearance of 1.5 inches between the top end flange and the camera lens, the source for this final image was uncertain.

The exact source of the image shown in Figure 4.5 was found once the RIGEX test structure was removed from the vacuum tank. At this point it was seen that what was assumed to have been a 20 inch z-folded tube initially mounted within the heater

Figure 4.5 Final Deployment Image: Deployment Test 1

box was actually a 24 inch tube. All prior designs and tests were conducted using 20 inch tubes, and upon ordering the z-folded tubes, 20 inch tubes were requested. However, it was later determined that the addition of 4 inches to the tube was a manufacturer error, which was not realized prior to the deployment of the tube during this test. Figure 4.6 shows the final results of the first test for the inflatable, rigidizable tube.

4.2.4.2 Deployment Test 2. Based on the results found in the first deployment test, several modifications were needed before a second tube could be deployed. The primary task was to provide the clearance needed for the 24 inch tube to fully deploy. Once this task was accomplished, the inflation rate of the tube was analyzed. In the first test, the tube inflated very quickly and very few images of the deployment were captured. While the primary source for the speed of the deployment is the affect gravity has on the top end flange, by slowing the inflation rate instigated by the inflation system, it was hoped that the deployment would occur over a slightly longer time span thus allowing more intermediate images of the deployment to be captured.

Figure 4.6 Final Deployed State: Deployment Test 1

In order to make use of the 24 inch tubes for ground tests, the test structure was modified to allow sufficient clearance for the tube to deploy. This was done by removing the camera from the inside of the test bay. By removing the camera, the 24 inch tube would be capable of fully deploying with a clearance of 0.25 inches between the top end flange and the top plate of the test structure. However, if the camera were fully removed, there would be no method for collecting images of the deployment. To resolve the issue, a two inch diameter hole was cut in the top plate of the test structure, and four 1.375 inch aluminum spacers were made that would allow the camera to be mounted on the top side of the top place directly above the newly cut hole as shown in Figure 4.7. This solution would allow for images to be taken throughout the deployment process while ensuring that sufficient clearance was provided for the 24 inch inflatable, rigidizable tube to fully deploy.

Once the camera was configured in the new location, the inflation system was modified to include a flow control valve in an effort to decrease the inflation rate of

Figure 4.7 Digital Camera in Modified Mounting Position

the tube. Figure 4.8 shows the Parker HR Series valve that was added to the inflation system (4). The flow valve was added to the system just after the inflation system solenoid in the direction of gas flow through the system as shown in Figure 4.9. This would allow the flow rate directly to the tube to be adjusted and set at a desired level.

With the flow control valve inserted into the inflation system, it was necessary to first reset the pressure regulator and then set the flow control valve to the desired level prior to removing the inflated tube from the first deployment test. This would allow the components to be set using the exact volume that would be used for the test. To set the pressure regulator, the flow control valve was first opened to allow the maximum flow through the system. The regulator was then set to allow a maximum of 4 psig into the tube. However, due to the addition of the flow control valve, even when set to allow a maximum flow rate, it took approximately fifteen minutes for the desired 4 psig level to be reached. Since the flow control valve was set at the maximum level, the only way to increase the pressurization rate was to increase the pressure allowed by the regulator. After several iterations, the regulator

Figure 4.8 Flow Control Valve

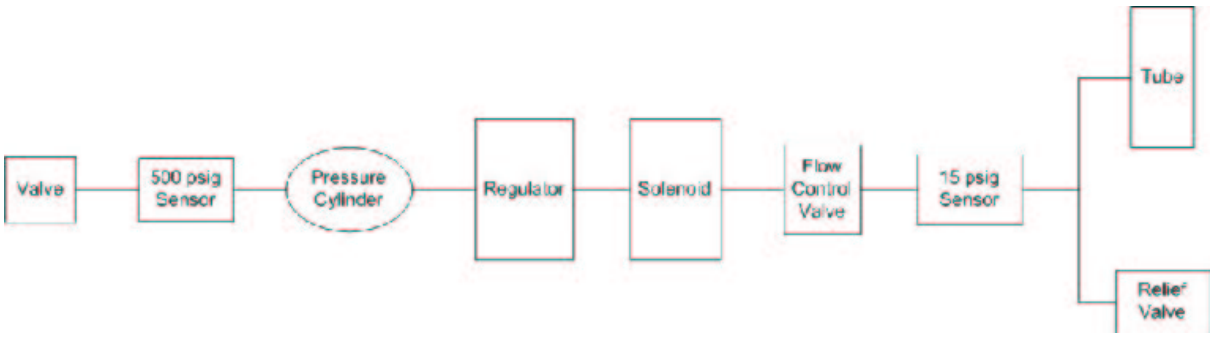

Figure 4.9 Modified Inflation System Schematic

was set so that the tube reached the desired pressure of 4 psig after approximately forty seconds, and after approximately two hours, the pressure level increased to only 8 psig. Based on results from the previous deployment test, this 8 psig level was determined to be acceptable due to the fact that in the first test, the tube safely reached a level of 9.381 psig.

In order to test that the inflation system was once again functioning properly, the inflation gas was released, and the pressure cylinder was pressurized to the desired 320 psig level. The N_2 gas source was then removed in order to allow the test of the inflation system to be conducted in the same manner as it would be operated during the deployment test. The inflation system solenoid was activated, and the results matched those found in the initial settings. The 4 psig level was reached after approximately forty seconds, and then the pressure slowly increased within acceptable limits, the inflation gas was then vented and the process was repeated. After several repetitions, identical results were found each time. For the actual flight experiment, further tests and calculations are needed to determine the optimal flow rate that will ensure a controlled and full deployment of the tube.

With the inflation system operational, the inflated tube was removed, and a new z-folded inflatable, rigidizable tube was mounted within the heater box. Once the tube was securely mounted, the RIGEX test structure was mounted inside the vacuum tank as in the first deployment test. Prior to the vacuum tank being sealed, the functionality of the digital camera along with its ability for images to be taken in the new orientation was verified through acquisition of the image shown in Figure 4.10.

Once the functionality of the camera was verified, the pressure cylinder within the inflation system was pressurized with N_2 gas as was done in preparation for the first deployment test. One variation however occurred during the pressurization of the pressure cylinder. For this test, the cylinder was only pressurized to a 305 psig level as opposed to the 320 psig level used in the first test. This was due to the

Figure 4.10 Digital Image Inside Vacuum Tank: Deployment Test 2

fact that all components had been set based on a 320 psig source. Given that there was an expected 14.7 psig increase in pressure due to the difference between ambient and vacuum conditions, the initial pressure was reduced in order to compensate for the expected increase. The vacuum tank was then sealed, and the pressure within the tank was reduced once again to 0.21 psia. As expected, the pressure within the pressure cylinder increased as the atmospheric pressure within the tank decreased and stabilized at a pressure of 319 psig.

With the vacuum tank prepared for testing, the testing procedures outlined in Table 3.1 were initiated. As expected, the heaters immediately responded to the initialization of power to the system, and followed a profile near identical to that found in the first test. The temperature profile of the heaters is shown in Figure 4.11. Once again, an initial dip in temperature is seen at the point of deployment, and the decrease in temperature is seen at the point where the power was terminated.

The temperatures being monitored on the inflatable, rigidizable tube followed a similar profile as in the first step, however, there were slight differences. In the first test, the two measurements remained within close proximity to one another and

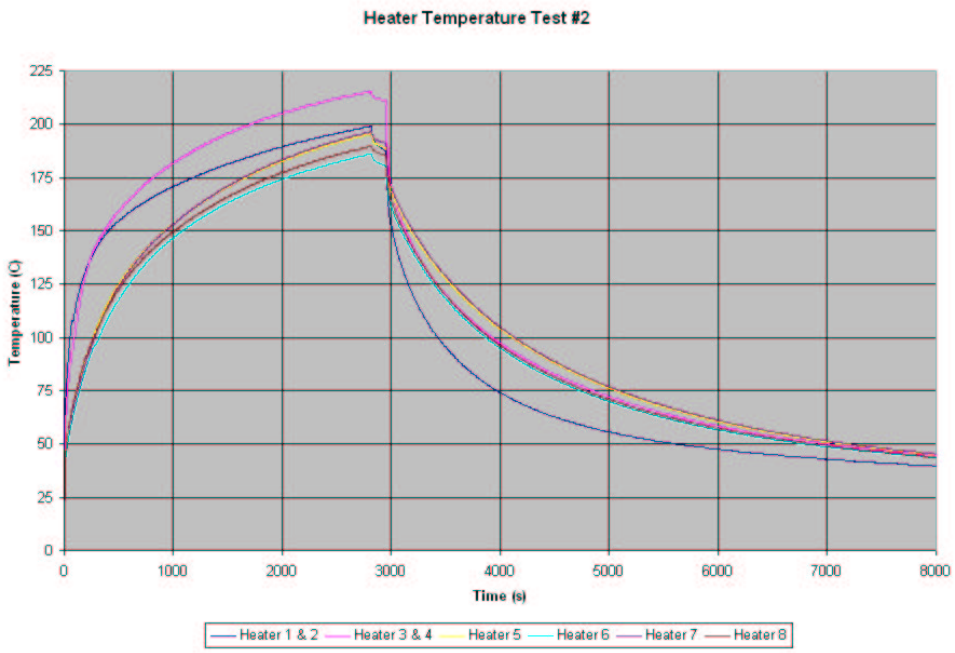

Figure 4.11 Heater Temperature: Deployment Test 2

only slowly separating to a maximum difference of approximately $44°C$ at the point of deployment. In this test, the temperatures separated much more rapidly to a maximum difference of approximately $61°C$ at the point of deployment. Figure 4.12 shows the temperature profile of the tubes throughout the test. The same criteria was used for deployment as was used in the first test, and as Figure 4.12 shows, the tube in this test took approximately 570 seconds longer to reach the desired $100°C$ temperatures readings for both thermocouples as did the tube in the first test. However, the thermocouple mounted within the fold of the tube reached a maximum temperature of $166°C$ as opposed to the $152°C$ of the first test while the thermocouple mounted just above the bottom flange measured a maximum temperature of only $105°C$ as opposed to the $108°C$ recorded in the first test.

Once again, the power and current used by the heaters within the heater box were monitored up until the deployment sequence was begun. The power applied to the heaters was again set and maintained at 24 volts throughout the test. Once the

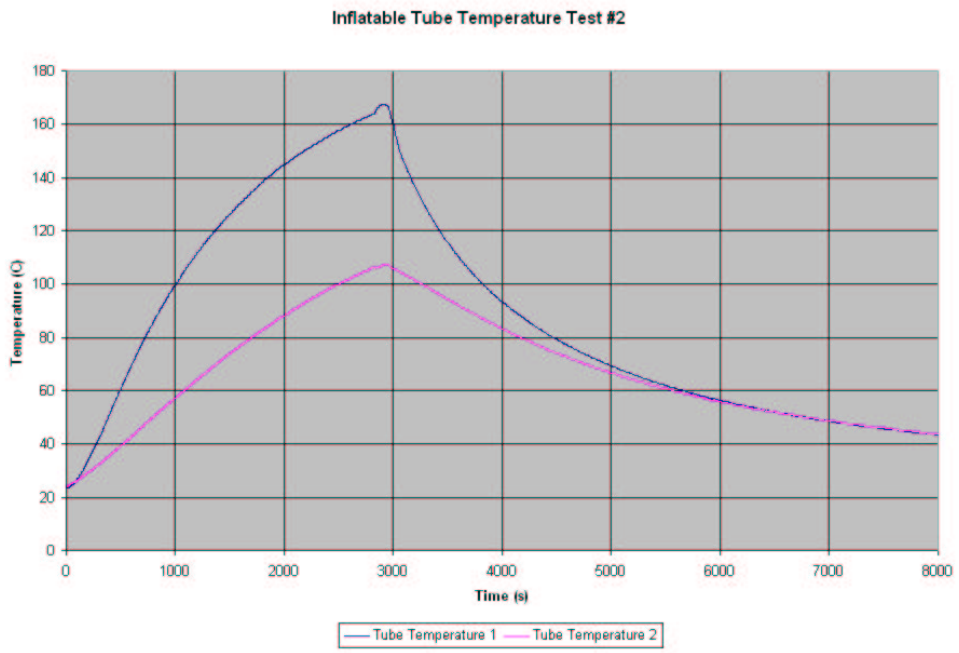

Figure 4.12 Tube Temperature: Deployment Test 2

heaters were powered on, they drew an initial current totalling 3.08 amps. Throughout the course of the test, this value slowly decreased, as expected based on data shown in the first test, and reached a value of 2.64 amps at the point where the deployment sequence was initiated. By following the same reasoning outlined for the first deployment test, given the maximum current used and a total deployment time of approximately 47 minutes, a total of 12 battery cells would be needed to power three inflatable, rigidizable tube assemblies, thus verifying the results of the first deployment test

Upon the initiation of the deployment sequence, one problem was immediately noticed. Based on testing results, the tube should have reached a pressure of 4 psig within approximately forty seconds. However, after initially rising to a value of 2.22 psig, pressure slowly increased to a pressure of only 2.48 psig after 85 seconds. An expected initial decrease was seen in the pressure of the cylinder, however, once the tube reached 2.48 psig, both the pressure within the tube and the pressure cylinder

decreased to essentially zero within six minutes. Plots of the pressure for both the tube and the pressure cylinder can be seen in Appendix A. Once the test structure was removed from the vacuum tank, all connections were checked with the exception of the connection to the heater box, the o-ring seal between the heater box and the bottom flange due to the inaccessibility of the connections. No leaks were found in the connections tested, which leads to the conclusion that a leak was present in one or both of the unchecked connections, or within the tube itself.

A second complication found within this test was associated with the digital camera. While the inflation rate was decreased by the flow control valve, only one intermediate deployment image was collected. In the initial design of the test structure and the lights for the digital imaging system, the lights were mounted in a location that would optimize the light on the end flange of a 20 inch tube. However, given that the tube was 24 inches, once fully deployed, the top of the end flange was above the light source. This in addition to the fact that only a 0.25 inch clearance remained between the end flange and the top plate of the test structure, caused all light to be blocked from the digital camera thus enabling no additional images to be collected. The time lapsed images that were taken can be seen in Appendix A. Further testing should be conducted to determine if, when using the inflatable, rigidizable tube, can the test structure be mounted in the upright configuration and achieve a full deployment. This would minimize the affects of gravity on the speed of deployment and thus allow multiple intermediate images to be collected.

The final results of the second deployment test were found once the structure was removed from the vacuum tank. It was then seen that despite the loss of pressure within the tube, a successfully deployment and rigidization was achieved. The fully deployed and rigidized tube is shown Figure 4.13.

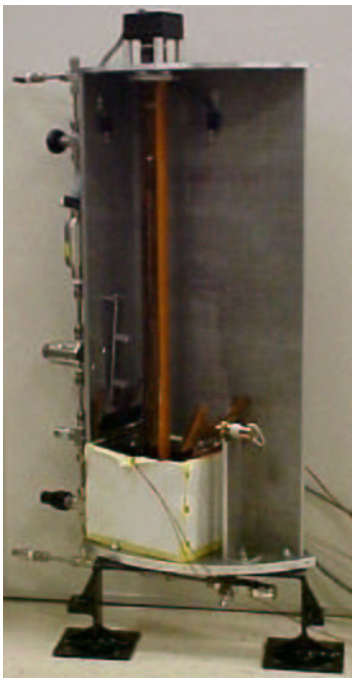

Figure 4.13 Final Deployed State: Deployment Test 2

4.3 Vibrations Results

The purpose of vibrational testing was to identify the natural frequencies and damping ratios of the inflatable, rigidizable tube as the boundary conditions of the tube varied. Initial test plans used the inflatable, rigidizable tube that had been inflated during deployment tests. However, due to complications in the fabrication and delivery of these tubes, these tests were conducted prior to the deployment tests, and were conducted using a previously inflated tube composed of identical materials. By taking the results found throughout this testing, estimates could be made to determine how the tube would respond once on orbit in an effort to correlate the ground testing data found to the actual space flight results. Multiple tests were run in order to verify the true properties of the tube. The following sections outline the results from each test.

4.3.1 Natural Frequency Identification. The first step in the vibrations testing was to identify the ω_n values for the tube given each of the four various

boundary conditions. By forming FRF's using the data collected through each of the four configurations outlined in Section 3.3.2.2, these values were easily identified by the frequencies corresponding to each peak value recorded. In each of the various configurations, FRF plots are shown for the data collected using the HP system while the frequencies of the peaks were simply recorded for the data using the PSV system in order to verify the HP system data.

The first step in the identification of the ω_n values was to find a baseline for future comparison. This baseline was formed by the values for the tube itself mounted in configurations 1a and 1b. Figure 4.14 shows the FRF of the tube.

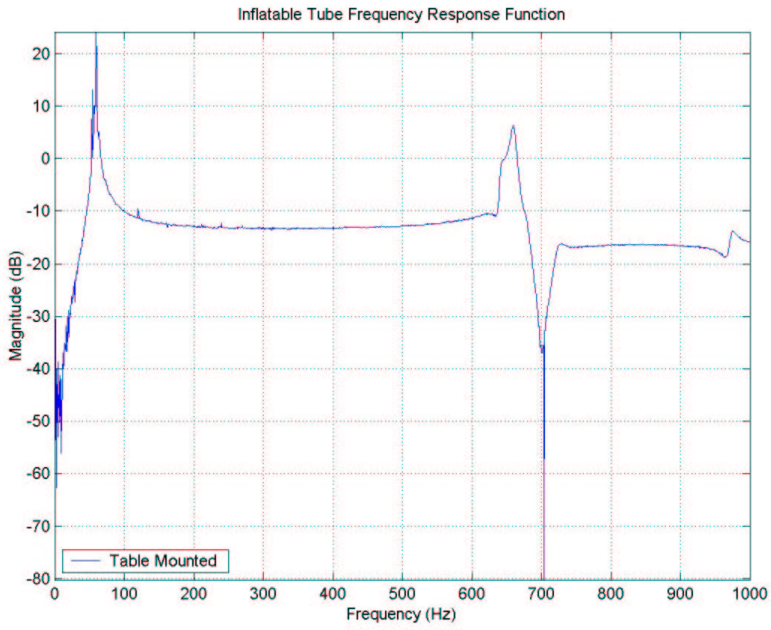

Figure 4.14 Inflatable, Rigidizable Tube FRF

Table 4.1 shows the values found using the HP system compared to those found using the PSV system. Due to the fact that only a single axis accelerometer was used to collect data for the HP system, the data found will only show the true bending modes of the tube assuming the axis of the accelerometer was aligned perfectly with

the axis excited by the PZT's. Therefore, the natural frequencies present within both test cases show the ω_n values for the bending modes of the tube.

Table 4.1 Table Mounted Results Comparison

Mode	HP System Data Frequency (Hz)	PSV System Data Frequency (Hz)
1^{st} Bending	59.6875	62.5
2^{nd} Bending	660.0	662.3
1^{st} Torsional		722.5

To verify that these are the true values for the bending modes, the mode shapes produced using the PSV system were analyzed. This analysis showed that the value seen at 722.5 Hz was clearly a torsional mode of the tube while an addition value seen in the PSV data at 345.8 Hz did not show a clearly defined shape. It was therefore determined to be a combination of both torsional and bending and not a true mode of the tube. In addition, the HP data showed a value at 976.5625 Hz that was determined to not be a mode of the tube due to the fact that it did not appear in the data collected using the PSV system. The exact source of this value is undetermined.

The tube was then placed on the test stand and the identical analysis was performed. Figure 4.15 shows the FRF of the tube mounted on the test stand in comparison to the tube mounted on the table while Table 4.2 compares the data found from during test configurations 2a and 2b.

The data shown in Figure 4.15 followed the expected result in that by changing the boundary conditions to a less rigid base, additional modes would be introduced in the system. It was then necessary to compare the results found for each of the two data collection methods along with the mode shapes produced by the PSV system to determine which were the true bending modes of the tube.

The first step in this data reduction process was to realize that the value at approximately 37.5 Hz appears in both cases and is therefore determined to be the

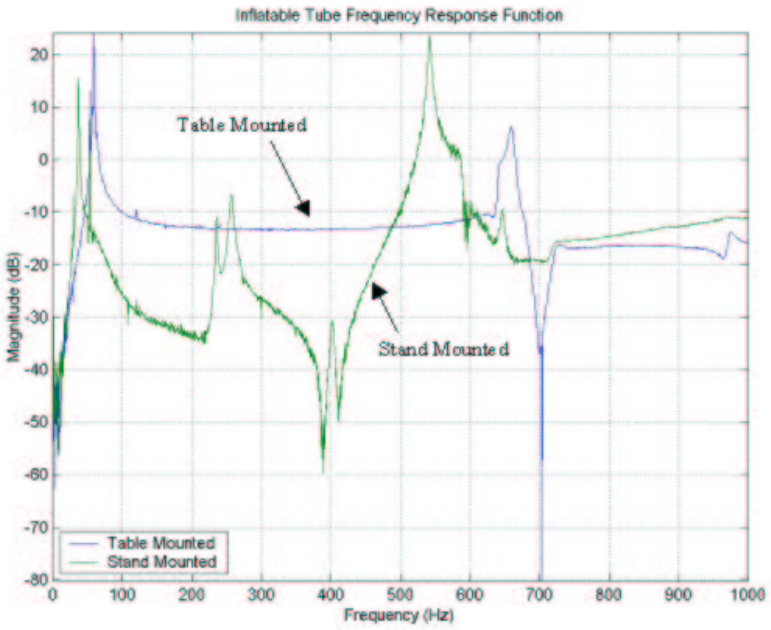

Figure 4.15 Table Mounted vs Stand Mounted FRF

Table 4.2 Stand Mounted Results Comparison

Mode	**HP System Data Frequency (Hz)**	**PSV System Data Frequency (Hz)**
1^{st} Bending	37.5	37.75
1^{st} Stand Bending		169.5
1^{st} Torsional	235.9375	237.0
2^{nd} Stand Bending		278.8
2^{nd} Bending	542.1875	540.0
2^{nd} Torsional	647.5	647.3

first mode of the tube. The modal shape data also supported this determination. Additionally, values appeared at approximately 236 Hz, 541 Hz, and 647 Hz in both cases, along with various modes in the PSV data between 160 Hz and 540 Hz, and at 716.8 Hz. It was then necessary to use the modal shape data to determine which values were the true modes of the tube.

When using the modal shape data, the values shown between 160 Hz and 402 Hz were clearly due to the motion of the test stand. This was seen in the fact that the free end of the tube remained fixed while the end attached to the test stand showed drastic motion. In addition, the values seen at 647.3 Hz clearly demonstrated the behavior of a torsional mode while the value at 716.8 Hz appeared to have no clearly defined shape. One source of ambiguity however is in the fact that the value of 235.9375 Hz and 647.5 Hz, which has been determined to be a torsional modes, appears in the data collected by the HP system using a single axis accelerometer. A possibly explanation as to why this value is seen by a single axis accelerometer is that the base motion of the tube due to the motion of the test stand is causing the axis of the accelerometer to become misaligned thus detecting the additional mode. Regardless, the second mode of the tube is identified as 542.1875 Hz. These values for the first and second bending mode correspond to the expected results in that by adding flexibility to the support of the tube the ω_n values should decrease.

The tube was then mounted within the RIGEX heater box and in turn mounted to the RIGEX test structure and tested in configurations 3a and 3b. The resulting FRF from this test is shown in Figure 4.16.

The results shown in Figure 4.16 did not follow as expected. It was thought that a similar response to that seen in Figure 4.15 would be seen given that the support structure was assumed to be less rigid than the table mounted configuration. Therefore, as seen in test configurations 2a and 2b, it was expected that additional modes would be present within the system, and that the ω_n values would decrease from those found for the table mounted tube.

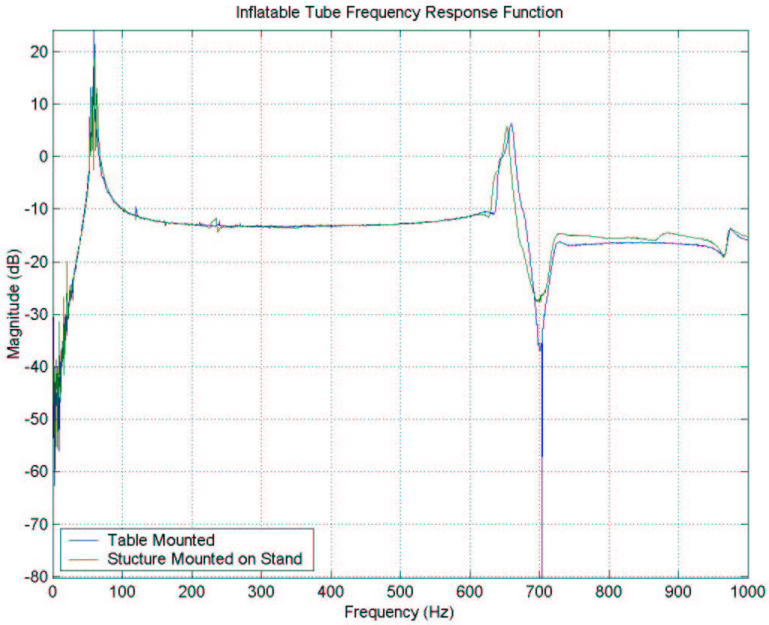

Figure 4.16 Table Mounted vs Structure Mounted FRF

By following the same pattern as in previous tests, the true modes were determined based on a comparison between the two configurations and verifying the values through the modal shape data. As shown in Table 4.3, it was seen that the ω_n values were almost identical to those found in test configurations 1a and 1b. This unexpected result was due to the fact that the RIGEX test structure provided a sufficient amount of mass loading to the system so that the support modelled that of the rigid table mounted configuration. Once again though, one additional value was seen at 975.0 Hz in the data collected using the single axis accelerometer that was not present in the data found using the PSV system. The exact source of this value is unknown.

The final test to be accomplished was to mount the tube within the RIGEX test structure inside the vacuum tank as described for configuration 4. This would allow testing to be conducted in a mounting orientation that would simulate how the experiment will be mounted inside the GAS canister. Figure 4.17 shows the FRF

Table 4.3 Structure Mounted Results Comparison

Mode	HP System Data Frequency (Hz)	PSV System Data Frequency (Hz)
1^{st} Bending	60.3125	62.75
1^{st} Torsional		236.5
2^{nd} Bending	654.0625	654.0

produced for this test configuration, which does vary slightly from that of the tube itself. While the peaks lie at similar frequencies, the basic shape of the FRF changed fairly significantly. For the purposes of determining the bending modes of the tube, the shape of the plot is not a key factor and therefore will not be analyzed.

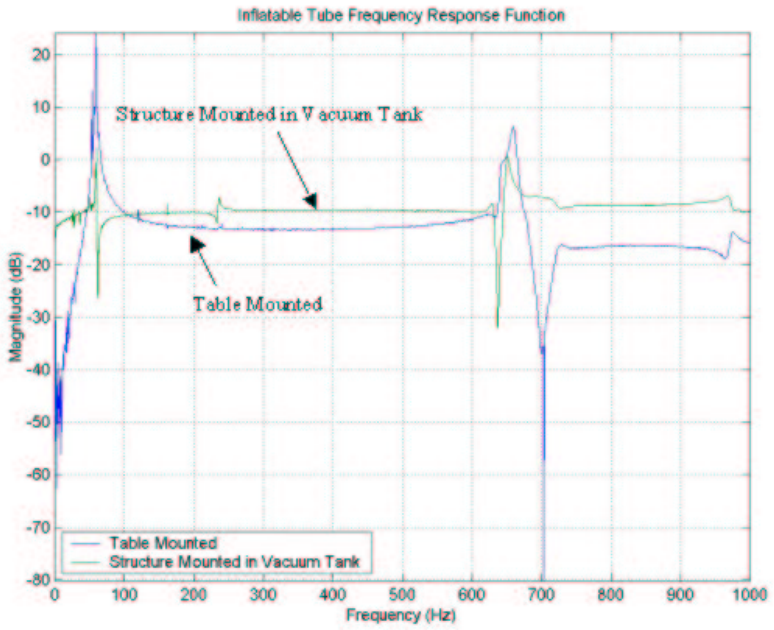

Figure 4.17 Table Mounted vs Vacuum Tank Mounted FRF

Table 4.4 outlines the exact ω_n values found using the HP system, and due to the fact that no data could be taken using the PSV system in this configuration because of the vacuum tank, all verification of the modes was accomplished by comparing the results to those found using test configurations 3a and 3b.

Table 4.4 Vacuum Tank Mounted Results

Mode	Frequency (Hz)
1^{st} Bending	60.625
1^{st} Torsional	235.9375
2^{nd} Bending	651.25

By comparing these results shown in Table 4.4 to those found by testing in configuration 3a and 3b, it was determined that the first mode was located at 60.625 Hz while the second mode was located at 651.25 Hz. The value seen at 235.9375 Hz is assumed to be a torsional mode of the tube due to the fact that it corresponds to the value seen at 236.5 Hz in test configuration 3b which by viewing the modal shape data was clearly a torsional mode. The reason this mode was detected with only a single axis accelerometer is assumed to be because of the misalignment of the accelerometer with respect to the axis being excited during the test. Once again, a mode was seen at 967.8125 Hz which correlates to those previously seen in the 900 Hz range. As in previous tests, the source of this mode is unknown. In addition, data plots showing the phase and coherence data in comparison to the FRF magnitude plots for each test configuration are shown in Appendix B.

In conclusion, by compiling the data for each test and comparing the results between the data collected through the HP system and the data collected through the PSV system, along with the modal shape data, the true first and second bending modes and their corresponding natural frequencies were found for the tube. Given that in the actual space flight experiment, only a single axis accelerometer mounted to the top end flange would be used, the frequencies identified as the first and second mode through the data collected by the HP system will be the only values used for further analysis. These values are shown in Table 4.5.

4.3.2 Damping Ratio Calculation. To calculate the damping ratios of the tube, only the first and second bending modes were analyzed, and only the data

Table 4.5 Natural Frequency Results

First Bending Mode		**Second Bending Mode**	
Table Mounted	59.6875 Hz	**Table Mounted**	660.0 Hz
Stand Mounted	37.5 Hz	**Stand Mounted**	542.1875 Hz
Structure Mounted	60.3125 Hz	**Structure Mounted**	654.0625 Hz
Vacuum Tank Mounted	60.625 Hz	**Vacuum Tank Mounted**	651.25 Hz

obtained by using the HP system in conjunction with the accelerometer was used. The reason for this limitation was to calculate the damping ratios based only on the data that would be achievable for the actual space flight of RIGEX. By applying the half power method described in Section 2.2.2 to the data collected, the damping ratios corresponding to the first and second bending modes of the tube were found. Table 4.6 shows the values found for each test configuration in comparison to the results found for the natural frequencies of each mode.

Table 4.6 Damping Ratio Results

First Bending Mode				
Parameter	**Table**	**Stand**	**Structure**	**Vacuum Tank**
Natural Frequency (Hz)	59.6875	37.5	60.3125	60.625
Damping Ratio (%)	0.78	0.83	0.52	1.04
Second Bending Mode				
Parameter	**Table**	**Stand**	**Structure**	**Vacuum Tank**
Natural Frequency (Hz)	660.0	542.1875	654.0625	651.25
Damping Ratio (%)	0.64	0.32	0.53	0.57

As shown in Table 4.6, the damping ratios for the tube vary between tests. It was expected that the damping values would remain essentially unchanged throughout each test due to the fact that the damping ratio is simply a material property and should not be dependent upon the boundary condition. As seen in Table 4.6 though, the damping ratios do not appear to remain constant, however, all values are within approximately the same order of magnitude. Therefore, the change in the values is assumed to be due to the limitation in the accuracy of the half power

method. In order to determine the exact values for the damping ratios, an accurate model of the tube is necessary.

4.4 Summary

Initial RIGEX ground tests were successful. They demonstrated that the preliminary design of the experiment, once minor modifications were made, was suitable for the mission, and initial test results showed the feasibility of deploying and rigidizing a tube. Initial vibrational tests demonstrated the expected shift in frequencies as the boundary conditions were modified, and additionally showed that flight results obtained while the tube was mounted within the actual RIGEX structure should match those of the tube itself due to the mass loading of the structure.

Despite the success of initial ground tests the need for improved ground testing methodologies in order to obtain sufficient data still remains. Improvements are still needed prior to the actual RIGEX space flight in order to determine the accuracy of the tube deployment and to correct various issues that were seen throughout the initial tests. Recommendations for future work needed to ensure a successful RIGEX mission are outlined in the next chapter.

V. Conclusions and Recommendations

5.1 Testing Evaluation

In general, the ground testing of RIGEX completed has been very successful. While minor set backs were seen throughout testing, the basic goal of the testing process was accomplished. Both successes and failures were seen in individual tests, however, the successes verified that the procedure or system operated as planned and within specified limits while failures allowed for the opportunity to make modifications to ensure the ultimate success of the mission. Current tests have yielded great knowledge into the details of the experiment that will lead to the future success of the RIGEX mission.

5.1.1 Deployment Testing. The primary objective of the deployment testing was to determine if given the current RIGEX design, could a tube successfully be inflated and rigidized. Throughout the course of testing, several flaws were found. These include the need for insulation around the heater box to prevent heat loss, the need to prevent direct contact between the heater box and the bottom plate of the structure which once again would yield heat loss from the heater, the need for a latch to hold the tube in place and provide a mechanism for triggering the opening of the heater box doors, and the need for various modifications to the inflation system in order to ensure a leak proof system that would maintain a controlled deployment of the tube. While some of these flaws were corrected, some are left for future research.

In addition, when testing the deployment of inflatable structures, the primary hinderance to accurate ground testing methods is in the affects due to gravity. When deciding which orientation the structure would be mounted in for the deployment, it was determined that a full deployment of the tube given the current design would be unattainable in the upright configuration. This is due to the fact that initial tests using the purely inflatable tube showed that in the upright configuration, the

tube would become wedged in the heater box thus preventing a full deployment. Therefore, it was determined to mount the structure in the inverted configuration for the tests. In addition to the fact that this would ensure a complete deployment, the inverted configuration most accurately modelled how the tube would react in space given that the force of the doors would provide an initial upward force to the tube. However, as seen in the speed at which the tube deployed, this did not yield an optimal means for collecting the desired data on the tube deployment. In addition, this also eliminates the ability to determine the accuracy of the deployment in that due to gravity, the tube will always deploy to a perfectly vertical state.

In conclusion, as with all testing programs, success can take on a variety of forms. There will constantly be areas for improvement regardless of how successful a test is accomplished. However, for the purposes of this research, given that a z-folded tube was successfully heated, inflated, cooled, and rigidized the current RIGEX deployment testing is considered a success.

5.1.2 Vibrations Testing. Throughout the course of RIGEX vibrations testing, several unexpected occurrences were seen. The tube itself, when mounted to a firm base thus yielding a cantilever support, responded as expected with a very clearly defined FRF. By changing the boundary conditions for the tube, and thus adding flexibility into the support, it was expected that additional modes would be seen, and that the actual ω_n values for the tube itself would be decreased. This exact occurrence was seen when the tube was mounted on the test stand, however, due to the mass of the test structure, once mounted within the RIGEX test structure, the tube responded as if it were mounted to a fixed support. This gives an initial estimate that once in space, very little change in the ω_n values of the tube should be seen.

A different outcome however was seen in the analysis of the ζ values for the tube, where the results seemed to follow no apparent pattern. Although no pat-

tern was seen, all values were within the same order of magnitude. Therefore, the ambiguity within the ζ values is due to the accuracy of the half power method. In order to decrease the error, within the ζ values, an accurate analytical model of the tube is needed. Initially, it was thought that the tube could be modelled simply as a cantilever beam. However, as testing has shown, the tube does not respond in this manner. The first bending mode of the tube did match the motion of the first bending mode of a purely cantilever beam. The second bending mode of the tube though modelled the motion of the first bending mode of a simply supported beam. Therefore, a dedicated model of the beam is needed if further analysis is desired.

As with the deployment tests conducted, the RIGEX vibrations tests were successfully completed. While some unexpected results were seen, and exact correlations between tests could not be completely made, the first and second bending modes of the tube along with the damping ratios associated with those modes were found for each of the test configurations. Given that the final testing configuration of the experiment simulated the actual space flight configuration, these results can be correlated to the actual space flight results, thus validating the ground testing methods and accomplishing the RIGEX mission.

5.2 Recommendations

In order to achieve the over all objective of the RIGEX mission and correlate the ground tests to space flight results, further research is required in a variety of areas. Current efforts have resolved some issues associated with the RIGEX mission, however, in resolving these issues, additional concerns have come about. The following paragraphs outline several key issues that should be addressed if the continuation of the RIGEX mission is desired.

As seen in testing, there are various issues involved with the inflation system. To resolve these issues, future work should focus on optimizing the gas flow between the pressure cylinder and the inflatable tube. Key aspects that should be analyzed in

order to accomplish this task are as follows. First, the regulator should be thoroughly tested to determine why it appeared to malfunction during testing. If a solution to this question can not be found, then the system should be modified to incorporate a new regulator. Once the regulator is operational, the flow rate should be optimized in order to yield the desired tube inflation time. The final task is to determine the cause for the leak within the pressure relief valve. This leak should be eliminated and the relief valve should be set in order to ensure over pressurization of the tube will not occur.

With the issues regarding the inflation system resolved, the connection between the inflation system and the tube should be modified. Currently, as previously mentioned, the inflation system is screwed into the base of the thermoplastic heater box and an o-ring provides the seal between the heater box and the tube. However, as tests showed, this seal is inadequate in that it allows numerous points of failure that cannot be tested prior to deployment. In addition, the connection between the inflation system and the heater box poses a point of concern for the actual flight design in that during launch, the vibrations seen by the heater box will cause this connection of metal screwed into plastic to loosen thus causing an additional leak within the inflation system. Therefore, the bottom end flange of the tube should be changed to match the top end flange. Once this is done, a hole can be drilled and tapped in the base of the bottom end flange thus allowing the inflation system to be screwed into the aluminum end flange. This will eliminate the need for the o-ring, and eliminate the potential for leaks during launch due to the connection to the tube.

In addition to the modification to the inflation system, the actual positioning of the inflation system as part of the flight experiment is needed. Current design calls for the inflation system to be mounted on the bottom side of the bottom plate of the experiment structure. However, due to the addition of the heater box latch, some of the space originally designed for the inflation system is now occupied. Therefore,

analysis should be done to determine physically where to mount the inflation system within the flight model of the experiment. This design should then be tested due to the fact that as the dimensions of the inflation system tubing change, the volume occupied by the inflation gas changes, thus changing the settings of the pressure regulator and the gas flow rate.

Various aspects of the structure along with potential mounting issues also need to be addressed. The current design for the structure was done in a manner that ensured adequate structural support for the experiment components, however, the potential exists for reduction in the mass of the structure if need be. Therefore, analysis should be done to determine the optimal thickness for the plates of the structure given the loads it must withstand. If analysis shows that the thickness of the plates can be reduced, this may open more space within the experiment bay, which will in turn allow a greater separation between the top end flange of the deployed tube and the camera, thus allowing better resolution of the deployed state of the tube.

The issue of how the tubes are mounted within the heater box should also be addressed. Currently a bolt is placed through the holes in the heater box and in turn through the holes in the end flange. A nut is attached to the bolt and tightened to secure the tube within the heater box. This yields two concerning issues. One is in the fact that due to a limited space, it is very difficult to tighten the nut on the bolt and provide a secure connection. The second is in the fact that during launch vibrations, the potential exists for the nuts to loosen thus once again eliminating the secure connection which will in turn decrease the quality of the vibrational data that will later be collected on the deployed tube. Therefore, as the bottom end flanges are modified, the bolt holes in the end flange should be changed to threaded holes so that the tube can be directly connected to the bolt thus eliminating the need for a nut to provide the connection.

In regards to the heater box, three issues should be addressed. The first is in the insulation used. Current design simply used a type of fiberglass insulation around the heater box. This solution was effective, however, it was not optimal. A better form of insulation is needed that can be more firmly mounted around the heater box. Additional testing should also be conducted to determine how much insulation is needed on all sides. Once again, if less insulation is needed on the bottom of the heater box, more space could be given to allow better resolution of the digital images. The second aspect in need of work is the latch solenoid. While this solenoid worked for initial testing, it will not suffice for space flight. In addition, the current solenoid had only a 23 oz pull force which in some instances was not sufficient. Therefore, a higher quality pin puller is needed for the latch system. The final aspect needed is simply higher quality springs for the heater box doors. While the current springs will work for ground tests, further tests are needed to determine if they will be capable of surviving the various vibrational launch loads within the GAS canister.

The final physical aspect that should be modified is in the actual parameters of the tube. Current design has set the T_g temperature of the tube at $125°C$. This was a user defined parameter that can be changed. This value was originally based on a 25% safety margin over the $100°C$ assumed maximum temperature within the GAS canister. However, further research showed that the maximum temperature was only $65°C$ which in using the same 25% margin, yields a T_g of only $81.25°C$. By lowering the T_g value, less time would be required for heating the tube thus reducing the required power for the heating process.

In addition to actual hardware issues within the experiment, various tests are needed to further analyze the feasibility of the mission given the current design. One such test includes a complete power analysis followed by and end to end test to verify the power consumed by the complete experiment. The results should be compared to the amount of battery power that can be supplied to determine if it is sufficient.

A complete heating test of the tube should be conducted using various data points on the tube. As seen in testing, the temperature can vary drastically from one point to the next and therefore, a temperature profile of the tube at various points is needed to truly determine at what point the tube has reached the T_g temperature. In addition, tests should be conducted to determine at what point the temperature sufficient rigidization has occurred so that the inflation gas can be vented from within the tube. By minimizing the time that pressure should be maintained, the power consumption of the inflation system can be minimized due to the fact that power must be continuously supplied to the inflation system solenoid in order to maintain pressure. Once power is removed, the inflation gas is vented. Therefore, if the time the tube pressure is maintained is reduced, the time that power is needed for the solenoid is reduced, thus reducing the power consumed.

The final task which should be accomplished is in solidifying an actual launch opportunity for the RIGEX mission. Given that RIGEX is a Department of Defense (DoD) sponsored experiment, the most efficient and cost effective way to obtain a flight opportunity is through the DoD Space Test Program (STP). STP is responsible for providing flight opportunities for experimental payloads approved by the Space Experiments Review Board (SERB). By briefing the SERB, and obtaining approval, a flight opportunity can be solidified. Appendix E outlines the process necessary to brief the SERB and obtain approval. This process should be started immediately in order to ensure a flight opportunity within two years.

5.3 Conclusion

In conclusion, the RIGEX mission is an excellent opportunity for AFIT. It provides a method for AFIT to make vital advances in the use of inflatable, rigidizable technology. Space assets are an essential part of today's world in both the civilian and military arenas, and as greater demands are placed on satellite providers, the necessity arises for technology that will allow those demands to be met. In an

age where budgets and capabilities are limited, inflatable, rigidizable technology provides a solution to current technological needs. The knowledge gained through the RIGEX mission is an excellent way to advance that technology and provide increased capability for both the commercial and DoD community.

Appendix A. Deployment Testing Results

A.1 Deployment Test 1 Digital Images

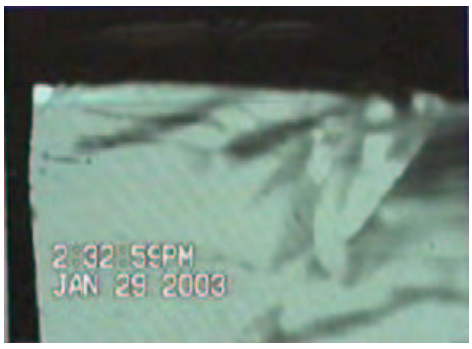

A.2 Deployment Test 1 Data Plots

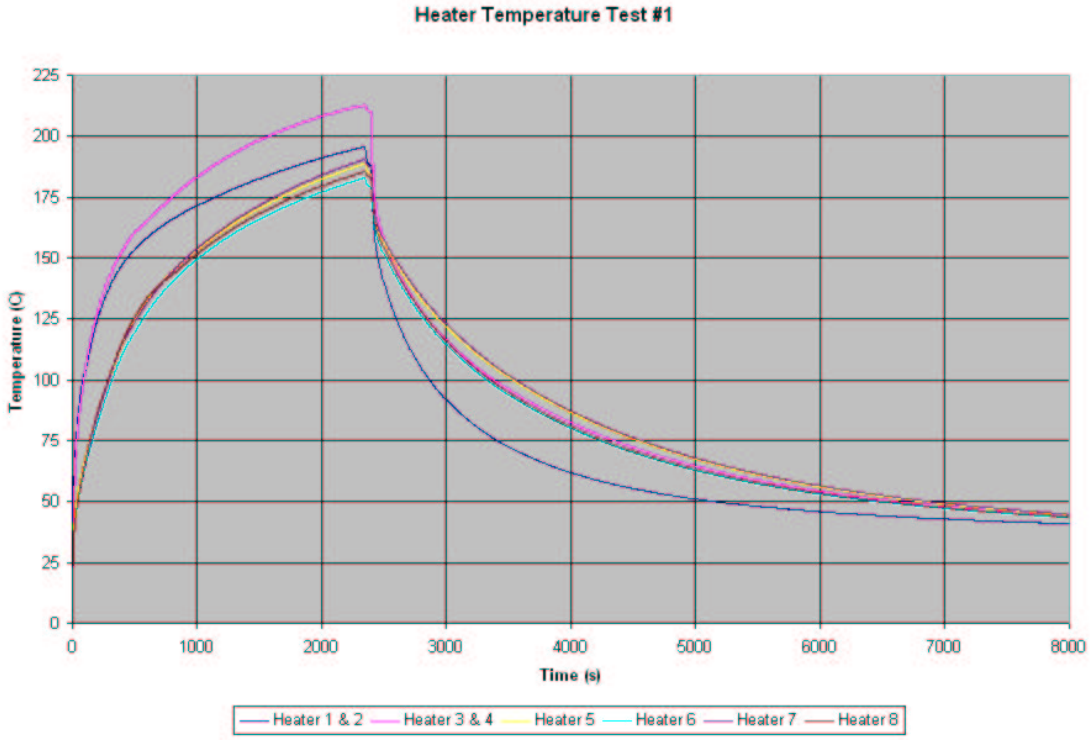

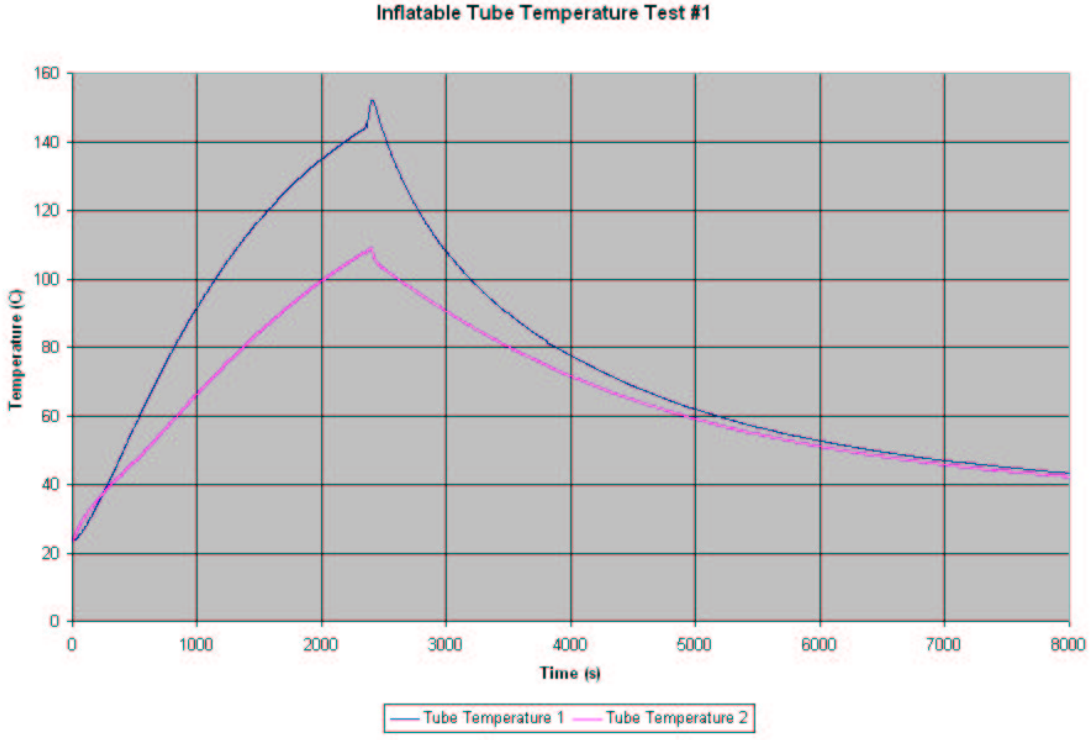

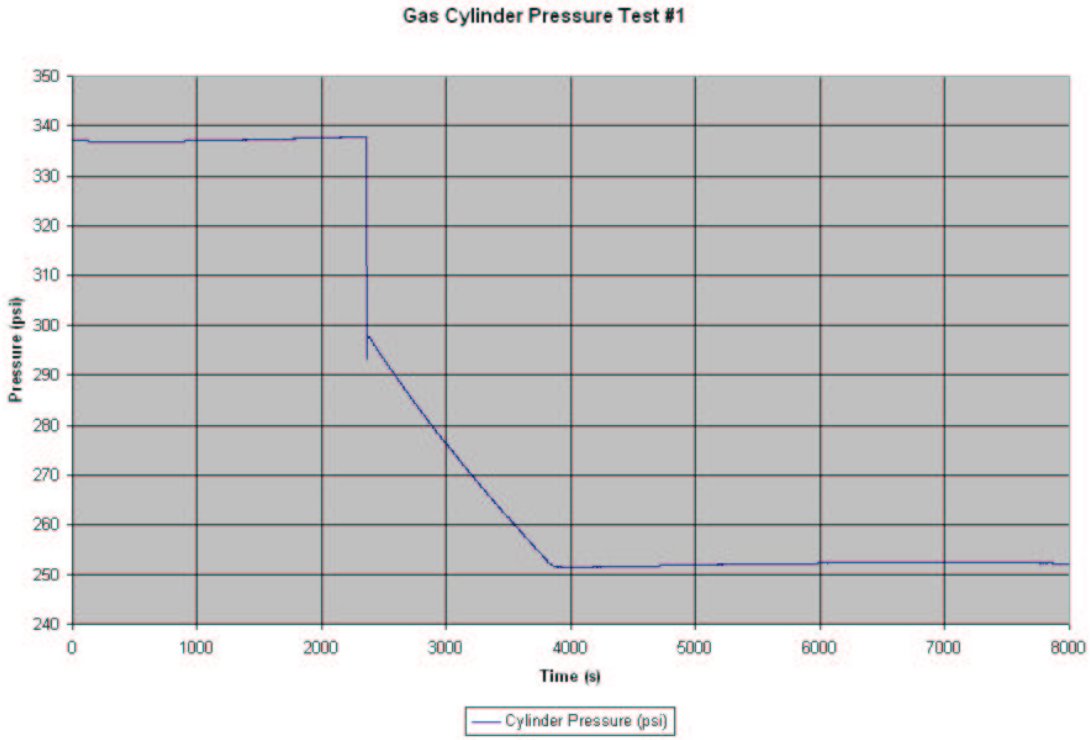
Gas Cylinder Pressure Test #1
Pressure (psi)
350
340
330
320
310
300
290
280
270
260
250
240
0
1000
2000
3000
4000
5000
6000
7000
8000
Time (s)
Cylinder Pressure (psi)

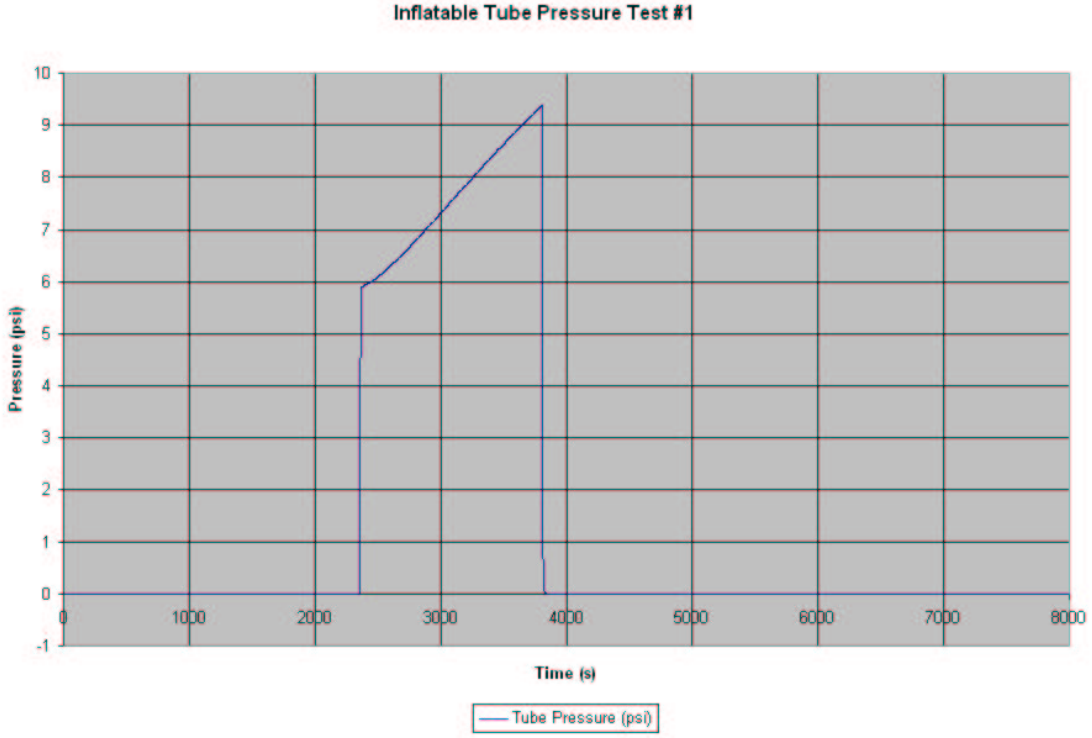
Inflatable Tube Pressure Test #1
Pressure (psi)
10
9
8
7
6
5
4
3
2
1
0
-1
0
1000
2000
3000
4000
5000
6000
7000
8000
Time (s)
Tube Pressure (psi)

A.3 Deployment Test 2 Digital Images

A.4 Deployment Test 2 Data Plots

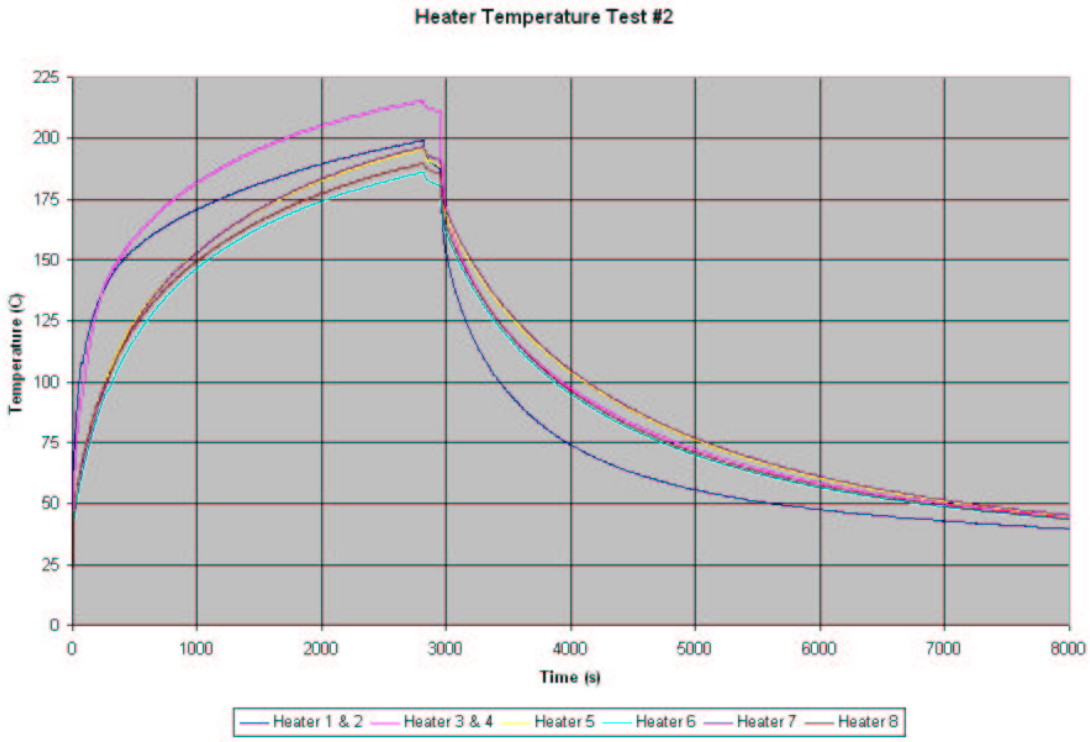

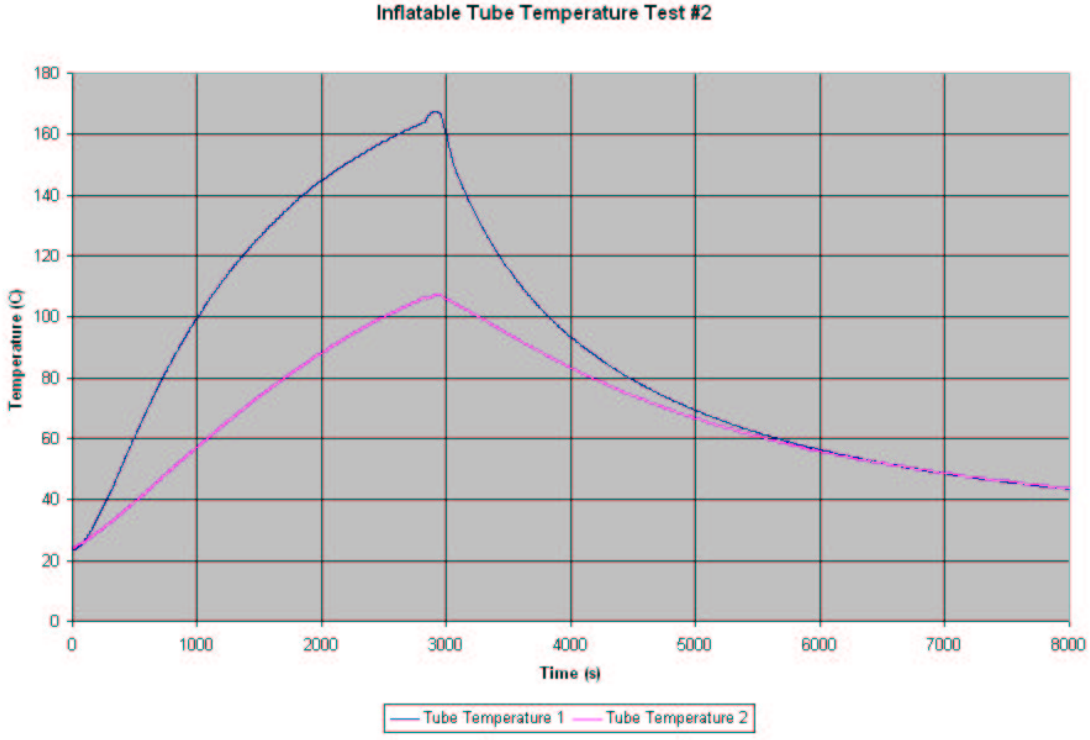

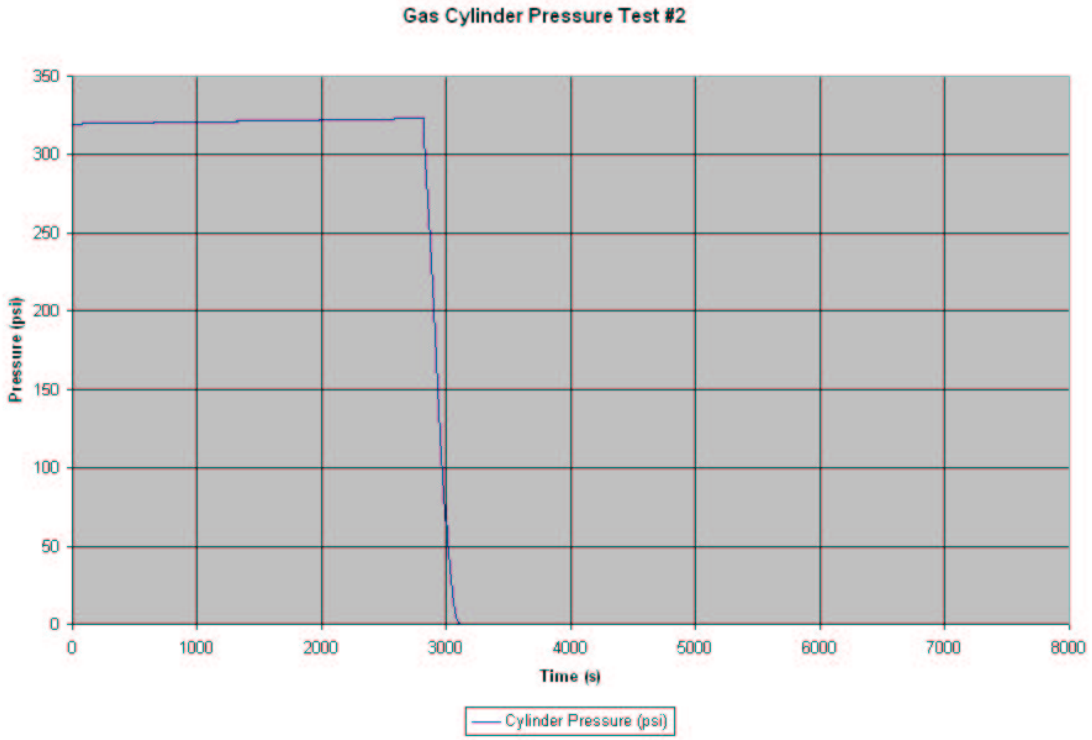
Gas Cylinder Pressure Test #2
Pressure (psi)
350
300
250
200
150
100
50
0
0
1000
2000
3000
4000
5000
6000
7000
8000
Time (s)
Cylinder Pressure (psi)

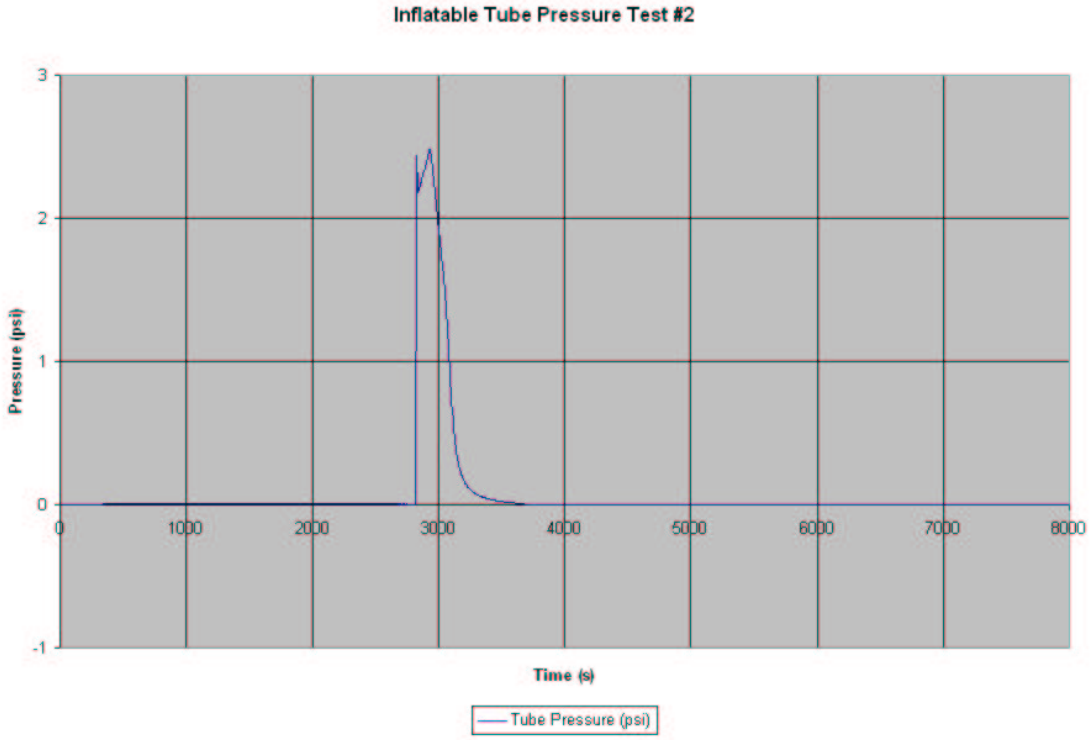
Inflatable Tube Pressure Test #2
Pressure (psi)
3
2
1
0
-1
0
1000
2000
3000
4000
5000
6000
7000
8000
Time (s)
Tube Pressure (psi)

Appendix B. Vibrations Testing Results

B.1 Table Mounted FRF Data Plots

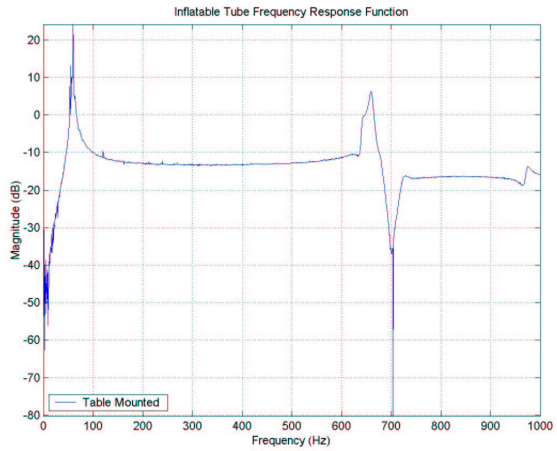

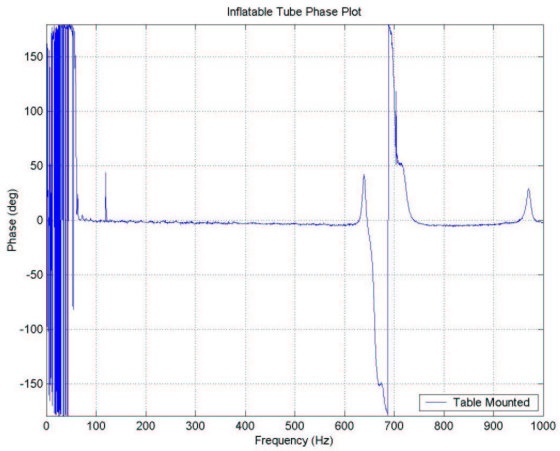

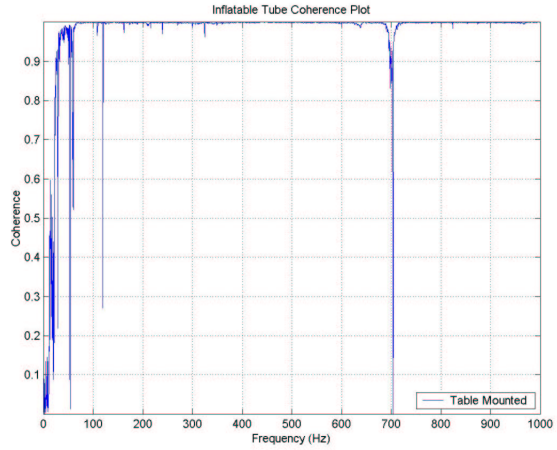

B.2 Stand Mounted FRF Data Plots

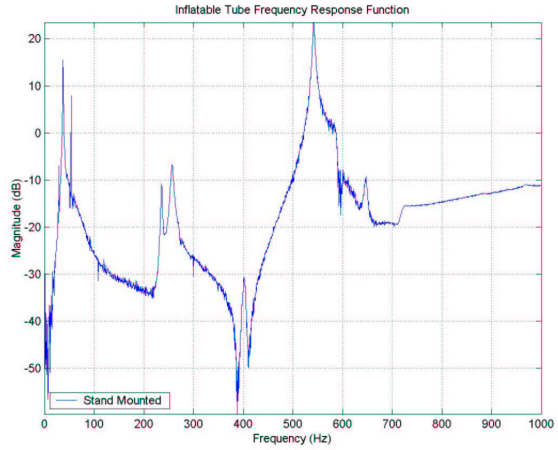

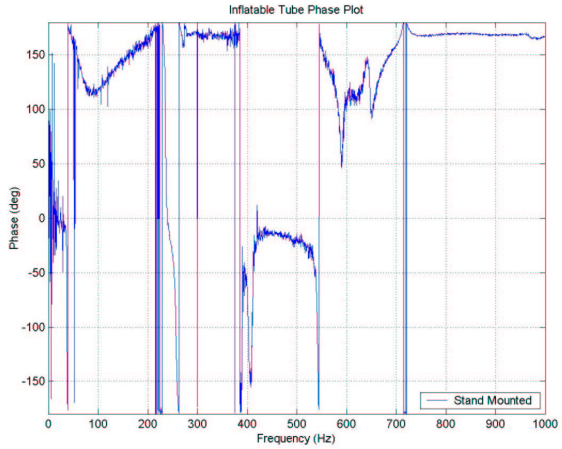

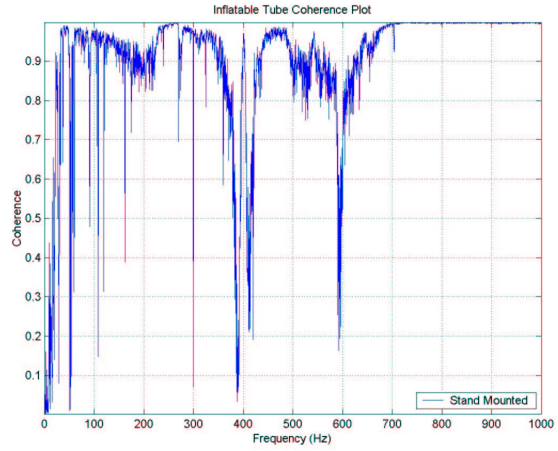

B.3 Structure Mounted FRF Data Plots

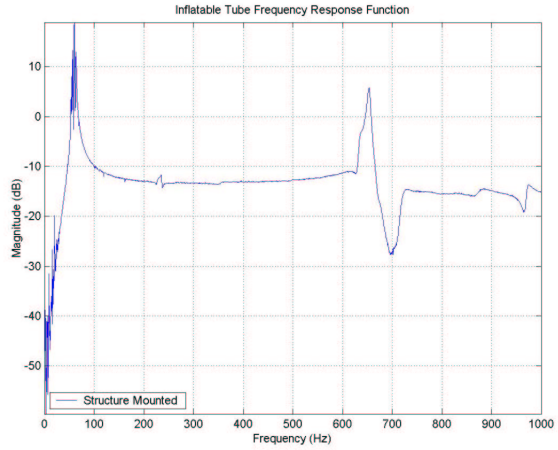

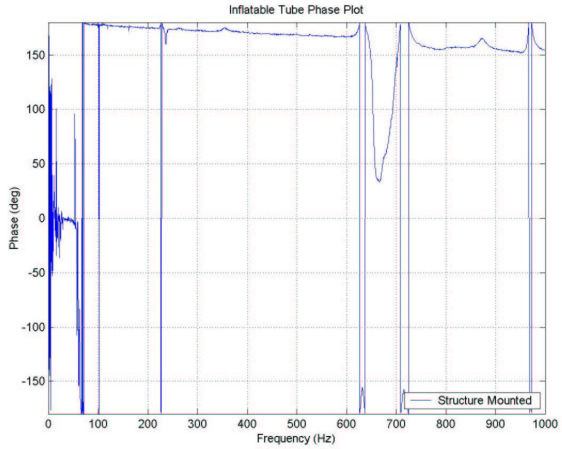

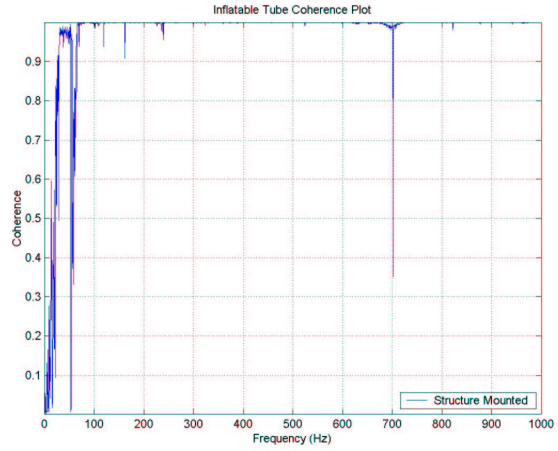

B.4 Vacuum Tank Mounted FRF Data Plots

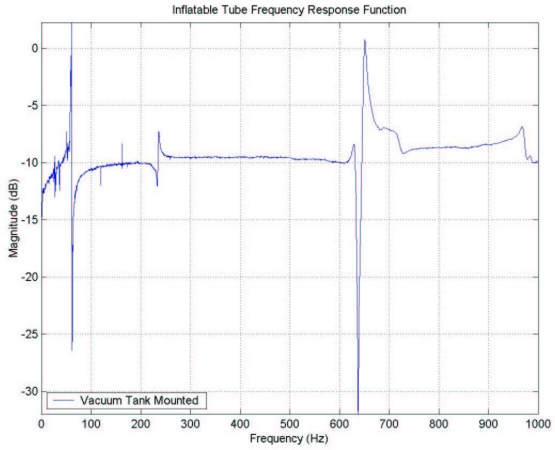

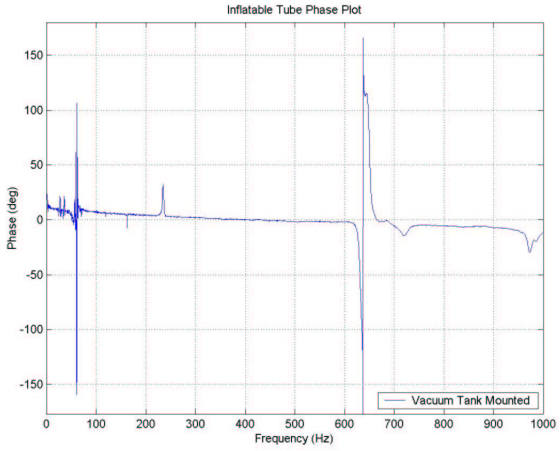

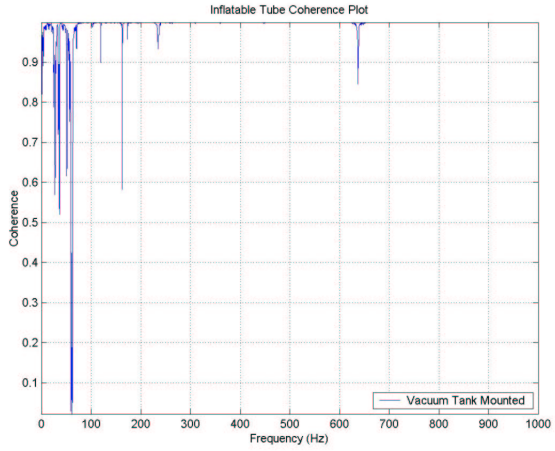

Appendix C. Heat Transfer Calculations

Initial estimates for the heat lost (Q) by the heater box can be found using the fundamental equation for one-dimensional, steady-state heat conduction as shown below:

$$Q = (\frac{kA}{L})\Delta T \tag{C.1}$$

Where k is the thermal conductivity of the material in $W/m{\cdot}K$, A is the surface area of the material perpendicular to the direction of heat transfer, L is the thickness of the material, and ΔT is the absolute temperature difference in Kelvin. Using equation C.1, the total heat lost for the box could be determined by the following:

$$Q_{total} = Q_{top} + Q_{bottom} + 2Q_{front,back} + 2Q_{side} \tag{C.2}$$

Where Q_x is the heat transfer for the various components of the box. Figure C.1 shows the configuration used for the top of the heater box, while Figure C.2 shows the layout all other sides of the heater box, given that all sides are insulated with the exception of the top.

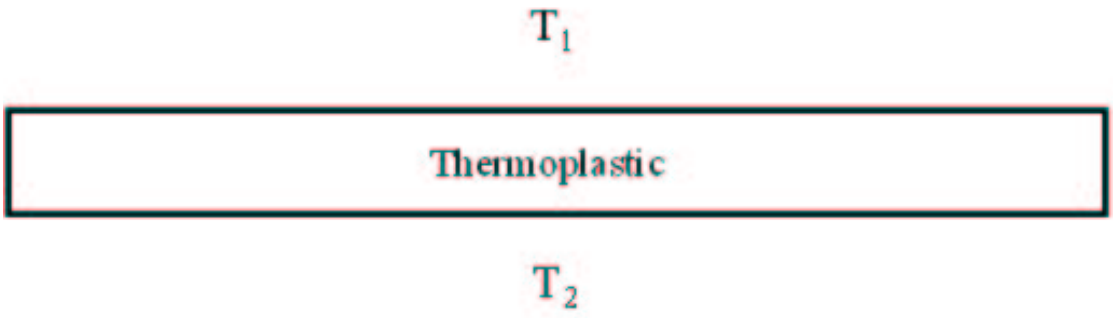

Figure C.1 Heat Transfer Diagram 1

In addition, in order to perform the calculations when the insulation was added, the total conductivity of the combined surface was defined. This was done through the calculation of the thermal resistance due to conduction (23). The thermal resis-

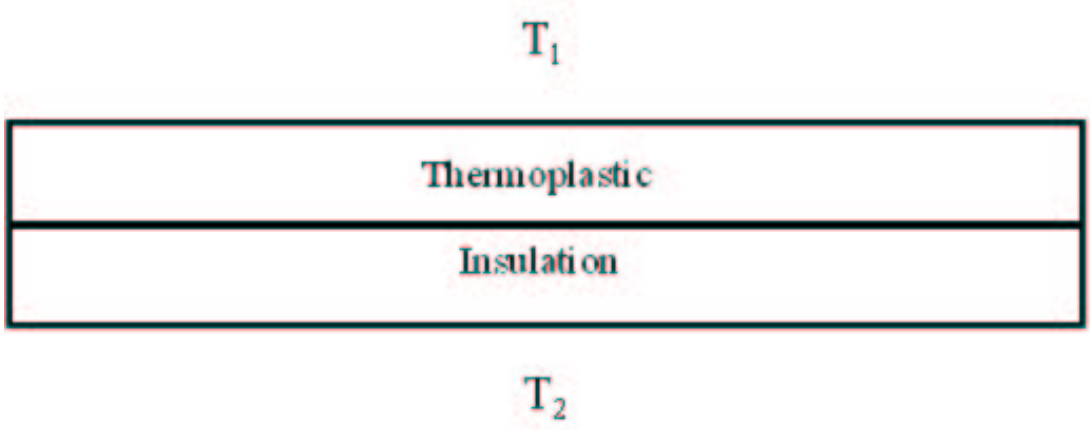

Figure C.2 Heat Transfer Diagram 2

tance ($R_{t,cond}$) of a material is defined by equation C.3:

$$R_{t,cond} = \frac{L}{kA} \tag{C.3}$$

When multiple materials are mounted to one another, the total thermal resistance (R_t) can then be found by simply adding the $R_{t,cond}$ values for each material as shown in equation C.4:

$$R_t = R_{t,1} + \ldots + R_{t,n} \tag{C.4}$$

Using these relationships, the heat transfer defined by equation C.1 can be redefined as shown in equation C.5:

$$Q = \frac{\Delta T}{R_t} \tag{C.5}$$

Using these relationships, the heat loss can be found for both the uninsulated and insulated cases.

In order to complete the necessary calculations, the material properties each portion of the box along with the material properties of the insulation must be defined. The thermal conductivity of the heater box material was found to be 0.12 while the thermal conductivity for the insulation is assumed to be approximately 0.0317 (8, 45). The additional properties needed to perform the thermal analysis

are outlined in Section 3.2.2. Additionally, it was assumed that only conduction was responsible for the heat loss from the box as the heat is conducted through the heater box material, and that when the insulation was added, there was assumed to be no space between the insulation and the thermoplastic. For all cases, T_1 was assumed to be $150°C = 423.15K$ and T_2 was assumed to be at ambient temperature of $22°C = 295.15K$, thus making $\Delta T = 128K$ for all cases.

In order to show the affects of the insulation, two sets of calculations were performed. First, the total heat loss was found without insulation using equation C.1 as the basis for finding the Q values. The heat loss with the insulation added was then found using equation C.5 as the basis for determining the Q values. This allowed the decrease in heat loss due to the insulation to be shown. In addition, for in order to convert from units of inches to meters, the conversion factor of $1meter = 39.37inches$ was used. The following sections show the calculations that were used to initially estimate the affects of the addition of insulation to the heater box.

$$A_{top,bottom} = (length)(width) \tag{C.6}$$

$$= (3.75in)(5.5in) = (0.0952m)(0.1397m) = 0.0133m^2 \tag{C.7}$$

$$Q_{top,bottom} = [\frac{(0.12)(0.0133)}{0.0063}](128) = 32.1869W \tag{C.8}$$

$$A_{sides} = (length)(width) \tag{C.9}$$

$$= (3.75in)(4.5in) = (0.0952m)(0.1143m) = 0.0109m^2 \tag{C.10}$$

$$Q_{sides} = [\frac{(0.12)(0.0109)}{0.0063}](128) = 26.3347W \tag{C.11}$$

$$A_{front,back} = (length)(width) \tag{C.12}$$

$$= (5.5in)(4.5in) = (0.1397m)(0.1143m) = 0.0160m^2 \tag{C.13}$$

$$Q_{sides} = [\frac{(0.12)(0.0160)}{0.0063}](128) = 38.6243W \tag{C.14}$$

$$Q_{total} = 2Q_{top,bottom} + 2Q_{sides} + 2Q_{front,back} \tag{C.15}$$

$$= 2(32.1869) + 2(26.3347) + 2(38.6243) = 194.2917W \tag{C.16}$$

$$A_{top,bottom} = 0.0133m^2 \tag{C.17}$$

$$A_{sides} = 0.0109m^2 \tag{C.18}$$

$$A_{front,back} = 0.0160m^2 \tag{C.19}$$

$$R_{t,top} = \frac{L_{top}}{k_{plastic}A_{top}} \tag{C.20}$$

$$= \frac{0.0063}{(0.12)(0.0133)} = 3.9768\frac{K}{W} \tag{C.21}$$

$$Q_{top} = \frac{128}{3.9768} = 32.1869W \tag{C.22}$$

$$R_{t,bottom} = (\frac{L_{bottom}}{k_{plastic}A_{bottom}}) + (\frac{L_{insulationbottom}}{k_{insulation}A_{bottom}}) \tag{C.23}$$

$$= (\frac{0.0063}{(0.12)(0.0133)}) + (\frac{0.0127}{(0.0317)(0.0133)}) = 34.0849\frac{K}{W} \tag{C.24}$$

$$Q_{bottom} = \frac{128}{34.0849} = 3.7553W \tag{C.25}$$

$$R_{t,sides} = (\frac{L_{sides}}{k_{plastic}A_{sides}}) + (\frac{L_{insulationsides}}{k_{insulation}A_{sides}}) \tag{C.26}$$

$$= (\frac{0.0063}{(0.12)(0.0109)}) + (\frac{0.0095}{(0.0317)(0.0109)}) = 32.4596\frac{K}{W} \tag{C.27}$$

$$Q_{sides} = \frac{128}{32.4596} = 3.9434W \tag{C.28}$$

$$R_{t,front,back} = (\frac{L_{front,back}}{k_{plastic}A_{front,back}}) + (\frac{L_{insulationfront,back}}{k_{insulation}A_{front,back}}) \tag{C.29}$$

$$= (\frac{0.0063}{(0.12)(0.0160)}) + (\frac{0.0063}{(0.0317)(0.0160)}) = 15.8590\frac{K}{W} \tag{C.30}$$

$$Q_{front,back} = \frac{128}{15.8590} = 8.0711W \tag{C.31}$$

$$Q_{total} = Q_{top} + Q_{bottom} + 2Q_{sides} + 2Q_{front,back} \tag{C.32}$$

$$= (32.1869) + (3.7553) + 2(3.9434) + 2(8.0711) = 59.9712W \tag{C.33}$$

Appendix D. RIGEX Drawings (17)

Due to the unique nature of the RIGEX mission, several key components of the experiment must be designed and fabricated. Specifically, the experiment structure, battery box, and end flanges for the inflatable, rigidizable tubes need the be analyzed in order to produce both test and flight components for the various remaining aspects of the RIGEX mission. The following drawings outline the current design for these various components. These designs should be used only as a starting point, and modifications should be made as necessary to optimize the operation of the experiment.

The first drawing shows the basic layout of the RIGEX components within the experiment structure. This provides a basis for how the experiment should appear in its final state. As with all designs, this is by no means a finalized design and only provides a basis for future work.

The experiment structure shown in this drawing will house all components of the experiment. The current design calls for all plates to be made of 0.25 inch thick aluminum with the exception of the bottom plate which requires 0.5 inch thick aluminum. The top plate requires 24 holes that will be used to mount the RIGEX structure to the experimental mounting plate within the GAS canister.

The battery box is designed to fit within the center column of the experiment structure, and is designed to prevent any leaks that should arise from the batteries from contaminating the experiment, or the GAS canister. The current design requires the box to be fabricated from 0.125 inch thick aluminum plates.

The next drawing illustrates the current design for the top end flange of the tube. Given the results of this research, this design is to be used for both the top and bottom end flange. The only exception is in the fact that the bottom end flange will need a threaded hole in the flange to allow for the connection of the inflation system. Variations to this design should be considered to optimize this connection.

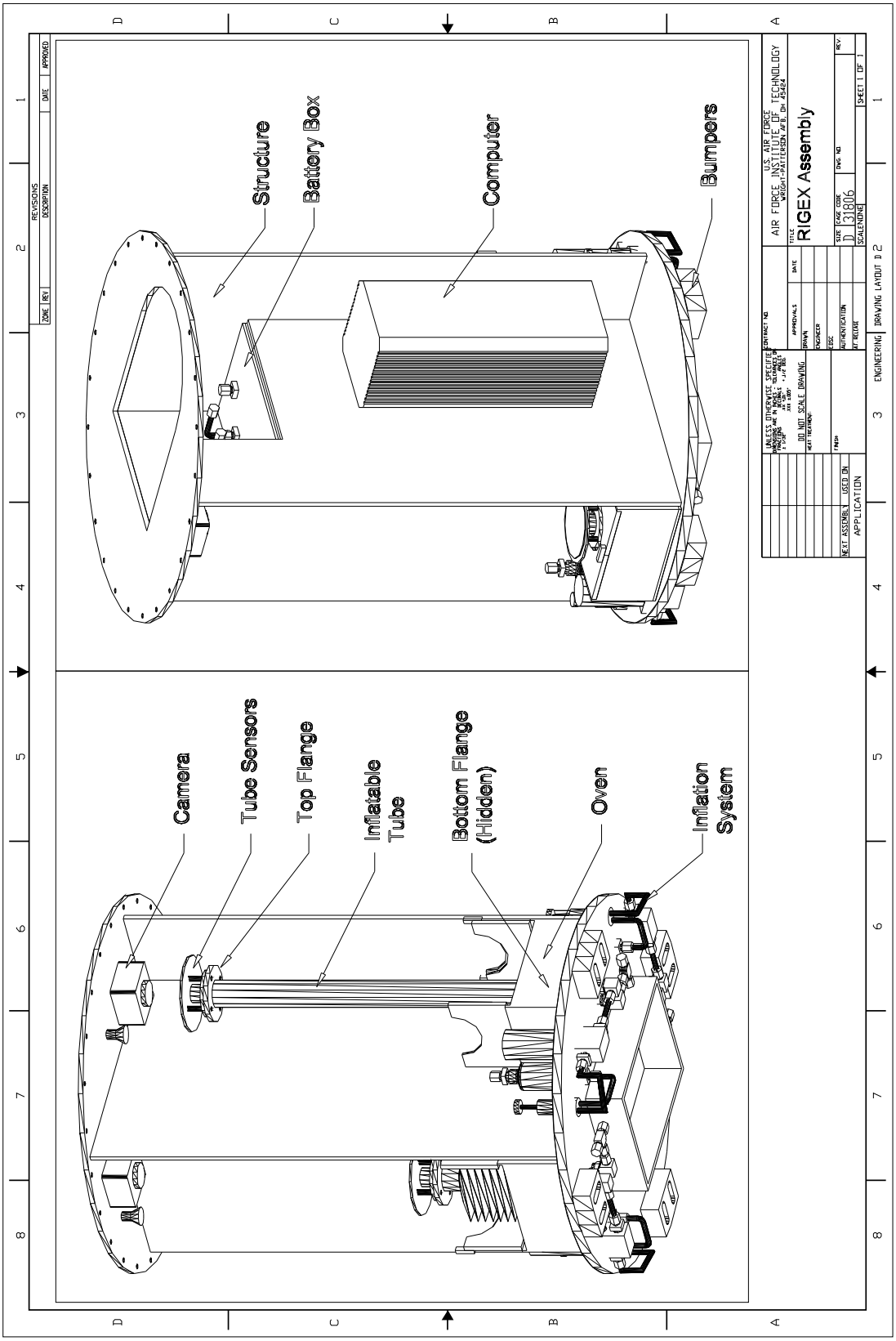
Structure
Battery Box
Computer
Bumpers
Camera
Tube Sensors
Top Flange
Inflatable Tube
Bottom Flange (Hidden)
Oven
Inflation System
AIR FORCE INSTITUTE OF TECHNOLOGY
RIGEX Assembly
DO NOT SCALE DRAWING
ENGINEERING DRAWING LAYOUT D 2

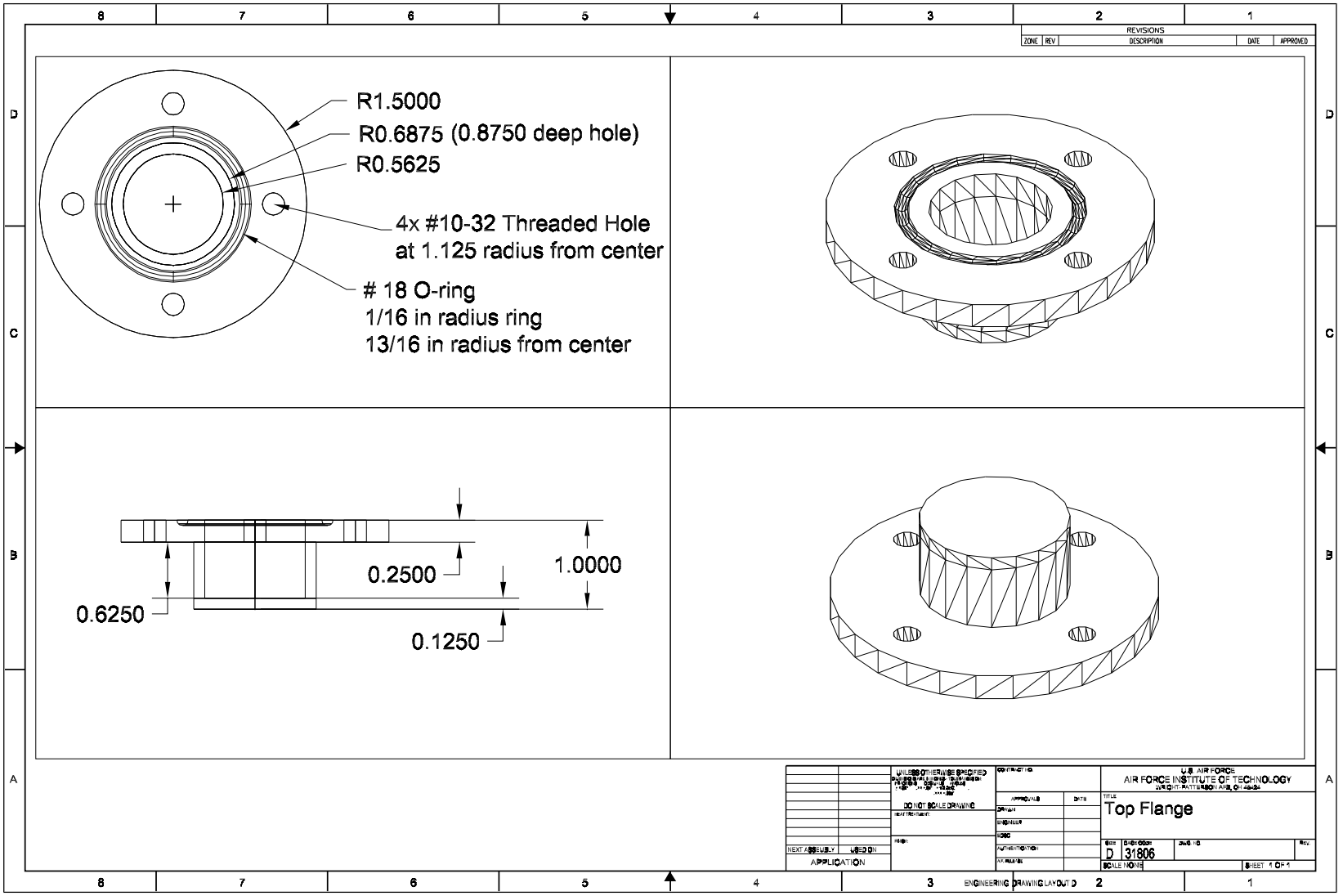
REVISIONS
ZONE REV DESCRIPTION DATE APPROVED
R1.5000
R0.6875 (0.8750 deep hole)
R0.5625
4x #10-32 Threaded Hole
at 1.125 radius from center
18 O-ring
1/16 in radius ring
13/16 in radius from center
0.2500
1.0000
0.6250
0.1250
UNLESS OTHERWISE SPECIFIED
DO NOT SCALE DRAWING
NEXT ASSEMBLY
USED ON
APPLICATION
ENGINEERING DRAWING LAYOUT D
U.S. AIR FORCE
AIR FORCE INSTITUTE OF TECHNOLOGY
WRIGHT-PATTERSON AFB, OH 45433
TITLE
Top Flange
SIZE
D
DWG NO
31806
REV
SCALE NONE
SHEET 1 OF 1

Appendix E. DoD SERB Process (10)

The purpose of the DoD Space Test Program is to be the single DoD source for providing space flight for experimental payloads. The payloads flown by STP include those that are part of the Space Experiments Review Board prioritized list. Once part of the list, STP incorporates three primary modes of space flight for the experiments to include free-flying satellites, secondary payloads on various spacecraft, and space shuttle flights. The choice for which method of flight is used it based on user defined requirements.

The first step in this process is to obtain a sponsor. Experiments can originate from a variety of sources to include DoD laboratories, NASA projects, and various research institutions, however, this is in no way an exhaustive list. The only limitation is that in order to proceed in the process, every experiment must be sponsored by a DoD agency.

Once a sponsor organization is identified, a request for space flight must be submitted to the Secretary of the Air Force for Acquisition (SAF/AQS). This request is submitted by the experimenters sponsoring agency, and is done by submitting a DD Form 1721 through organizational channels to SAF/AQS. This form will then be used by the SERB to evaluate and prioritize the experiments.

The SERB is composed of members of the Army, Air Force, Navy, and other various DoD organizations, and once a year, experimenters who have submitted a request for space flight are required to present their experiments to the board. Each experiment is then evaluated, and is given a ranking based on its DoD relevance as well as the quality of the experiment and the priorities given to the experiment by the sponsoring service. This ranking is then passed on to STP for further analysis.

Upon receipt of the prioritized SERB list, STP develops a mission model for upcoming years which takes into account all launch opportunities available given budget constraints along with the quantity of experiments present on the list. As

listed described previously, the opportunities available include dedicated free-flyer mission, secondary missions and space shuttle opportunities. All available options are included in the model, and experiments are analyzed to determine the applicability of particular opportunities. In addition, priority with various launch opportunities is given based on the experiments DoD SERB ranking.

Once a particular space flight opportunity has been identified, all experiments are reviewed to determine compatibility with a given opportunity. All compatible experiments are sent a payload questionnaire in an effort to refine and update the experiment requirements from the previously submitted DD Form 1721. This information in conjunction with the specifics of the particular opportunity are studied in order to determine the best qualified experiment. Once the experiment has been identified and assigned to a particular launch option, the mission must be approved by SAF/AQS.

The next step in the process is to develop an agreement between the STP, the experimenter, and the agency providing the launch option. The method for accomplishing this task is directly dependent upon the launch option being used. If the experiment is being flown as either a secondary payload or as GAS payload on the space shuttle, typically only a memorandum of agreement (MOA) is necessary to transfer funds from STP to the program office providing the launch. However, if the experiment is being flown as a primary mission requiring STP to procure a satellite for the experiment, along with launch services, STP must go through the standard DoD procurement process in order to acquire a contract for the mission.

With an agreement in place and a host vehicle or space craft and launch option identified, various studies and designs are formulated by both the experimenter and the integration contractor in an effort to produce an interface control document. This document will be used to outline the technical interface requirements defined by the experimenter in order to ensure the capability of mating the experiment with

the host system. Once this point is reached, all changes will require contractual changes and will increase the mission cost.

The final stage in the SERB process is the actual launch and on orbit operations of the experiment. Once the experiment is integrated to the host vehicle, it is launched and a one year period of on orbit operations begins. Throughout this one year of operations, experiment data is collected, formatted, and transmitted to the experimenter. Any data required past the one year point is then the responsibility of the experimenter.

Vita

First Lieutenant Thomas Lee Philley Jr. graduated from Galena Park High School in Galena Park, Texas in May 1996. He entered undergraduate studies at the United States Air Force Academy in Colorado Springs, Colorado where he graduated with a Bachelor of Science Degree in Astronautical Engineering in May 2000.

His first assignment was as a space test developmental engineer for the Department of Defense Space Test Program located at Kirtland AFB, New Mexico. While assigned there, he was the mission manager for several experimental space payloads. In August 2001, he began the Graduate Astronautical Engineering program at the Air Force Institute of Technology, Wright-Patterson AFB, Ohio. Upon graduation, he will be assigned to the National Reconnaissance Office located in Chantilly, Virginia.

Bibliography

1. "Minco Products, Inc.." http://www.minco.com, 1999.
2. "Duracell Alkaline-Manganese Dioxide Battery." http://www.duracell.com, 2000.
3. "ELECTRIM Corporation." http://www.electrim.com/EDC-104.pdf, 2001.
4. "Parker Hannifin Corporation." http://www.parker.com, 2001.
5. "Atlas V Family." http://www.ilslaunch.com/atlas/atlasv/prebody.html, 2002.
6. "Delta IV Launch Vehicles." http://www.boeing.com/defense-space/space/delta/delta-4/delta4.htm, 2002.
7. "GO Regulator, Inc.." http://www.goreg.com, 2002.
8. "Quadrant Engineering Plastic Products." http://www.quadrantepp.matweb.com, 2002.
9. "TiNi Aerospace, Inc.." http://www.tiniaerospace.com, 2002.
10. "STP DoD-SERB." http://www.smc.kirtland.af.mil//dodserb.html, 2003.
11. Canfield, Robert A. Lecture Notes, Mech 515, Theory of Vibrations. School of Engineering and Management, Air Force Institute of Technology, Wright-Patterson AFB OH, Winter Quarter 2002.
12. Cassapakis, Dr. Costa and Dr. Mitch Thomas. "Inflatable Structures Technology Development Overview," *American Institute of Aeronautics and Astronautics*, (AIAA 95-3738) (1995).
13. Clem, A. L., et al. "Experimental Results Regarding the Inflation of Unfolding Cylindrical Tubes," *American Institute of Aeronautics and Astronautics*, (AIAA 01-1264) (2001).
14. Cobb, Richard G. Lecture Notes, Mech 719, Vibrations Damping and Control. School of Engineering and Management, Air Force Institute of Technology, Wright-Patterson AFB OH, Fall Quarter 2002.
15. Derbes, Billy. "Case Studies in Inflatable Rigidizable Structural Concepts for Space Power," *American Institute of Aeronautics and Astronautics*, (AIAA 99-1089) (1999).
16. Disebastian III, John D. and Gregory S. Agnes. "RIGEX: Preliminary Design of a Rigidized Inflatable Get-Away-Special Experiment," *American Institute of Aeronautics and Astronautics*, (AIAA 02-1373) (2002).

17. DiSebastian III, John Daniel. *RIGEX: Preliminary Design of a Rigidized Inflatable Get-Away-Special Experiment*. Master's Thesis, Air Force Institute of Technology, Dayton, OH, March 2001.

18. Freeland, R. E. and G. Bilyeu. "In-Step Inflatable Antenna Experiment," *International Astronautical Federation*, (IAF 92-0301) (1992).

19. Freeland, R. E., et al. "Development of Flight Hardware for a Large, Inflatable-Deployable Antenna Experiment," *International Astronautical Federation*, (IAF 95-1501) (1995).

20. Freeland, R. E., et al. "Inflatable Deployable Space Structures Technology Summary," *International Astronautical Federation*, (IAF 98-1501) (1998).

21. Freeland, R. E., et al. "Large Inflatable Deployable Antenna Flight Experiment Results," *International Astronautical Federation*, (IAF 97-1301) (1997).

22. Guidanean, Dr. Koorosh and Geoffrey T. Williams. "An Inflatable Rigidizable Truss Structure With Complex Joints," *American Institute of Aeronautics and Astronautics*, (AIAA 98-2105) (1998).

23. Incropera, Frank P. and David P. DeWitt. *Fundamentals of Heat and Mass Transfer* (Second Edition). New York, NY: John Wiley and Sons, 1985.

24. Jenkins, Christopher H. M., editor. *Gossamer Spacecraft: Membrane and Inflatable Structures Technology for Space Applications*, *191*. Reston, VA: American Institute of Aeronautics and Astronautics, Inc., 2001.

25. Lou, M. C. and V. A. Feria. "Development of Space Inflatable/Rigidizable Structures Technology." http://techreports.jpl.nasa.gov/1999/99-2110.pdf, 1999.

26. Maddux, Michael. "RIGEX Heater/Storage Box Design and Testing." School of Engineering and Management, Air Force Institute of Technology, Wright-Patterson AFB OH, Summer Quarter 2002.

27. Main, John Alan. *Analysis and Design of Inflatable Aerospace Structures*. PhD Dissertation, Vanderbilt University, Nashville, TN, May 1993.

28. Marker, Dan K. and Dr. Mark Gruneisen. "Thirty-Meter Diameter Diffraction-Limited Gossamer Telescopes in Space," *AFRL Technology Horizons*, (DE-01-02) (2001).

29. Meirovitch, Leonard. *Elements of Vibration Analysis* (Second Edition). Boston, MA: McGraw Hill, Inc., 1986.

30. Miyazaki, Yasuyuki and Michiharu Uchiki. "Deployment Dynamics of Inflatable Tube," *American Institute of Aeronautics and Astronautics*, (AIAA 02-1254) (2002).

31. NASA. *1986 Get Away Special Experimenter's Symposium*, 1986.

32. Salama, Moktar and Michael Lou. "Simulation of Deployment Dynamics of Inflatable Structures," *American Institute of Aeronautics and Astronautics*, (AIAA 02-1521) (2002).

33. Satter, Celeste M. and Robert E. Freeland. "Inflatable Structures Technology Applications and Requirements," *American Institute of Aeronautics and Astronautics*, (AIAA 95-3737) (1995).

34. Shuttle Small Payloads Project Office, Goddard Space Flight Center. *Carrier Capabilities*, 1999.

35. Simburger, Edward J., et al. "Development of a Multifunctional Inflatable Structure for the Powershpere Concept," *American Institute of Aeronautics and Astronautics*, (AIAA 02-1707) (2002).

36. Single, Thomas G. *Experimental Vibration Analysis of Inflatable Beams for an AFIT Space Shuttle Experiment*. Master's Thesis, Air Force Institute of Technology, Dayton, OH, March 2002.

37. Smith, S. W., et al. "Post-Flight Testing and Analysis of Zero-Gravity Deployment of an Inflating Tube," *American Institute of Aeronautics and Astronautics*, (AIAA 01-1265) (2001).

38. Special Payloads Division, Goddard Space Flight Center. *Get Away Special Small Self-contained Payloads Experimenter Handbook*.

39. Steiner, Mark, et al. "Spartan 207/Inflatable Antenna Experiment Flown on STS-77–Preliminary Mission Report." http://www.lgarde.com/people/papers/207.pdf, 1997.

40. Thomas, Mitchell. "Inflatable Space Structures: Redefining Aerospace Design Concepts Keeps Costs From Ballooning." http://www.lgarde.com/people/papers/structures.pdf.

41. Ulvestad, James S., et al. "ARISE: A Space VLBI Mission Using an Inflatable Antenna Structure," *American Institute of Aeronautics and Astronautics*, (AIAA 95-3794) (1995).

42. Veal, Gordon and Robert Freeland. "In-Step Inflatable Antenna Description," *American Institute of Aeronautics and Astronautics*, (AIAA 95-1193b) (1995).

43. Wada, Ben K. and Michael Lou. "Pre-Flight Validation of Gossamer Structures," *American Institute of Aeronautics and Astronautics*, (AIAA 02-1373) (2002).

44. Wang, John T. and Arthur R. Johnson. "Deployment Simulations of Ultra-Lightweight Inflatable Structures," *American Institute of Aeronautics and Astronautics*, (AIAA 02-1261) (2002).

45. Wertz, James R. and Wiley J. Larson, editors. *Space Mission Analysis and Design* (Second Edition). Boston, MA: Kluwer Academic Publishers, 1992.

REPORT DOCUMENTATION PAGE

Form Approved
OMB No. 074-0188

1. REPORT DATE *(DD-MM-YYYY)*	**2. REPORT TYPE**	**3. DATES COVERED** *(From – To)*
14-03-2003	**Master's Thesis**	Jun 2002 – Mar 2003

4. TITLE AND SUBTITLE

DEVELOPMENT, FABRICATION AND GROUND TEST OF AN INFLATABLE STRUCTURE SPACE-FLIGHT EXPERIMENT

5a. CONTRACT NUMBER

5b. GRANT NUMBER

5c. PROGRAM ELEMENT NUMBER

6. AUTHOR(S)

Philley, Thomas L., Jr., First Lieutenant, USAF

5d. PROJECT NUMBER
03-299

5e. TASK NUMBER

5f. WORK UNIT NUMBER

7. PERFORMING ORGANIZATION NAMES(S) AND ADDRESS(S)
Air Force Institute of Technology
Graduate School of Engineering and Management (AFIT/EN)
2950 P Street, Building 640
WPAFB OH 45433-7765

8. PERFORMING ORGANIZATION REPORT NUMBER

AFIT/GA/ENY/03-3

9. SPONSORING/MONITORING AGENCY NAME(S) AND ADDRESS(ES)
IMINT/RNTS
Attn: Maj. Dave Lee
14675 Lee Road — DSN: 898-3084
Chantilly VA 20151 — e-mail: David.Lee@nro.mil

10. SPONSOR/MONITOR'S ACRONYM(S)

11. SPONSOR/MONITOR'S REPORT NUMBER(S)

12. DISTRIBUTION/AVAILABILITY STATEMENT

APPROVED FOR PUBLIC RELEASE; DISTRIBUTION UNLIMITED.

13. SUPPLEMENTARY NOTES

14. ABSTRACT

Inflatable, rigidizable structures provide a solution to reduce the costs associated with design, fabrication and launch of a space system while simultaneously increasing the deployment reliability and mission success of the system. This research focused on the follow on design, fabrication, and ground test of the Rigidizable Inflatable Get-Away-Special Experiment (RIGEX). RIGEX is a self-contained experiment that will test the deployment and structural characteristics of three inflatable rigidizable tubes. Once inflated and rigidized, each tube will be excited using piezoelectric transducers in order to collect vibration data for structural characterization. The goal of this research was to collect ground testing data that will later be used in conjunction with actual space flight results in an effort to validate ground testing methodologies.

15. SUBJECT TERMS

Inflatable Structures, Rigidizable Structures, Ground Testing, Vibrations Testing, RIGEX, Get-Away-Special, GAS, Space Structures

16. SECURITY CLASSIFICATION OF:			**17. LIMITATION OF ABSTRACT**	**18. NUMBER OF PAGES**	**19a. NAME OF RESPONSIBLE PERSON**
a. REPORT	**b. ABSTRACT**	**c. THIS PAGE**			Richard G. Cobb, Maj, USAF (ENY)
U	**U**	**U**	**UU**	152	**19b. TELEPHONE NUMBER** *(Include area code)* (937) 255-3636, ext 4559; e-mail: Richard.Cobb@afit.edu